

**CADMIUM SELENIDE BASED CORE-SHELL
QUANTUM DOTS FOR BIOSENSING AND
IMAGING APPLICATIONS**

THESIS SUBMITTED TO
COCHIN UNIVERSITY OF SCIENCE AND TECHNOLOGY (CUSAT)
IN PARTIAL FULFILMENT OF THE REQUIREMENTS FOR THE DEGREE OF
DOCTOR OF PHILOSOPHY
IN CHEMISTRY UNDER THE FACULTY OF SCIENCE

BY
VINAYAKAN R.

UNDER THE SUPERVISION OF
Dr. K. GEORGE THOMAS



**PHOTOSCIENCES AND PHOTONICS
CHEMICAL SCIENCES AND TECHNOLOGY DIVISION
NATIONAL INSTITUTE FOR INTERDISCIPLINARY
SCIENCE AND TECHNOLOGY (NIIST), CSIR
TRIVANDRUM - 695019
KERALA, INDIA**

MAY 2009

Dedicated to
My Parents and Teachers...

STATEMENT

I hereby declare that the matter embodied in the thesis entitled: “Cadmium Selenide Based Core-Shell Quantum Dots for Biosensing and Imaging Applications” is the result of investigations carried out by me at the Photosciences and Photonics, Chemical Sciences and Technology division of the National Institute for Interdisciplinary Science and Technology (NIIST), (formerly, Regional Research Laboratory, RRL), CSIR, Trivandrum, under the supervision of Dr. K. George Thomas and the same has not been submitted elsewhere for any degree.

In keeping with the general practice of reporting scientific observations, due acknowledgement has been made wherever the work described is based on the findings of other investigators. Any omission that might have occurred due to oversight or error in judgment is deeply regretted.



May 11, 2009

Vinayakan R.

NATIONAL INSTITUTE FOR INTERDISCIPLINARY SCIENCE AND TECHNOLOGY



(Formerly Regional Research Laboratory)
Council of Scientific & Industrial Research (CSIR)
Industrial Estate P.O., Trivandrum - 695019
Kerala, India.



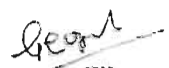
Dr. K. George Thomas, FASc.
Scientist E II
E-mail: kgt@vsnl.com

Tel : 0471 2515364
Fax: 0471 2490186

May 11, 2009

CERTIFICATE

This is to certify that the work embodied in the thesis entitled: "Cadmium Selenide Based Core-Shell Quantum Dots for Biosensing and Imaging Applications" has been carried out by Mr. Vinayakan R., under my supervision and the same has not been submitted elsewhere for any degree.


K. George Thomas
(Thesis Supervisor)

ACKNOWLEDGEMENTS

First and foremost, I express my deep sense of gratitude to Dr. K. George Thomas, my thesis supervisor, for extending me a strong hand into the fascinating world of research, suggesting the problem and in giving all freedom, leading to the successful completion of this work.

I would like to express my sincere thanks to Professor M. V. George, for being an inspiring model, through his systematic and prompt approach in addressing various tasks as well as for all his advices and encouragement during my stay in Photosciences and Photonics.

I wish to thank Professor T. K. Chandrashekar, former Director and Dr. B. C. Pai, Director in Charge, National Institute for Interdisciplinary Science and Technology (NIIST), Trivandrum, for allowing me to avail fellowship under UGC scheme and also for providing basic amenities to carry out the research work.

I sincerely thank Prof. P. Ramamurthy, Director, NCUEP, Chennai, Dr. Suresh Das, Head, Chemical Sciences and Technology Division, NIIST, Trivandrum, and Dr. K. R. Gopidas, Scientist, Photosciences and Photonics, NIIST, Trivandrum for their valuable discussions and suggestions, during the different stages of this work.

I thank Dr. D. Ramaiah, Dr. A. Ajayaghosh and Dr. A. Srinivasan, scientists of the Photosciences and Photonics, for all their whole hearted help and support extended to me. I thankfully remember Dr. G. Vijay Nair (former Director, NIIST, Trivandrum) for all his support and advice.

I gratefully acknowledge Dr. Annie John and Ms. Susan, SCTIMST, Trivandrum, for cytotoxicity analysis experiments. I gratefully acknowledge Dr. E. Sreekumar and Dr. T. R. Santhosh Kumar, scientists, RGCB, Trivandrum, for their help in blood serum analysis experiments.

I am deeply indebted to my seniors, Dr. P. K. Sudeep, Dr. Binil Ity Ipe, Dr. P. V. James, Dr. S. T. Shibu Joseph, Mr. K. Yoosaf and in particular to Dr. Mahesh Hariharan for all their affectionate care, support and valuable guidance in stream lining my work to its perfection.

I thankfully remember the selfless support provided by my seniors, Dr. Joshy Joseph, Dr. S. Sumalakshmy, Dr. Bijitha Balan, Dr. V. K. Praveen, Dr. Reji Varghese, Dr. G. Narayan, Dr. E. Arunkumar and Dr. K. T. Arun.

I express my happiness in being with the members of Photosciences and Photonics, especially with Dr. P. Pramod, Mr. A. R. Ramesh, Mr. Pratheesh V Nair, Mr. Jatishkumar, Mr. Jino George, Mr. M. Shanthil and Mr. Anoop Thomas.

I also thank Mr. Sitansh Sharma, Summer Research Fellow, JNCASR, Bangalore and Ms. T. Shanmughapriya, Research Scholar, NCUEP, Chennai, for their valuable help.

I extend my affectionate love to all my friends in this laboratory for all their selfless help and support.

My sincere thanks are also due to:

- *Mr. Robert Philip and Mrs. Sarada Nair of Photosciences and Photonics.*
- *Mrs. Saumini Mathew, Mr. Tirumalai and Mr. Adarsh for NMR Analysis.*
- *Mrs. S. Viji for HRMS Analysis.*
- *Ms. Priya A. Nair for GCMS and IR Analysis.*
- *Dr. U. Shyamaprasad and Mr. P. Guruswamy for XRD Analysis.*
- *Dr. T. Pradeep, IIT, Chennai, Dr. V. S. Prasad and Mr. Narendraraj, NIIST, Trivandrum, for HRTEM Analysis.*
- *Mrs. A. Nesamany and others in the Finance wing of NIIST, Trivandrum for their whole hearted support.*
- *Mr. G. Ramachandran Nair and others in the Stores and Purchase Section of NIIST, Trivandrum for their help.*
- *DRDO and UGC for financial assistance and CSIR, Govt. of India for providing research facilities.*

With immense gratitude, love and respect, I acknowledge, Dr. T. U. Mathai, former Head (Rtd), Department of Chemistry, CMS College, Kottayam, who gave me a chance to pursue Post Graduation in Chemistry, which became the reason to lead a research career in my life. I thankfully remember the whole hearted support given by Mr. James C. Joseph, Lecturer, Department of Chemistry, K. E. College, Mannanam, especially while I was stuck up with the bitter realities in life.

I express my extreme happiness in getting strong support from my family members and friends. Words are not just enough to express my satisfaction in being with my wife, Archana, who stands as the reason for my confidence.

May 11, 2009

Vinayakan R.

CONTENTS

	<i>Page</i>
<i>Statement</i>	<i>iii</i>
<i>Certificate</i>	<i>iv</i>
<i>Acknowledgements</i>	<i>v</i>
<i>Contents</i>	<i>vii</i>
<i>Preface</i>	<i>x</i>
Chapter 1: Quantum Dots (QDs): An Overview	
1.1. Introduction to Nanoscience and Nanotechnology	1
1.2. Quantum Dots: An Overview	4
1.3. Quantum Confinement Effect	6
1.3.1. Quantum Confinement Effect: Theoretical Predictions	11
1.4. Synthesis of Quantum Dots	19
1.4.1. Epitaxial Growth Method	20
1.4.2. Chemical Methods	22
1.5. Characterization of Quantum Dots	26
1.5.1. UV-Vis Spectroscopy	26
1.5.2. X-ray Diffraction (XRD)	27
1.5.3. Electron Microscopy	27
1.5.4. Energy Dispersive X-ray Spectroscopy (EDS)	29
1.6. Exciton Dynamics and Optical Properties of Quantum Dots	29
1.7. Quantum Dots: Applications in Modern Technology	31
1.8. Focus of the Current Work	33
1.9. References	34

Chapter 2: Optimization of the Shell Thickness of CdSe-ZnS Core-Shell Quantum Dots

	Abstract	39
2.1.	Introduction	40
2.2.	Results and Discussion	44
2.2.1.	Characterization of CdSe and CdSe-ZnS Quantum Dots	44
2.2.2.	Effect of Electron Donors	52
2.2.3.	Optimization of Shell Thickness	57
2.3.	Conclusions	64
2.4.	Experimental Section	65
2.5.	References	68

Chapter 3: Silica Overcoated CdSe Quantum Dots for Biological Applications

	Abstract	72
3.1.	Introduction	73
3.1.1.	Toxicological Effects of Quantum Dots	74
3.1.2.	Synthesis of Water Soluble Quantum Dots	75
3.1.3.	Quantum Dots for Multiphoton Fluorescence Imaging	76
3.2.	Results and Discussion	78
3.2.1.	Overcoating CdSe Quantum Dots with Silica	78
3.2.2.	<i>In Vitro</i> Cell Cytotoxicity Studies	86
3.2.3.	Two-Photon Absorption Studies	88
3.3.	Conclusions	93
3.4.	Experimental Section	93
3.5.	References	96

Chapter 4: Silica Overcoated CdSe Quantum Dots as Sensors

	Abstract	100
4.1.	Introduction	101
4.2.	Detection of Sulfhydryl Containing Biomolecules	104
4.2.1.	Results and Discussion	105
4.3.	Selective Detection of Hg^{2+} Using Silanised Quantum Dots	117
4.3.1.	Results and Discussion	117
4.4.	Conclusions	124
4.5	Experimental Section	125
4.6.	References	128
	<i>Appendix</i>	133
	<i>List of Publications</i>	136

PREFACE

Semiconductor materials in its nanoscale dimension possess unique physical and chemical properties. Luminescence properties of semiconductor materials are sensitive to their size and shape; for example, on decreasing the size below the Bohr exciton radius the emission band shifts from 740 nm to 450 nm in the case of spherical CdSe QDs. The tunability of optical properties of QDs, by controlling their physical dimension in nanometer length scale, allows the fabrication of display devices, cascade lasers and light sources of different colors from materials possessing same chemical composition. Recent studies have shown that QD based hybrid systems are useful in the design of photovoltaic devices and in biomedical applications (for e.g., sensing and imaging). The present thesis, entitled "Cadmium Selenide Based Core-Shell Quantum Dots for Biosensing and Imaging Applications" is mainly focused on the synthesis and characterization of CdSe QDs overcoated with different shell materials for various biological and chemical sensing applications. Main objectives of the present investigation are (i) to develop a novel method for the optimization of shell thickness in core-shell QD systems, (ii) to synthesis water soluble QDs for biological applications, and (iii) to develop QD based sensors.

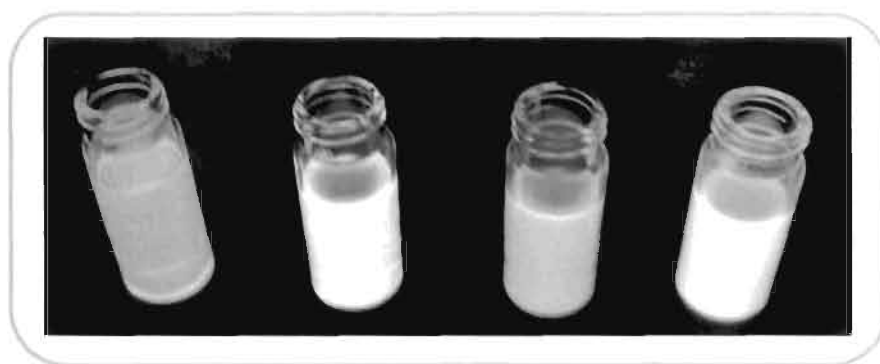
The thesis is divided into four chapters; first chapter provides an introduction to the size, shape and composition dependent properties of QDs. A theoretical insight into quantum confinement effect in QDs is also presented. Second chapter presents a novel method based on photoinduced charge transfer process to optimize the shell thickness of CdSe-ZnS core-shell QDs. Spectroscopic investigations indicate that phenothiazine binds to the surface of bare CdSe QDs, resulting in luminescence quenching, by an electron transfer process. Further, experiments with ZnS overcoated CdSe QDs showed that two monolayers of ZnS prevent the electron transfer processes while retaining good luminescence quantum yields. Methodologies presented, based on photoinduced charge transfer process, can provide quantitative information on the optimum shell thickness of core-shell QDs, which can suppress the undesired electron transfer and provide maximum photoluminescence yield.

Synthesis and characterisation of silica overcoated, water soluble CdSe QDs, *in vitro* cytotoxicity analysis, cell imaging and two-photon absorption (TPA) properties are presented in the third chapter. *In vitro* studies using human bone marrow derived mesenchymal stem cells (hMSC) showed that the silanised QDs are cytocompatible at nanomolar levels. Use of silanised QDs in cell imaging is also illustrated. Multiphoton absorption studies showed that silanised QDs possess improved two-photon absorption characteristics in aqueous media, which makes them an excellent candidate for biological labeling, imaging and sensing applications.

Final chapter demonstrates the use of silica overcoated CdSe QDs in the selective detection and quantification of (i) biologically important molecules under physiologically relevant conditions and (ii) trace quantities of Hg^{2+} ions in the presence of interfering metal ions. Amino acids and peptides containing free sulphydryl group (cysteine, homocysteine and glutathione) selectively quenches the luminescence of silica overcoated CdSe QDs by an electron transfer process. In contrast, molecules which possess disulphide linkage (e.g. cystine) or thiol derivatives (e.g. methionine) did not influence the luminescence of silica overcoated CdSe QDs. The ability of this core-shell nanohybrid system to selectively detect free thiols in the presence disulphides have been explored and further utilized for the selective detection of total free thiol content in human blood serum samples. Among various metal ions, Hg^{2+} selectively quenches the emission of silanised QDs in aqueous medium with a concomitant bathochromic shift in the absorption and emission bands. These changes are attributed to the modification of the electronic structure of CdSe QDs due to the surface reconstruction; mercuric ion react with CdSe to yield quantum sized HgSe on QD surface. This extremely elegant fluorimetric method, based on silica overcoated CdSe QDs allows the detection of biomolecules at physiologically relevant conditions and mercuric ions without the aid of any specialized instruments.

CHAPTER 1

QUANTUM DOTS (QDs): AN OVERVIEW



CdSe QDs of different size under UV excitation

1.1. Introduction to Nanoscience and Nanotechnology

Nanoscience and Nanotechnology deals with the engineering of materials by controlling their size and shape in the nanoscale size regime ($1 \text{ nm} = 10^{-9} \text{ m}$). A comparison of the size domains of various naturally existing and man made systems is presented in Figure 1.1. By definition, nanoscience is the study of phenomena and manipulation of materials in the nanometer scale wherein their properties differ significantly from that of bulk.¹ The word 'nano' is originated from the Greek "νᾶνος", meaning 'dwarf' and it was Lohmann who used the prefix 'nano' for the first time in 1908, to address small organisms having size in the order of $\sim 200 \text{ nm}$ scale.² The visionary idea of controlling matter in the nanoscale regime was proposed by Nobel laureate Richard P. Feynman, in his famous lecture entitled "There's Plenty of

Room at the Bottom”, delivered at California Institute of Technology, in 1959.³ In this talk, he outlined the theoretical concept of manipulating matter in the atomic/molecular level and the potential applications of nanoscale systems. Fifteen years later, Aviram and co-workers proposed single molecular electronic device based on donor π and acceptor π system, separated by a methylene bridge (molecular rectifiers).⁴ In the same year, Norio Taniguchi proposed the term ‘Nanotechnology’, as a successor of microtechnology.⁵ Theoretical concepts developed in the early years highlighted the need for precise control of matter in the nanoscale, however the nonavailability of instrumental techniques for their characterization was a major limitation.

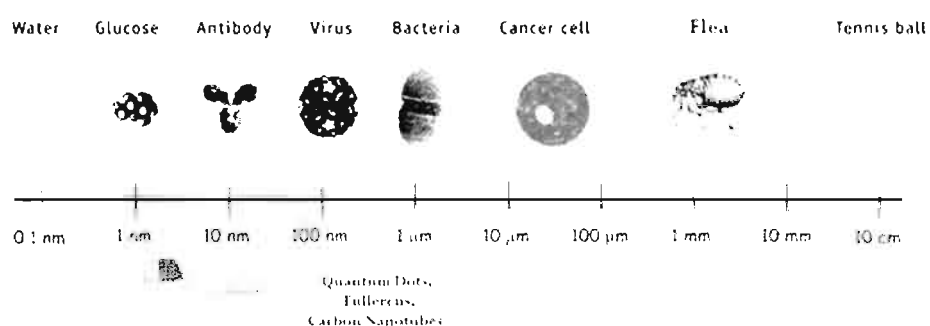


Figure 1.1. Comparison of the size domains of naturally existing and man-made systems.

Nanomaterials can be generally classified as organic, inorganic and organic-inorganic hybrid systems. Among various inorganic nanomaterials, semiconductor and metal nanoparticles have gained interest in last two decades due to their unique optical and electronic properties, governed not

only by its composition, but also by size and shape.⁶ Metal nanoparticles in its colloidal state have attracted mankind even centuries ago; the medicinal value of metal nanoparticle in its colloidal state have attracted the civilization in east, which is well documented in books of ancient Indian Ayurveda like 'Charaka Samhita' and Vedas.⁷ Metal nanoparticles have been used for decorating glass windows (stained glass windows) in many ancient cathedrals in Europe.^{8a} Another example is famous Lycurgus cup of the 4th century, which is now displayed in British museum.^{8b} This glass cup is embedded with a small quantity of an alloy of gold and silver having a diameter of ~70 nm in the molar ratio of (3:7). Interestingly, the glass cup appears green when viewed in reflected light and transmits red colour when illuminated from inside. Today, we attribute the special color display in Lycurgus cup to surface plasmon resonance of the alloy. The first systematic documentation on the synthesis of nanomaterials was reported by Michael Faraday in 1857.^{9a} On reducing sodium tetrachloroaurate ($\text{Na}[\text{AuCl}_4]$) with a solution of phosphorous in carbon disulphide, a deep ruby coloured solution was obtained which he attributed as 'finely divided metal'. Recent developments in the classical wet chemistry methods have enabled the synthesis of various metal nanoparticles and their alloys by controlling their size and shape.^{9b} Further, various functional properties of metal nanoparticles were correlated with the size as well as shape and these aspects are well documented.^{9c,d} Excellent research on the synthesis and study of colloidal semiconductor has

been carried out by Henglein and coworkers and these aspects were summarized in an earlier review.¹⁰ Theoretical insight on the tunable absorption and emission properties of semiconductor nanoparticles, when the size is brought below the Bohr Exciton radius, was provided by Louis Brus in 1984.¹¹ Later several experimental methods have been developed for the synthesis of semiconductor nanoparticles and a brief overview is summarized in the following section.

1.2. Quantum Dots: An Overview

Quantum Dots (QDs) form an important class of low dimensional structures with size, shape and composition dependent physical as well as chemical properties.¹² Photoexcitation of a bulk semiconductor results in the formation of a bound electron-hole pair, called 'exciton', through the transfer of an electron from valence band to conduction band. The freedom of charge carrier motion is completely restricted when all the three dimensions of the material are confined in nanometer length scale (for example, excitons in semiconductors when confined below the exciton Bohr radius). Such materials are termed as quantum dots (QDs) or zero-dimensional materials (0D).^{12c} One-dimensional (1D) semiconductor nanostructures can be obtained by confining two of the dimensions of a semiconductor material below the Bohr exciton radius and quantum rods or quantum wires are the best examples. Further, a (2D) quantum well structure is obtained by limiting quantum confinement in one of its dimensions i.e., only one dimension of the

material is in nanoscale regime. The extent of confinement of charge carrier motion results in the change in electronic energy levels as illustrated in Figure 1.2: the continuum in case of bulk semiconductor material was transformed to discrete atomic like energy levels due to quantum confinement, with a concomitant increase in the lowest energy states.

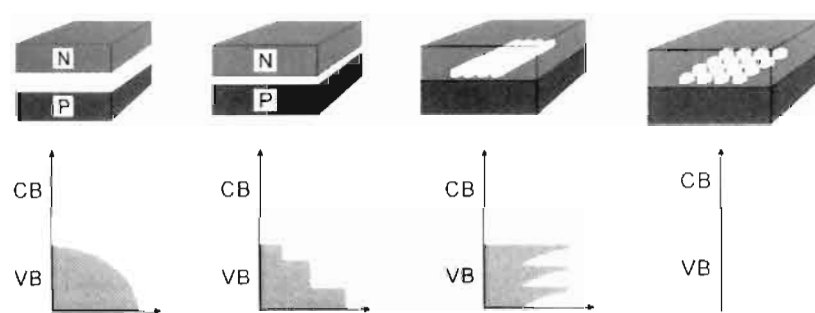


Figure 1.2. Schematic diagram of the density of states (DOS) in semiconductor structures; from left, bulk material, quantum well, quantum wire/rod, quantum dot array with quantum confinement in 0D, 1D, 2D and 3D respectively (*adapted from reference 12d*).

A reduction in size of a material leads to an increase in the surface area per unit volume as schematically shown in Figure 1.3. In QDs, significant percentage of atoms are occupied at the surface. For example, a 2.1 nm size CdSe QD contains ~1400 atoms of which 25 % lie on the surface and most of them possess dangling bonds.^{12c} Surface environment of semiconductor nanoparticle plays a key role in dictating its properties. Thus, the unique properties of QDs originate mainly from two factors: large surface to volume ratio and the spatial confinement of charge carriers, called as quantum

confinement effect or quantum size effect.^{12d} These aspects are discussed in the forthcoming sections.

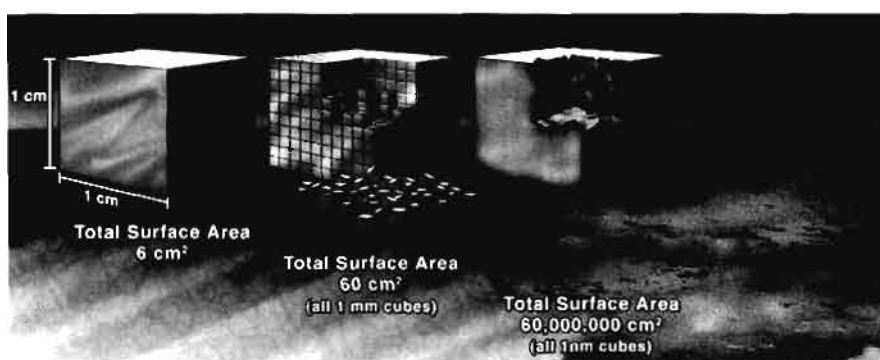


Figure 1.3. A simple thought experiment showing why nanoparticles have such phenomenal surface area per unit volume (*adapted from reference 12c*).

1.3. Quantum Confinement Effect

The physical and chemical properties of a material are directly related to the type of the charge carrier motion as well as the space in which their motion is confined.¹³ For example, the energy levels of an electron are not quantized until it is bound to an atom, molecule or a material. Once bound, their motion becomes highly confined in a potential well and quantization sets in, resulting in quantized energy levels. The extent of confinement is directly related to the spatial freedom allowed for electron movement: smaller the space in which the bound motion takes place, stronger the confinement and larger will be the energy separation between the allowed energies levels. The nuclear confinement is the strongest type of confinement as the motion of the nucleons is confined to a femtometer size scale. This is followed by electronic

confinement in atoms. For example, in hydrogen atom the electron is confined to a length scale of ~ 50 pm.⁶

The spatial restriction in the motion of charge carriers in metals or semiconductors can be brought about by reducing the physical dimension of matter to nanometer size regime. In the case of semiconductors, a reduction in the size to nanometer length scale of ~ 10 nm results in the (i) splitting of energy levels of valance band and conduction band to discrete quantized atomic like energy levels and (ii) an increase in the band gap energy. This phenomenon is explained on the basis of quantum confinement effect.¹³ Both these effects are directly observable in the electronic absorption and emission spectra of direct band gap semiconductor nanoparticles, which is illustrated by considering cadmium sulphide as a typical example.

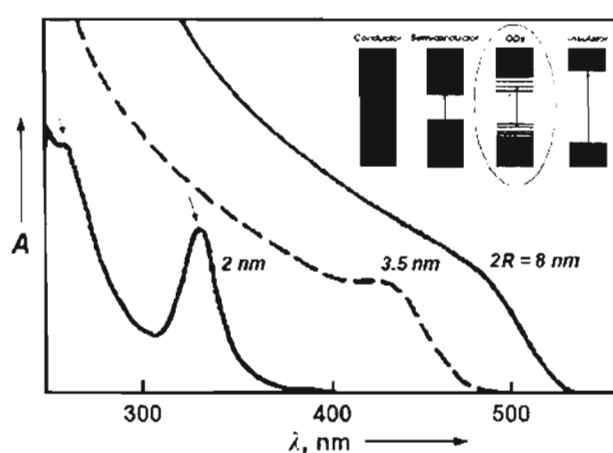


Figure 1.4. Quantum confinement effect in the electronic absorption spectrum of CdS QDs of different sizes. (inset) A comparison of energy states while moving from a metal to an insulator (*adapted from reference 14a*).

Macrocrystalline CdS has an absorption onset at 515 nm, corresponding to bandgap energy of 2.58 eV; a hypsochromic shift in the absorption band was observed when its size is decreased to a nanoscale dimension (Figure 1.4).^{14a} The absorption spectrum of CdS QDs having 8 nm size showed a considerable blue shift in absorption onset with evolution of a shoulder, close to 500 nm. These changes can be ascribed to an increase in bandgap energy as well as to the replacement of continuous energy levels with quantized states. The small hump in the absorption trace represents the lowest optical transition or first excitonic transition ($1S_h - 1S_e$), as schematically represented (dotted arrow) in the inset of Figure 1.4. The effects due to spatial confinement of charge carriers in QDs are more pronounced with further reduction in physical dimension. On decreasing the CdS QD size to 3.5 and 2 nm, the absorption onset showed considerable blue shift with evolution of sharp first and second excitonic transition in the absorption profile (Figure 1.4).

Cadmium selenide (CdSe) QDs are another important class of semiconductor nanomaterial wherein the quantum size effect on the optical properties as a function of size is well explored (Figure 1.5).^{14b} The absorbance as well as photoluminescence of CdSe is tuned from around 700 to 450 nm, covering the entire visible spectral window, just by controlling the size in the range of 6 to 2 nm. In summary, semiconductor nanomaterial having same chemical composition can emit light through out the visible

region by inducing quantum confinement effects, i.e., just by controlling the physical dimension in nanometer length scale.

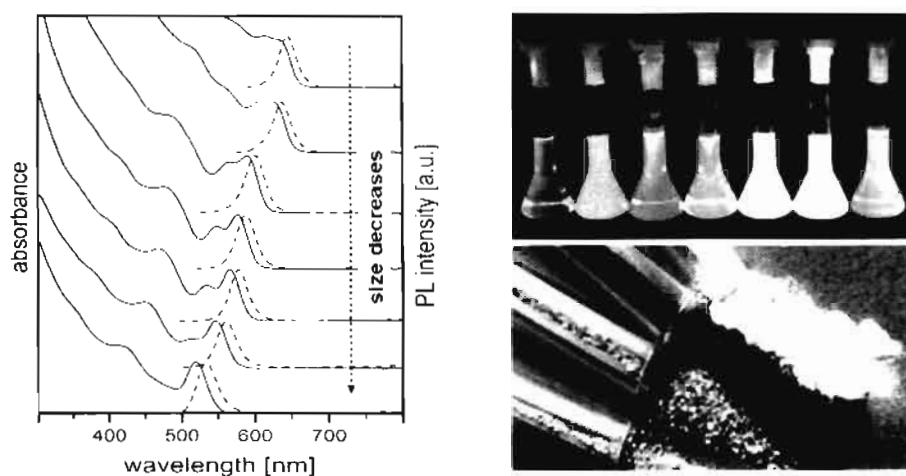


Figure 1.5. (left) Absorption (solid trace) and emission spectra (dotted trace) of CdSe QDs, as a function of size. (right) Photoluminescence from CdSe QDs in solution and in powder form: A visual evidence of quantum confinement effect in CdSe QDs (adapted from reference 14b).

Many other properties of semiconductor nanomaterials such as oscillator strength, intraband transitions, exciton binding energy, redox potential of the conduction band edge and valence band edge, dielectric constant and (one and two-photon) absorption cross section are dependent on their physical dimension.^{11,13} For example, oscillator strength accounts for the probability of the lowest energy electronic transition, which depends on the joint density of states of energy levels in the conduction and valence band wherein the optical transition occurs. Further more, it also depends on the extent of overlap of the envelope wave functions of electrons and holes. Both these factors produce a large enhancement in the oscillator strength as a

function of quantum confinement experienced in the system. Indirect band gap semiconductors are known to be poor light emitters since optical transition in these systems require a change in momentum and thus involves phonon contribution. However, the momentum selection rule is not involved in the quantum confined structures, allowing radiative recombination of excitons. For example, in contrast to silicon (an indirect bandgap semiconductor), silicon QDs show size dependent photoluminescence with high quantum yield.¹⁵

The intraband transitions, i.e., electron-hole transition within the conduction band and valence band are also influenced by quantum size effect. In bulk, these processes require a change in momentum and thus become a phonon assisted process. Hence, the intraband transitions are weak in bulk compared to interband transitions, as the latter requires little change in momentum during electronic transition. In the nanoscale regime, the quantum confinement relaxes the selection rule and electron can jump from one sublevel to another without changing the momentum, allowing the new transitions in the IR region. This process has been utilized to produce quantum cascade lasers and detectors based on quantum confined heterostructures.^{13a} Similarly, the exciton binding energy is enhanced due to quantum confinement effect in nanostructures compared to that of bulk. Also, the redox potential of the conduction band and valence band are also sensitive

to size of the QDs which shifts to more positive values for valence band and negative values for conduction band with decrease in the size of QDs.¹⁶

1.3.1. Quantum Confinement Effect: Theoretical Predictions

Semiconductors are characterized by their well separated, continuous energy levels labeled as conduction band and valence band with an energy gap in the order of few electron volts (< 5 eV). As mentioned earlier, promotion of an electron from the valence band to the conduction band by external stimuli such as photons creates a bound electron-hole pair called as exciton.¹⁷ Minimum energy required to generate an exciton in a semiconductor material is known as the bandgap energy (E_g). The electron and hole in such an exciton is weakly bound (Wannier-Mot type), due to the larger distance and high dielectric constant of the medium. For example, the exciton binding energy in the case of cadmium sulphide (CdS) is 0.05 eV and the charge carriers are separated by 2.5 nm. In contrast, the electron-hole pair formed in an organic insulator (Frenkel exciton), is tightly bound in the same lattice site within a small radius (exciton binding energy in the order of 0.1-1 eV). These systems can be compared with hydrogen atom wherein the exciton binding energy is 13.5 eV and the charge carriers are separated by 0.053 nm. The small binding energy observed in semiconductor offers a very rapid dissociation of excitons into free charge carriers which results in electrical conductivity in semiconductors. This 'quasiparticle' (i.e., exciton) can be

treated as hydrogen like system and energy (E_n) associated with the spatially confined system can be deduced from Bohr approximation as follows;^{13a}

$$E_n(k) = E_g - R_y/n^2 + (\hbar^2 k^2)/2m \quad (1.1)$$

In the above expression, ' R_y ' represents the exciton Rydberg energy, which is an estimation of electron hole binding energy, ' \hbar ' denotes $(h/2\pi)$ where ' h ' is the Plank's constant, ' k ' is the wave vector for exciton (regarded as zero for optically generated excitons) and ' m ' stands for mass of electron. The Rydberg energy is given by the expression 1.2,

$$R_y = e^2/2\epsilon a_B \quad (1.2)$$

where ' e ' stands for electron charge, ' ϵ ' for permittivity and ' a_B ' for the distance separating an electron and hole in an exciton, termed as exciton Bohr radius. This is an intrinsic parameter for a particular material, given by the expression 1.3;

$$a_B = \epsilon \hbar^2 / \mu e^2 \quad (1.3)$$

where ' μ ' represents the reduced electron-hole mass expressed as,

$$\mu = 1/(1/m_e^* + 1/m_h^*) \quad (1.4)$$

where m_e^* and m_h^* are effective mass of electron in conduction band and that of hole in valance band, respectively. The exciton Bohr radius for various semiconductor materials is listed Table 1.1, which can be approximately deduced in the order of few nanometers ($\sim 1-10$ nm).

According to the quantum confinement theory, electrons in the conduction band and holes in the valence band are confined spatially by the

potential barrier of the surface when the size of the material is comparable to its exciton Bohr diameter. Due to the confinement of both electrons and holes, the lowest energy optical transition from the valence band to the conduction band shows an increase in energy, effectively increasing the band gap. The extent of quantum confinement depends on the relative physical size of material and its exciton Bohr size.¹⁸ When the physical dimension is slightly larger than the exciton Bohr diameter, it results in a weak confinement. A strong confinement is experienced when the physical size is comparable or substantially smaller than the exciton Bohr diameter.

Various theoretical approaches have been reported to predict the basic principles governing the relationship between the size of semiconductor nanoparticle and their band gap, band structure, exciton energies and other parameters. All efforts are based on a quantum mechanical point of view, in which QDs can be treated as a “particle-in-a-box” type system where the energy of the particle is a function of box dimension. The first experimental evidence for the quantum confinement in clusters came from the findings by Ekimov and Onushchenko in case of CuCl clusters having a size of 3 nm.^{20a} Authors observed a blue shift (0.1 eV) in the excitonic absorption as a function of decrease in cluster size. A qualitative theoretical analysis of this confinement effect on the bandgap energy was put forward by Efros and Efros utilizing particle in a sphere and effective mass models as expressed below:^{20b}

$$E_g(R) = E_g(\infty) + (\hbar^2 \pi^2) / 2\mu R^2 \quad (1.5)$$

where ' $E_g(R)$ ' and ' $E_g(\infty)$ ' represent the band gap energy of the cluster as a function of cluster radius ' R ', and that of bulk, respectively.

Henglein reported a similar size dependent shift in the absorption spectrum in case of CdS and ZnS colloidal solutions.^{20c} The theoretical model proposed in case of CuCl cluster was quite elementary; it ignored many important factors including the electron-hole coulombic interactions and used infinite potential wells. Using the widely accepted effective mass model (EMM), a more reliable theoretical approximation was reported by Brus in 1984, describing the size dependent optical properties of CdS QDs.²¹ In this model, Brus retained the effective mass model approximation and incorporated a new potential energy term related to dielectric polarization to account for the coulomb effects. These aspects are explained as follows.

Absorption of light creates an electron-hole pair which interacts with the lattice, as well as with each other. The strong coupling of electron and hole with the periodic potential of the lattice makes them to behave as “pseudoparticles” with an ‘effective mass’ m_e^* and m_h^* respectively (the ratio of the mass of the electron and hole in a semiconductor to the mass of the electron in vacuum; often smaller than their free masses). Effective masses of charge carriers for a few semiconductor materials are provided in Table 1.1.

Table 1.1. Physical constants for some semiconductor materials.¹³

Material	Eg, eV	aB, nm	m _e [*]	m _h [*]
CdS	2.58	2.8	0.19	0.80
CdSe	1.89	4.9	0.13	0.80
CdTe	1.50	7.5	0.11	0.35
GaAs	1.42	12.5	0.07	0.68
GaN	3.42	2.8	0.20	0.8
Si	1.11	4.3	0.9	0.52

This forms the basis of EMM approximation and mathematically represented as follows (equation 1.6);

$$E_g(QD) = E_g(bulk) + (\hbar^2 \pi^2 / 2 \mu R^2) - (1.786 / \epsilon R) \tag{1.6}$$

This simple approximation, which correlates the bandgap energy and QD size contains two size dependent terms. An additive term for the kinetic energy gained for exciton by quantum confinement effect with $1/R^2$ dependence on E_g and a subtractive term for the columbic interaction (V_{Coul}) with a $1/R$ dependence, which accounts for the mutual attraction between electron and hole in an exciton. Quantum confinement effect becomes prominent in case of very small QD sizes since the additive term has $1/R^2$ dependence. For QDs having larger size, the theoretical model predicted showed good agreement with the experimental data, however deviations were observed for smaller QDs due to strong quantum confinement effects. Some of the basic assumptions used such as (i) the electron and hole in exciton are

uncorrelated, (ii) use of infinite potential well, (iii) considering QDs as spherically symmetric entity, (iv) ignoring the coupling of electronic states with vibrational levels are responsible for the deviation observed for smaller QDs.

Brus model was further modified keeping effective mass approximation, and by introducing more parameters. The electron-hole spatial correlation effect was accounted by Kayanuma and modified the Brus equation as follows (equation 1.7);²²

$$E_g(\text{QD}) = E_g(\text{bulk}) + (\hbar^2 \pi^2 / 2\mu R^2) - (1.786/\epsilon R) - (0.248 E_{\text{Ry}}) \quad (1.7)$$

Weller and coworkers introduced finite well depth conditions to confine exciton and accounted for the size dependence of the energy values for higher excited states.^{23a} Later, Nosaka used particle-in-a-box finite depth spherical well model calculation for semiconductor nanoparticle.^{23b} However, none of these improvisations were fully successful in correlating theory and experiment in the case of strongly quantum confined structures.

A different treatment, deviating from the effective mass approximation was introduced by Wang and coworkers (PbS, CdS) and Lippens and coworkers (CdS and ZnS), using a molecular orbital calculation method named as Tight Binding Hamiltonian (TBH).²⁴ Rama Krishna and coworkers came up with a more precise model named 'empirical pseudopotential method' (EPM),²⁵ incorporating more parameters related to surface effects, lattice structure, lattice constants, cluster shape etc. The results were in good

agreement with that of experimental data, especially for small sized clusters where strong quantum confinement exists. Comparison between experimental data and various theoretical models is illustrated in Figure 1.6.

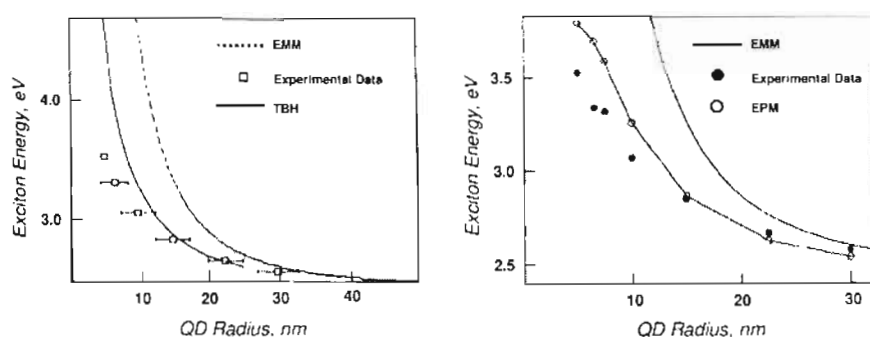


Figure 1.6. A comparison of experimental and calculated data (based on effective mass model (EMM), empirical pseudopotential model (EPM) and tight binding hamiltonian (TBH)) for the dependence of the optical bandgap (exciton energy) on the cluster size for CdS clusters (*adapted from references 24 and 25*).

Many efforts have been reported to improve the above discussed theoretical models, adaptable for any QD system irrespective of their composition and size range, to fit with experimental data. Generally, all these are by incorporating more complex functions, different potential barrier heights etc., which essentially makes calculations more complicated and time consuming. For example, conventional EPM was modified by Zunger and coworkers as semiempirical pseudopotential method (SEPM) by introducing local density approximation (LDA),^{26a} while Kim and coworkers used plane wave pseudopotential approach which includes spin-orbit coupling, screened electron-hole coulomb interactions, and exchange interactions.^{26b} Recently

Wang *et al.* used a charge patching method, with advantages over EPM to compare the quantum confinement effect in zero and one dimensional nanostructures.²⁷ Though there were many drawbacks, modified forms of EMM are still used, owing to the simplicity and speed in calculations. A couple of recent variants of this method include multiband EMM by Efros *et al.* and EMA-TBH combination by Carceller *et al.*²⁸ In latter approach, introduced for silicon QDs, features of tight binding method was adopted to improve precision of EMA calculations.

A physical picture of size effects in QDs can be understood from the electronic structure of semiconductors in the atomic, molecular and bulk size domains.^{11,13b,19} The basic building blocks of matter are atoms, which constitutes electrons orbiting around atom nucleus. The individual path of an electron is designated as atomic orbital (AO) with an associated discrete or quantized energy levels. A combination of several atoms generate molecule, where electrons orbit collectively around more than one nucleus. Thus the AOs are shared between atoms, and labeled as molecular orbitals (MOs), which still have atomic like discrete energy levels. When atoms combine to generate crystalline solids (e.g. silicon atoms to give crystalline silicon), the electronic structure can be described in terms of a periodic combination of atomic orbitals. Compared to atoms or molecules, the electronic structure of the solid no longer consists of discrete energy levels, in contrast they form broad, continuous energy levels, called as energy bands (This is illustrated in

Figure 1.7. with Si as an example). The intermediate size regime of nanometer scale exists between molecules having discrete energy levels and a bulk solid having energy bands. The concept of energy bands are retained in this size regime with discrete energy levels in band edges. The bandgap energy in the case of nanomaterials is not identical with bulk matter and depends on the size and in turn the number of atoms present.

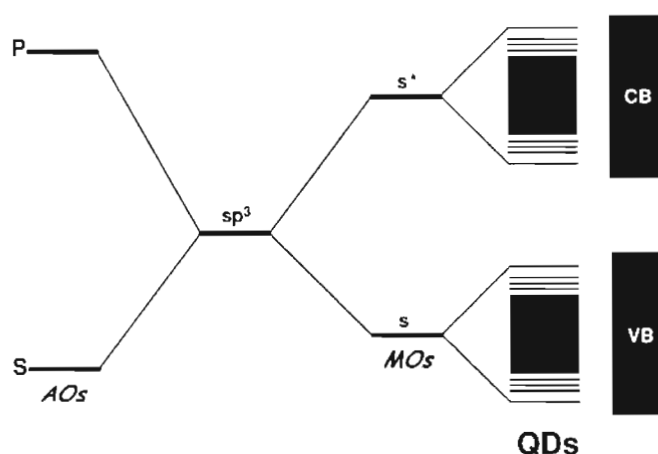


Figure 1.7. Comparison of electronic energy levels for atoms, molecules (with discrete, quantized energy levels) and semiconductors. QDs fall in between molecules and bulk semiconductors, with discrete energy levels at the band edges (adapted from reference 13b).

1.4. Synthesis of Quantum Dots

An ideal strategy for the synthesis of semiconductor nanoparticle should have the following characteristics: (i) control on the size and shape, (ii) high monodispersity and good crystallinity, (iii) high luminescence quantum yield and (iv) reproducibility. Two different methods adopted for the synthesis of nanocrystals include “top-down” and “bottom-up” approaches. In the “top-down” approach, bulk

crystal is crushed down mechanically to nanoscale size regime using various physical methods. In “bottom-up” approach, the constituent ions or molecules are grown atom by atom to nanocrystal of desired shape and size using solution-phase colloidal chemistry. A brief summary of various methods adopted for the synthesis of semiconductor QDs is given below.

1.4.1. Epitaxial Growth Method

The simplest way of producing quantum dots is directly generating semiconductor particles in gaseous or liquid phase, followed by their controlled condensation as nanoparticles. Again, the crystallinity and morphology of the resulting nanostructures can be guided by using templates or substrates on which the condensation is performed. This type of growth is called ‘epitaxial growth’, where the substrate (the template) and the growing semiconductor layer are having matching crystal lattice parameters. Various epitaxial methods employed for QD synthesis are briefly discussed below.¹³

In molecular beam epitaxy (MBE), the growth is performed in a vacuum chamber wherein the precursors in its elemental or homoatomic form are vaporized into a ‘molecular beam’ and deposited on a substrate (Figure 1.8.). MBE chamber incorporates *in situ* characterisation techniques such as reflection high-energy electron diffraction (RHEED), which allows the real time monitoring of crystallinity and morphology of the growing layer. When the precursor is in the form of a metal-organic complex, it is called metal-organic chemical vapor deposition method (MOCVD) or as metal-organic vapor-phase epitaxy (MOVPE). This method is

simple and offers higher growth rate, but lacks real time characterisation as in the case of MBE. A combination of MBE and MOCVD offers another technique called as chemical beam epitaxy (CBE) where metal organic precursors are used. The reaction is performed in vacuum, which offers advantages of both the parent methods. When high deposition rate and high crystallinity are requisites, liquid phase epitaxy (LPE) is preferred, where the substrate is brought into contact with a saturated solution of film material at appropriate temperature and duration. Even though this method is cost effective, the surface properties of the nanostructure obtained is of poor quality due to low control over morphology.

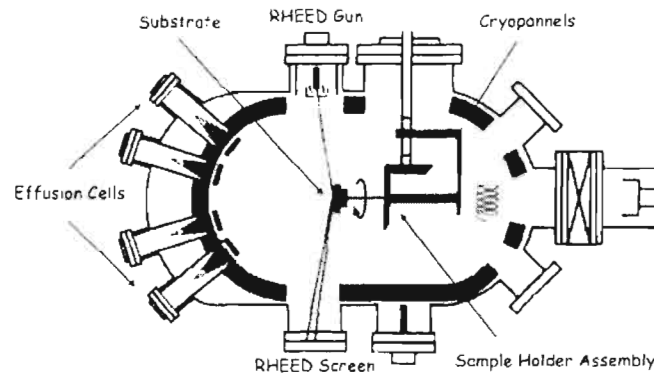


Figure 1.8. Schematic illustration of MBE growth chamber. The precursors are fed through effusion cells and the molecular beam generated is deposited on the substrate (*adapted from reference 13a*).

Another simple method is to use a laser beam to produce metal/semiconductor vapor, called as laser assisted vapor deposition (LAVD). Laser ablation of a solid target leads to production of ablated materials which can be deposited itself on a substrate or can be directed to substrate with an inert gas flow. This may also be performed in a liquid phase by keeping the material in a solvent.

which contains an appropriate capping agent to protect and stabilize the laser generated nanoparticles. Physical methods are useful in the mass production of nanocrystals, however it lacks control over size, shape and dispersity. In addition, these techniques require sophisticated instrumental set up and skilled manpower which makes it economically unviable.

1.4.2. Chemical Methods

Soft chemistry follows a colloidal synthesis route, a more viable and cost effective approach, that can be performed in any laboratory environment. It offers several advantages over physical methods. Chemical methods allow the preparation of wide range semiconductor nanoparticles and core-shell nanostructures with excellent control over size, shape and dispersity. This method also allows the functionalisation of surfaces of semiconductor nanoparticles with various ligands, and the design of higher order nanostructures through self-assembly.

Colloidal synthesis offers a versatile route, where nanoparticles are grown by chemical reaction of their precursors in an appropriate solvent. It follows the usual nucleation and crystal growth mechanism where the latter process is controlled by the use of an appropriate surfactant or capping agent (sometimes the solvent molecule itself serves as capping agent). Control over the size, shape, dispersity and crystallinity can be achieved by adjusting the reaction conditions such as time, temperature, concentration of the precursor, chemical nature of the capping ligands and surfactants.

The history of colloidal semiconductor synthesis starts in 1980s, with the initial interest of using semiconductors for the splitting of water to produce oxygen and hydrogen simultaneously.^{29a} Earlier attempts to produce extremely small particles include (i) size selective precipitation of dilute colloidal solution and (ii) growing them in confined matrix (templates) such as zeolites, micelles, molecular sieves, polymers, ionomers, hollow biological molecules, lipid bilayers etc (Figure 1.9).^{29b,c,30}

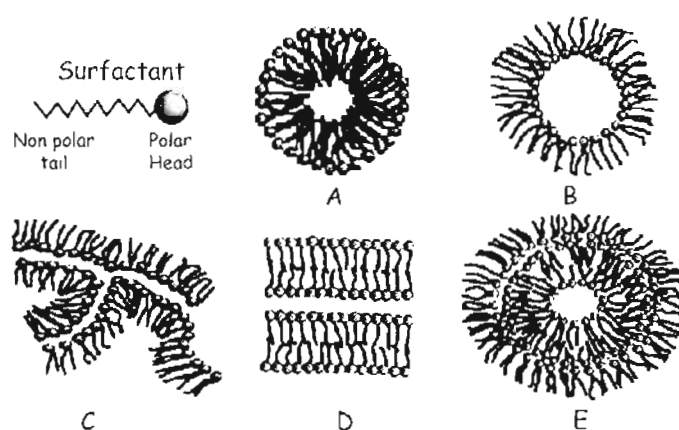


Figure 1.9. Various self-assemblies of surfactant in colloidal solutions resulting in (A) normal micelles (B) reverse micelles (C) interconnected cylinders (D) planar lamellar and (E) onion-like lamellar phase (*adapted from reference 30*).

A break through in producing monodispersed QDs of cadmium chalcogenide such as CdS, CdSe, CdTe, (II-VI semiconductors) was reported by Bawendi and coworkers in 1993.³¹ The authors were able to synthesize highly crystalline QDs using organometallic precursors in the presence of a coordinating solvent, trioctylphosphine oxide (TOPO). The reaction was carried out at elevated temperatures (~360 °C) under vacuum, using selenium

precursor (TOPSe; selenium coordinated to trioctylphosphine) which was injected rapidly into solution of dimethylcadmium in TOPO (Figure 1.10). This resulted in burst nucleation followed by crystal growth leading to formation of crystalline quantum dots. TOPO served as the main capping agent and QDs produced possessed narrow size distribution ($\sigma_r < 10\%$), having excellent solubility in nonpolar solvents. Low surface defects, compared to other synthetic methods is another advantage of the high temperature organometallic synthesis. An excellent control over crystal growth was achieved by controlling the precursor concentration, temperature, reaction duration etc. Further, the organic capping agent, which is electrostatically bound to the QD surface, could be replaced by functionalisation with thiol. It is possible to introduce photoactive or electroactive groups on to the surface of nanoparticle by following this method (place exchange reaction).

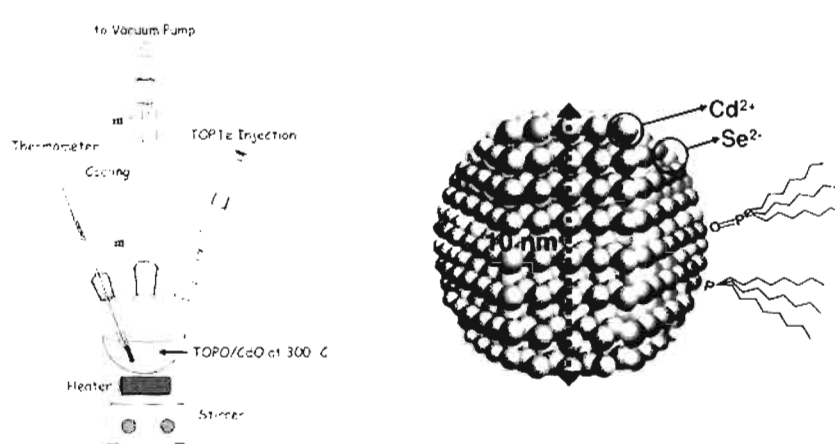


Figure 1.10. Figure presents an experimental set-up for QD synthesis by high temperature organometallic method, along with an schematic illustration of CdSe QD capped with TOPO (bound to Cd^{2+}) and TOP (bound to Se^{2-}) (*adapted from reference 36a*).

Numerous attempts have been made to replace dimethyl cadmium with other organometallic precursors due to its extreme toxicity, pyrophoric nature, expensiveness and instability.^{32a} A marked improvement in the above synthesis strategy was achieved by Peng and coworkers, by using a non-pyrophoric and stable cadmium precursor, cadmium oxide instead of dimethylcadmium. A significant reduction in reaction temperature ($\sim 300^\circ\text{C}$) as well as in size distribution ($\sigma_r < 5\%$) was observed for the resulting nanocrystals (Figure 1.11.). This was attributed to the thermal stability as well as slow decomposition of the cadmium oxide compared to dimethylcadmium, which led to a slow and homogeneous nucleation and crystal growth (avoiding Ostwald's ripening).^{32b}

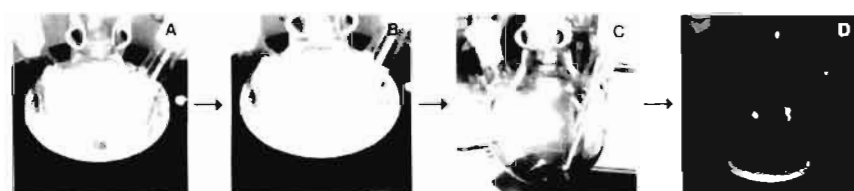


Figure 1.11. Photographs illustrating the various steps in the synthesis of CdSe QDs; (A) commencement of reaction with CdO and TOPO mixture, (B) after selenium injection (at 300°C), (C) after reaction under day light and (D) under UV illumination.

Several other synthesis protocols were reported by varying the cadmium precursor (e.g. cadmium acetate, cadmium stearate), reaction medium (e. g. octadecene, olive oil) and capping agents such as amines, fatty acids, phosphonic acids etc.³³ Design and fabrication of anisotropic

semiconductor nanostructures such as nanorods (quantum rods), nanowires (quantum wires), dipods, tripods and tetrapods have drawn attention in recent years. These nanostructures are having high potential especially in fabricating nanoelectronic, photovoltaic and energy storage devices due to their shape dependent properties. For example, CdSe nanorods possess polarized emission related with their cylindrical symmetry which makes them a novel photonic material (for e.g., laser systems).³⁴ A collection of recent reviews on the synthesis of isotropic and anisotropic semiconductor nanostructures, their characterisation and investigation of their properties are listed in References 35 and 36.

1.5. Characterization of Quantum Dots

A wide range of spectroscopic as well as microscopic techniques are available for the characterisation of semiconductor nanoparticles. A brief description of various techniques used in subsequent chapters for characterization of nanomaterials is discussed below.

1.5.1. UV-Vis Spectroscopy

Among spectroscopic methods, UV-Vis absorption and emission spectroscopy is a very simple technique which is widely used for the preliminary characterisation of QDs. QDs show size dependent absorption and emission spectra and the theoretical determination of its size is possible from these data. For example, the size of CdSe QDs having diameter ' D ' can

be predicted from the corresponding absorption spectrum by using following relationship (1.8), where ' λ_1 ' is the first excitonic absorption maximum.^{37a}

$$D = (1.6 \times 10^{-9})\lambda_1^4 - (2.7 \times 10^{-6})\lambda_1^3 + (1.6 \times 10^{-3})\lambda_1^2 - (0.4)\lambda_1 + 41.5 \quad (1.8)$$

Similarly, stokes shift and the broadness of emission peak (FWHM) is also an indirect measure of the surface imperfections and size distribution of the nanocrystals.³⁷

1.5.2. X-ray Diffraction (XRD)

X-ray diffraction analysis is a versatile tool, which provides information about the size as well as the crystallinity of the nanostructure. The elastic scattering of a beam of monochromatic X-rays (of wavelength ' λ ') by the periodic lattice of the sample can be analyzed based on Bragg's relation. The XRD pattern of the nanoparticles is usually characterized by broad diffraction peak. The width of the diffraction peak (B) at an angle (θ) can be correlated to the size of the material using Debye-Scherrer equation as given below;^{37b}

$$\text{Particle size (D)} = 0.90\lambda/B\cos\theta \quad (1.9)$$

1.5.3. Electron Microscopy

Electron microscopy is one of the most powerful microscopic techniques used for characterizing nanomaterials wherein electrons and magnetic lenses are used to image the sample, instead of photons and optical lenses in optical microscope. The maximum theoretical resolution that can be achieved with visible light, based on Abbe's equation, is in the order of 220

nm. There is an obvious advantage in using electron beam for imaging. For example, spatial resolution down to 1 nm can be achieved by using an electron beam accelerated at 100 keV (possesses a wavelength of ~ 370 pm). This forms the basic principle of the various electron microscopic techniques such as scanning electron microscopy (SEM) and transmission electron microscopy (TEM). In the case of TEM, a focused electron beam (1-4 keV) is allowed to interact with the specimen and the transmitted electrons are collected on a fluorescent screen to generate the (2D) images. Typical examples for TEM images for CdSe semiconductor nanoparticles of various shapes are shown in Figure 1.12.

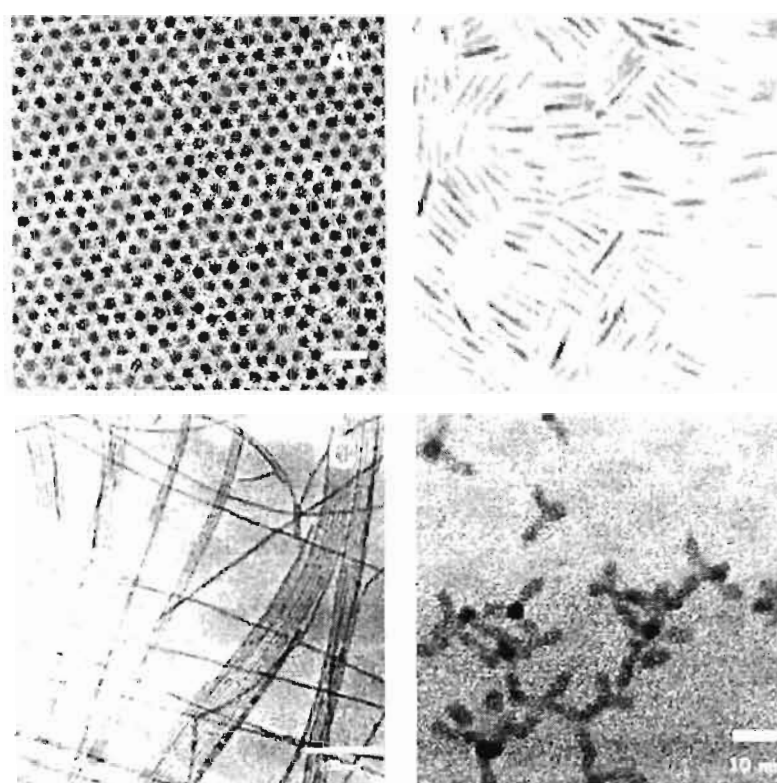


Figure 1.12. Bright field TEM images of CdSe nanocrystals of different shapes: (A) quantum dots, (B) rods (C) wire and (D) tripods (*adapted from reference 36*).

1.5.4. Energy Dispersive X-ray Spectroscopy (EDS)

Energy dispersive X-ray spectroscopy (EDS or EDX) is an electron spectroscopic technique used to explore the chemical composition of the sample. In this technique, an electron beam is allowed to impinge the sample surface leading to the ejection of an electron from the inner shell (e. g., K shell), leaving a vacancy. This vacant space is filled by an electron from an outer higher-energy shell (e. g., L shell) and the difference in energy between the higher and lower energy shell may be released in the form of X-rays ('K α ' emission). The number and the energy of the X-rays emitted from a specimen is the fingerprint of the constituent elements in the sample.

1.6. Exciton Dynamics and Optical Properties of QDs

In semiconductor nanoparticles, excitons could be generated by external stimuli such as, photons (photoluminescence), by injection of an electron-hole pair (electroluminescence), by electron impact (cathodoluminescence) or by chemical reaction (chemiluminescence).³⁸ The study of charge carrier generation as well as their recombination dynamics has received considerable attention in recent years. Issues of interest include multiexciton generation, recombination, trapping, carrier-carrier interaction and their dependence on particle size, shape and surface characteristics. Figure 1.13 illustrates major pathways of charge carrier relaxation for an exciton in QDs.

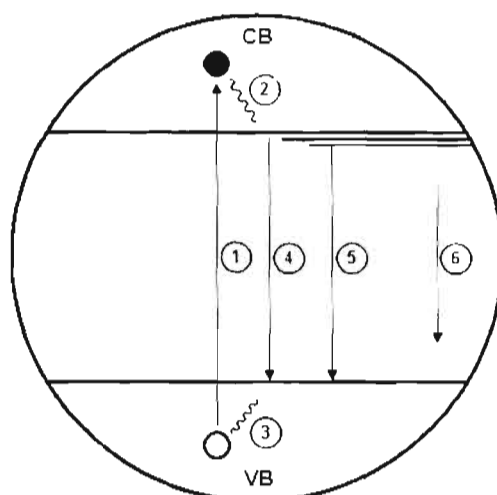


Figure 1.13. Schematic illustration of exciton recombination modes in QDs: (1) Single exciton generation, (2) & (3) electron-hole relaxation, (4) band edge emission, (5) trap state emission and (6) nonradiative recombination.

Excitation of QD with photons of energy higher than its bandgap energy leads to generation of an electron in conduction band and a hole in the valence band. The first step is the relaxation of electron and hole to the conduction band edge and valence band edge, respectively. Due to the interaction of electron/hole and phonon, the energy is released as local lattice vibrations. This process occurs in the time scale of 100 femtoseconds or less. Once the electron is relaxed to the bottom of the conduction band and the hole to the top of the valence band, they can recombine radiatively or nonradiatively. The radiative recombination is called as 'band edge' recombination and the lifetime is in the order of nanoseconds or longer. As in the case of organic fluorophores, QDs show 'Stokes shift' in emission, i.e., a

shift in the emission maximum to longer wavelengths compared to the first excitonic absorption maximum. When lower lying energy levels or 'trap states' are present within the bandgap (due to surface defects, internal defects, unsaturated bonds etc.), the charge carriers are trapped, inhibiting the band edge recombination process. Such trap states can be close to band edges (shallow traps) or away (deep traps), to which exciton migrates at a faster time scale, typically in a few picoseconds. Trapped charge carriers when recombine radiatively, produce trap-state emission (usually broad), considerably red shifted with respect to band edge emission. Depending on the nature of the trap states, the exciton lifetime may vary from nanoseconds to microseconds or even longer.

Other important aspects of charge carrier relaxation in QDs include generation of multiexcitons, luminescence intermittency etc.³⁹ In former process, more than one exciton is generated from a single photon, exceeding quantum efficiency beyond one. Luminescence intermittency originates from the relaxation of a high energy exciton creating another exciton, which follows an auger process, making QD ionized and nonluminescent.

1.7. Quantum Dots: Applications in Modern Technology

The potential applications of semiconductor nanoparticles cover a wide area from production of energy to storage, electronics to photonics, biomedical science to biotechnology and so on. Among these, QD based solar cell systems have received much attention.^{40a} Tunable bandgaps of

semiconductor allows the absorption of the broad spectrum of wavelengths that reach earth and there by fabrication of 'rainbow solar cells' are considered. Another aspect of recent interest is the multiple exciton generation efficiency in quantum dots, which boosts the light harvesting ability in QD based solar cells.^{40b}

Electronics is another field wherein novel materials are required for further miniaturization. QDs possess superior electron transport and optical properties, and they actively considered as elements in diode lasers, amplifiers and light emitters (e.g. Light emitting diodes).^{41a}

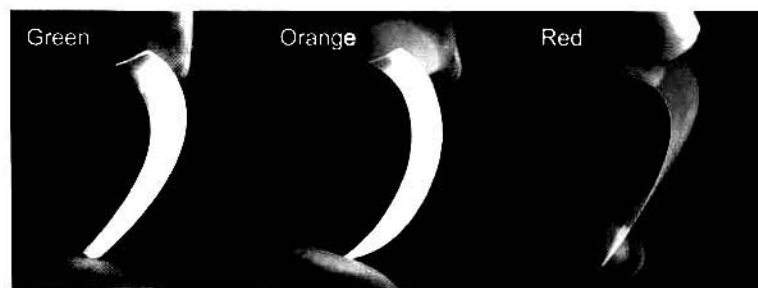


Figure 1.14. Emission from flexible CdSe/ZnS-clay films having nanocrystals of varying size, excited using UV light (adapted from reference 41b).

Emission of QD has specific Gaussian distributions: displays based on these systems can more accurately render the colors that the human eye can perceive (Figure 1.14). Also, QDs require very little power since they are not color filtered. This is an added advantage as in an ordinary liquid crystal display, two-thirds of the light is lost in filters, which are used to produce red, green, and blue pixels.

Another innovative application of QDs is in modern biomedical analysis (cell imaging and targeting, therapeutics) and in the development of novel chemical sensors. The unique physicochemical properties of QDs, coupled with the inherent increase in signal-to-noise ratio makes these systems promising candidates for sensing applications.⁴² A detailed review on the use of QDs as biosensors, exploiting their outstanding properties, is described in Section 4.1.

1.8. Focus of the Current Work

The overall focus of the thesis involves the synthesis and characterization of CdSe QDs overcoated with shell materials for various biological and chemical sensing applications. Second chapter deals with the synthesis and characterization of CdSe and CdSe/ZnS core shell QDs. The primary attention of this work is to develop a simple method based on photoinduced charge transfer to optimize the shell thickness. Synthesis of water soluble CdSe QDs, their cytotoxicity analysis and investigation of nonlinear optical properties form the subject of third chapter. Final chapter deals with development of QD based sensor systems for the selective detection of biologically and environmentally important analytes from aqueous media.

1.9. References

1. Joachim, C. *Nat. Mater.* **2005**, *4*, 107.
2. Lohmann, H. *Weiss. Meeresunters Kiel* **1908**, *10*, 129.
3. Feynman, R. P. *Eng. Sci.* **1960**, *23*, 22.
4. Aviram, A. ; Ratner, M. A. *Chem. Phys. Lett.* **1974**, *29*, 277.
5. Taniguchi, N. *Proc. Int. Congress Proc. Eng. (JSPE, Tokyo)* **1974**, *2*, 18.
6. (a) El-Sayed, M. A. *Acc. Chem. Res.* **2001**, *34*, 257. (b) El-Sayed, M. A. *Acc. Chem. Res.* **2003**, *37*, 326.
7. Mishra, L. C. *Scientific Basics for Indian Ayurvedic Therapies*. CRC Press, **2004**, 560.
8. (a) Hunt, L. B. *Gold Bull.* **1976**, *4*, 134. (b) Barber, D. J.; Freestone, I. C. *Archaeometry* **1990**, *32*, 33.
9. (a) Edwards, P. P.; Thomas, J. M. *Angew. Chem. Int. Ed.* **2007**, *46*, 5480. (b) Grzeleczak, M.; Pérez-Juste, J.; Mulvaney, P.; Liz-Marzán, L. M. *Chem. Soc. Rev.* **2008**, *37*, 1783. (c) Daniel, M.; Astruc, D. *Chem. Rev.* **2004**, *104*, 293. (d) Susie Eustis, S.; El-Sayed, M. A. *Chem. Soc. Rev.* **2006**, *35*, 209.
10. Henglien, A. *Chem. Rev.* **1989**, *89*, 1861.
11. Steigerwald, M. L.; Brus, L. E. *Acc. Chem. Res.* **1990**, *23*, 183.
12. (a) Eychmüller, A. *J. Phys. Chem. B* **2000**, *104*, 6514. (b) Nirmal, M.; Brus, L. E. *Acc. Chem. Res.* **1999**, *32*, 407. (c) Oberdörster, G.; Stone,

- V.; Donaldson, K. *Nanotoxicology* **2007**, *1*, 2. (d) Henini, M. *Materials Today* **2002**, 48. (e) Nirmal, M.; Dabboussi, B. O.; Bawendi, M. G.; Macklin, J. J.; Trautman, J. K.; Harris, T. D.; Brus, L. E. *Nature* **1996**, 383, 802.
13. (a) Prasad, P. N. *Nanophotonics*. Wiley VCH: New Jersey, **2004**. (b) Schmid, G. (Ed.) *Nanoparticles: From Theory to Application*. Wiley VCH: Weinheim, **2004**. (c) Fahlman, B. D. *Materials in Chemistry*. Springer, **2007**. (d) Rao, C. N. R.; Müller, A.; Cheetham, A. K. (Ed.) *Nanomaterials in Chemistry*. Wiley VCH: Weinheim, **2007**.
14. (a) Weller, H. *Angew. Chem. Int. Ed.* **1993**, 32, 41. (b) Talapin, D. V.; Rogach, A. L.; Kornowski, A.; Haase, M.; Weller, H. *Nano Lett.* **2001**, *1*, 207.
15. (a) Service, R. F. *Science* **2009**, 323, 1000. (b) Kim, T.-Y., Park, N.-M.; Kim, K.-H.; Sunga, G. Y.; Ok, Y.-W.; Seong, T.-Y.; Choi, C.-J. *Appl. Phys. Lett.* **2004**, 85, 5355.
16. Guyot-Sionnest, P.; Shim, M.; Matranga, C.; Hines, M. *Phys. Rev. B* **1999**, 60, R2181.
17. (a) Scholes, G. D.; Rumbles, G. *Nat. Mater.* **2006**, 5, 683. (b) Scholes, G. D. *ACS Nano* **2008**, 2, 523.
18. Wise, F. W. *Acc. Chem. Res.* **2000**, 33, 773.
19. Wang, Y.; Herron, N. *J. Phys. Chem.* **1991**, 95, 525.

20. (a) Ekimov, A. I.; Onushchenko, A. A. *JETP Lett.* **1981**, 34, 345. (b) Efros, Al. L.; Efros, A. L. *Sov. Phys. Semicond.* **1982**, 16, 772. (c) Henglein, A. *Pure Appl. Chem.* **1984**, 56, 1215.
21. (a) Brus, L. E. *J. Chem. Phys.* **1984**, 80, 4403. (b) Rossetti, R.; Nakahara, S.; Brus, L. E. *J. Chem. Phys.* **1983**, 79, 1086. (c) Brus, L. E. *J. Chem. Phys.* **1983**, 79, 5566.
22. Kayanuma, Y. *Phys. Rev. B* **1988**, 38, 9797.
23. (a) Weller, H.; Schmidt, H. M.; Koch, U.; Fojtik, A.; Baral, S.; Henglein, A.; Kunath, W.; Weiss, K.; Diemann, E. *Chem. Phys. Lett.* **1986**, 124, 557. (b) Nosaka, Y. *J. Phys. Chem.* **1991**, 95, 5054.
24. (a) Wang, Y.; Herron, N. *Phys. Rev. B* **1990**, 42, 7253. (b) Lippens, P. E.; Lannoo, M. *Phys. Rev. B* **1989**, 39, 10935.
25. Rama Krishna, M. V.; Friesner, R. A. *J. Chem. Phys.* **1991**, 95, 8309.
26. (a) Wang, L.-W.; Zunger, A. *Phys. Rev. B* **1995**, 51, 17398. (b) Zhao, Q.; Graf, P. A.; Jones, W. B.; Franceschetti, A.; Li, J.; Wang.; Kim, K. *Nano Lett.* **2007**, 7, 3274.
27. Li, J.; Wang, L.-W. *Chem. Mater.* **2004**, 16, 4012.
28. (a) Efros, Al. L.; Rosen, M. *Annu. Rev. Mater. Sci.* **2000**, 30, 475. (b) Rodríguez-Bolívar, S.; Gómez-Campos, F. M.; Carceller, J. E. *J. Appl. Phys.* **2008**, 104, 104309.
29. (a) Henglein, A. *Ber. Bunsenges. Phys. Chem.* **1982**, 86, 301. (b) Petit,

- C.; Lixon, P.; Pileni, M. P. *J. Phys. Chem.* **1990**, *94*, 1598. (c) Herron, N.; Wang, Y.; Eddy, M. M.; Stucky, G. D.; Cox, D. E.; Moller, K.; Bein, T. *J. Am. Chem. Soc.* **1989**, *111*, 530.
30. Pileni, M.-P. *Nat. Mater.* **2003**, *2*, 145.
31. Murray, C. B.; Norris, D. J.; Bawendi, M. G. *J. Am. Chem. Soc.* **1993**, *115*, 8706.
32. (a) Hambrock, J.; Birkner, A.; Fischer, R. A. *J. Mater. Chem.* **2001**, *11*, 3197. (b) Peng, Z. A.; Peng, X. *J. Am. Chem. Soc.* **2001**, *123*, 183.
33. (a) Liu, H.; Owen, J. S.; Alivisatos, A. P. *J. Am. Chem. Soc.* **2007**, *129*, 305. (b) Chen, O.; Chen, X.; Yang, Y.; Lynch, J.; Wu, H.; Zhuang, J.; Cao, Y. C. *Angew. Chem.* **2008**, *120*, 8766.
34. Alivisatos, A. P. *Science* **1996**, *271*, 933.
35. (a) Park, J.; Joo, J.; Kwon, S. G.; Jang, Y.; Hyeon T. *Angew. Chem. Int. Ed.* **2007**, *46*, 4630. (b) Rosenthal, S. J.; McBridea, J.; Pennycookc, S. J.; Feldmanb, L. C. *Surf. Sci. Rep.* **2007**, *62*, 111. (c) Masala, O.; Shesadri, R. *Annu. Rev. Mater. Res.* **2004**, *34*, 41. (d) Cushing, B. L.; Kolesnichenko, V. L.; O'Connor, C. J. *Chem. Rev.* **2004**, *104*, 3893.
36. (a) Kuno, M. *Phys. Chem. Chem. Phys.* **2008**, *10*, 620. (b) Burda, C.; Chen, X.; Narayanan, R.; El-Sayed, M. A. *Chem. Rev.* **2005**, *105*, 1025. (c) Peng, X. *Adv. Mater.* **2003**, *15*, 459. (d) Lee, S.-M.; Cho, S.-N.; Cheon, J. *Adv. Mater.* **2003**, *15*, 441.

37. (a) Yu, W. W.; Qu, L.; Guo, W.; Peng, X. *Chem. Mater.* **2003**, *15*, 2854.
(b) Patterson, A. L. *Phys. Rev.* **1939**, *56*, 978.
38. (a) Poznyak, S. K.; Talapin, D. V.; Shevchenko, E. V.; Weller, H. *Nano Lett.* **2004**, *4*, 693. (b) Rodriguez-Viejo, J.; Jensen, K. F.; Mattoussi, H.; Michel, J. *Appl. Phys. Lett.* **1997**, *70*, 2132.
39. (a) Empedocles, S.; Bawendi, M. *Acc. Chem. Res.* **1999**, *32*, 389. (b) Mahler, B.; Spinicelli, P.; Buil, S.; Quelin, X.; Hermier, J.; Dubertret, B. *Nat. Mater.* **2008**, *7*, 659.
40. (a) Sargent, E. H. *Adv. Mater.* **2008**, *20*, 3958. (b) Guyot-Sionnest, P. *Nat. Mater.* **2005**, *4*, 653.
41. (a) Rogach, A. L.; Gaponik N.; Lupton, J. M.; Bertoni, C.; Gallardo, D. E.; Dunn, S.; Pira N, L.; Paderi, M; Repetto, P.; Romanov, S. G.; O'Dwyer, C.; Sotomayor Torres, C. M. S.; Eychmüller, A. *Angew. Chem. Int. Ed.* **2008**, *47*, 6538. (b) Tetsuka, H.; Ebina, T.; Mizukami, F. *Adv. Mater.* **2008**, *20*, 3039.
42. (a) Sheehan, P. E.; Whitman, L. J. *Nano Lett.* **2005**, *5*, 803. (b) Jain, P. K.; Huang, X.; El-Sayed, I. H.; El-Sayed, M. A. *Acc. Chem. Res.* **2008**, *41*, 1578. (c) Rosi, N. L.; Mirkin, C. A. *Chem. Rev.* **2005**, *105*, 1547. (d) Liang, S.; Pierce, D. T.; Amiot, C. ; Zhao, X. J. *Synth. React. Inorg. Met. Org. Chem.* **2005**, *35*, 661.

CHAPTER 2

Optimization of the Shell Thickness of Core-Shell Quantum Dots



Abstract

Photoinduced charge transfer process between cadmium selenide (CdSe) quantum dots (QDs) possessing varying monolayers of zinc sulphide (ZnS) shell and hole scavengers such as phenothiazine (PT) and N-methylphenothiazine (NMPT), were investigated for optimizing the shell thickness of core-shell quantum dots. Spectroscopic investigations indicate that phenothiazine binds onto the surface of bare CdSe QDs, resulting in the photoluminescence quenching, by scavenging the hole formed in the valence band of photoexcited QDs. Further, experiments with ZnS overcoated QDs showed that two monolayers of ZnS prevent the electron transfer processes while retaining good luminescence quantum yields. Methodologies presented here, based on photoinduced charge transfer process can provide quantitative information on the optimum shell thickness of core-shell QDs, which can suppress the undesired electron transfer and provide maximum photoluminescence yield.

2.1. Introduction

The unique photophysical properties of semiconductor quantum dots (QDs) offer considerable promise as components in optoelectronic devices (for example, in photovoltaics)¹ and as tags for bioimaging, labeling, and sensing.² Excitation of QD yields highly reactive electron-hole (exciton) charge carrier pair. The photogenerated electron or hole can be transferred into the molecular adsorbates, and the transfer rate depends on many factors such as relative redox potential, size and shape of the nanoparticle, QD-acceptor distance, interfacial environment etc.³ In a recent investigation, Scaiano and co-workers have observed nonlinear effects in the quenching of the photoluminescence (PL) of CdSe QDs by free radicals, namely, TEMPO (2,2,6,6-tetramethylpiperidine-N-oxide free radical) and 4-amino-TEMPO involving an electron exchange mechanism which is dependent on the size of QDs.^{4,5}

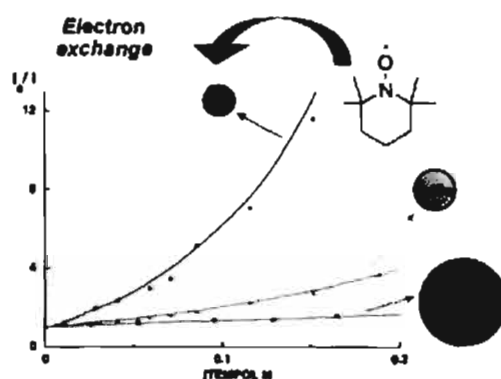


Figure 2.1. Nonlinear effects (dependent on nanoparticle size) in the quenching QD luminescence by nitroxyl free radicals (*adapted from reference 4*).

The luminescence properties of bare QDs are highly influenced by the surrounding medium: for example their interactions with biomolecules such as adenine and dopamine, result in luminescence quenching through an electron transfer process, thereby limiting their use in biological systems as fluorescent labels or biosensors.⁶ Also, bare QDs are highly susceptible to oxidation; exposed selenium sites on CdSe QDs react with molecular oxygen, resulting in the formation of SeO₂ and Cd²⁺, thereby leading to toxicity and degradation.^{7,8} One of the most successful strategies adopted for imparting photostability and improving the photoluminescence efficiency of QD is to overcoat with an inorganic shell material having similar lattice parameters and higher bandgap energy (E_g). Preferred shell materials in case of CdSe QDs include zinc sulphide (ZnS), zinc selenide (ZnSe) and cadmium sulphide (CdS).⁹⁻¹¹ A comparison of lattice parameters and bandgap energy for various overcoating materials used for CdSe QDs is given in Figure 2.2. Among these, ZnS is more preferred as an overcoating material, owing to its higher bandgap energy, imparting more confinement of exciton in core material.

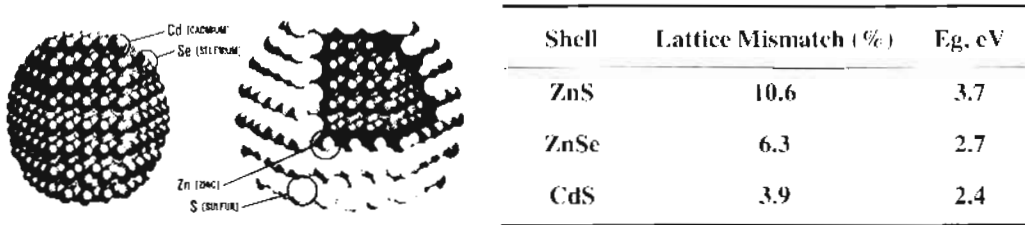


Figure 2.2. (Left) A cartoon representation of bare and core-shell QDs. (Right) Lattice mismatch and bandgap energy (E_g) of various shell materials recommended for CdSe QDs (E_g: 1.7 eV) (*references 9-11*).

Overcoating also prevents the leakage of core materials thereby reducing the toxicity of QDs.¹³ However, the luminescence quantum yield decreases with increase in shell thickness, limiting their use in optoelectronic devices.⁹ These results clearly indicate the need of optimizing the shell thickness of the overcoating layer. A few attempts have been made to follow the overcoating process using X-ray photoelectron spectroscopy (XPS) and Raman spectroscopy^{9,15-18} and these aspects are summarized below.

Bawendi and co-workers have investigated the overcoating of ZnS over CdSe QD by following the SeO₂ peak in X-ray photoelectron spectrum, along with TEM and small angle X-ray scattering analysis. The peak corresponding to SeO₂ peak was not observed for the samples having >1.3 monolayers (MLs) of ZnS, upon exposure to air for 80 h.⁹

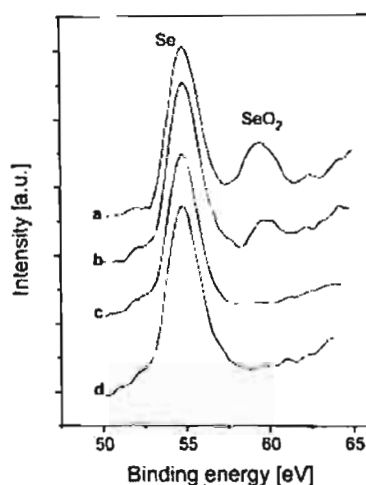


Figure 2.3. X-ray photoelectron spectra of ZnS overcoated CdSe QDs: (a) bare CdSe, (b) 0.65, (c) 1.3, and (d) 2.6 monolayers of ZnS. (adapted from reference 9).

A method based on Raman spectroscopy has been proposed by Baranov *et al.* to control the quality of ZnS overcoated CdSe (CdSe-ZnS core-shell) QDs.¹⁵ Authors have suggested a morphological transition from semi-disordered coherent to incoherent epitaxial growth when the shell thickness is more than 2 MLs. Recently, Lu and coworkers extended the same technique for determining the shell thickness and interface parameters of CdS overcoated CdSe QDs, based on the first-order and higher-order Raman scattering studies.¹⁶

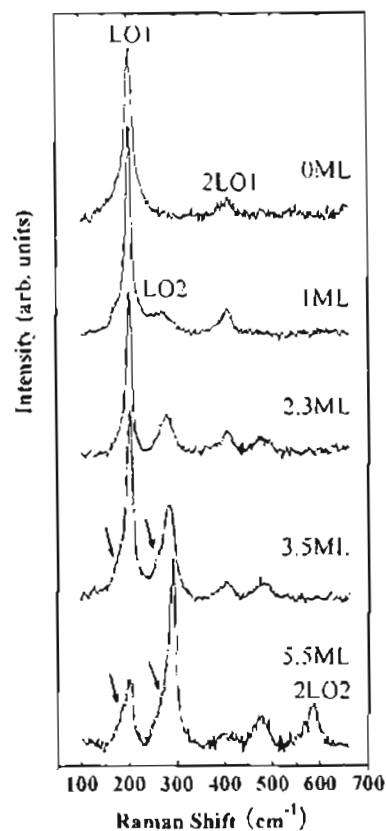


Figure 2.4. Optical Raman spectra for bare CdSe QDs and CdSe-CdS core-shell QDs with different shell thickness. The blue shift in the longitudinal optical phonons of CdS shell is a function of shell thickness (*adapted from reference 16*).

Synthesis of core-shell QDs is now routinely carried out in many laboratories; procedures that do not require any specialized instrumentation are more desirable for monitoring the overcoating process. Photoinduced charge transfer dynamics between core-shell QDs possessing varying shell thickness and hole scavengers may be a convenient method for probing the overcoating process. Herein, we present a novel methodology for probing the overcoating process by following the luminescence quenching of core-shell quantum dots, possessing varying shell thickness, in the presence of various hole acceptors.

2.2. Results and Discussion

2.2.1. Characterization of CdSe and CdSe-ZnS QDs

CdSe QDs capped with trioctylphosphine oxide (TOPO) and a small percentage of trioctylphosphine (TOP) were synthesized (referred as “bare QDs”) and overcoated with ZnS of varying shell thickness (0.65-3.9 MLs) by following reported procedures (details of QD synthesis and ZnS overcoating are provided in the experimental section).^{12,14} QDs of three different sizes were synthesized and characterized using absorption and emission spectroscopy. Corresponding spectra and their photographs under UV illumination are presented in Figures 2.5 and 2.6, respectively. The absorption spectra clearly showed the evolution of multiple excitonic peaks, indicating the change from continuum in energy levels to discrete energy levels, arising due to size quantization effect.¹⁹ The first excitonic peak ($1S(c)-1S_{3/2}(h)$)

transition) is a measure of minimum energy required for electronic transition (bandgap energy: E_g), which shifts to longer wavelengths with an increase in the crystal size. A similar red shift is also observed in the corresponding emission maxima, with an increase in QD size. The Stokes shift (~ 12 nm) observed in these systems is found to be small indicating that band edge emission is the predominating radiative decay channel. The presence of surface defects can broaden and shift the emission band to longer wavelength. These results confirm that the QDs produced are of high quality with minimum surface defects. Also, the low full-width at half-maximum (FWHM < 30 nm), which is an indicator of dispersity, suggests that the QDs obtained are monodisperse and is further confirmed by HRTEM images presented in Figure 2.9A.

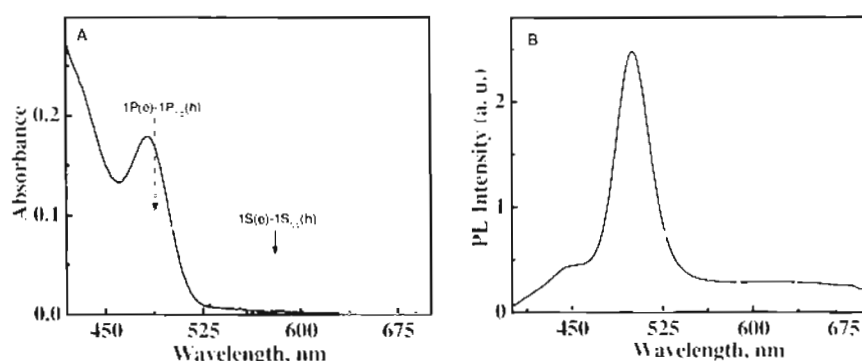


Figure 2.5. (A) Absorption and (B) emission spectra of CdSe QDs of three different size in toluene, excited at 390 nm.

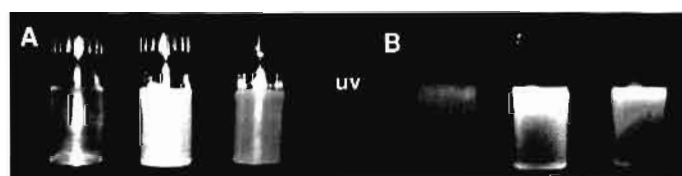


Figure 2.6. CdSe QDs of three different size (A) in day light and (B) under UV illumination.

The diameter (D) of the quantum dots can be theoretically estimated from the wavelength corresponding to the first excitonic transition (λ) in the UV-Vis spectrum by following relationship, reported by Peng and coworkers (equation 2.1).²⁰ From these results, concentration of QDs (C) were obtained by using Beer-Lamberts law (equation 2.2-2.3).

$$D = (1.61 \times 10^{-9})\lambda^4 - (2.66 \times 10^{-6})\lambda^3 + (1.62 \times 10^{-3})\lambda^2 - (0.43)\lambda + 41.57 \quad (2.1)$$

$$C = A / [l \times \epsilon] \quad (2.2)$$

$$C = A / [l \times 5857 (D)^{2.65}] \quad (2.3)$$

where 'A' is the absorbance, 'l' is the optical path length (cm) and 'ε' is the molar extinction coefficient.

Cadmium Selenide can form either 'hexagonal-wurtzite' or 'cubic-zinc blende' type structure (JCPDS files No. 8-459 and 19-191). We have carried out X-ray diffraction (XRD) analysis and the results are presented in Figure 2.7. Analysis of the X-ray diffractogram indicated the presence of hexagonal, wurtzite-type structure. It is reported that the QDs produced by high temperature synthetic method adopt a hexagonal, wurtzite-type structure. The X-ray diffractogram contains broad peak instead of sharp line like spectra, which is reported as a characteristic feature of small size particles. The XRD pattern can be further correlated to the size of the nanoparticle (D) using Debye-Sherrer formula (equation 2.4),^{21,22}

$$D = (0.89 \lambda) / (B \cos \theta)_h \quad (2.4)$$

where ' λ ' is the wavelength of X-ray, ' B ' is the FWHM ($\Delta\theta$) in radians of the corresponding diffraction peak angle ' θ_B '. The lattice spacing (d) was calculated as 0.346 nm from the Bragg's equation (2.5), corresponding to the strong diffraction peak at [002] plane. This result is in good agreement with the standard JCPDS d -value reported for CdSe hexagonal structure.

$$d = (n\lambda) / (2\sin\theta) \quad (2.5)$$

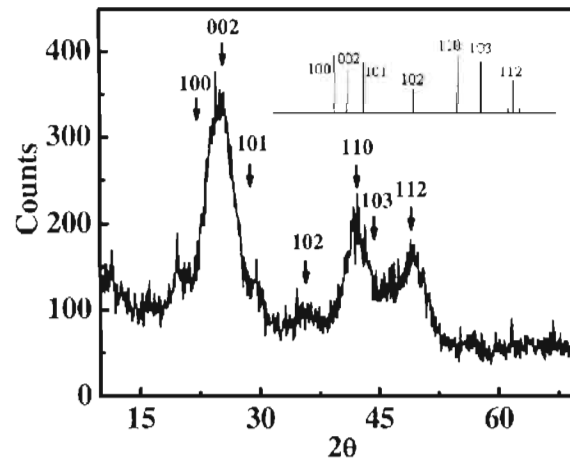


Figure 2.7. Powder XRD pattern of TOPO capped CdSe QDs, exhibiting hexagonal, wurtzite structure. (Inset) Theoretical XRD pattern for bulk CdSe crystal.

Energy dispersive spectroscopy (EDS), which is a surface chemical analysis technique, was used for the elemental identification of the QDs. The characteristic $K\alpha$ and $L\alpha$ lines in the EDS spectrum (Figure 2.8) corresponding to 'Cd' and 'Se', is in good agreement with the reported values.²³

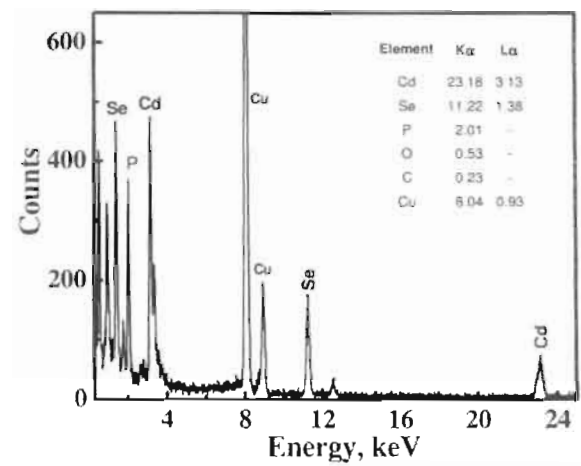


Figure 2.8. EDS spectrum of TOPO capped CdSe QDs prepared on a copper grid. Inset shows the theoretical ‘Kα’ and ‘Lα’ line energy values.

As a representative example, the size of the QD emitting at ~600 nm was deduced from absorption and emission spectroscopy, XRD analysis and from HRTEM images and these results are presented in Table 2.1. Based on the ‘D’ value obtained from various techniques, the average size was estimated as 4.16 nm (error between various techniques: ± 5 %).

Table 2.1. Estimation of size of QDs, emitting at ~600 nm, from spectroscopic and microscopic methods.

Method	QD size (D), nm
Absorption spectrum	4.01
Emission spectrum	4.30
XRD	4.01
HRTEM	4.30
Average Size	4.16

We have further varied the thickness of ZnS shell around CdSe core and all further studies were carried using the CdSe QDs having an average size of 4.2 nm (emitting at ~600 nm). Overcoated samples were capped with TOPO in all the cases. It is earlier reported by Bawendi and coworkers that the ZnS core-shell system having shell of 3.1 Å corresponds to one monolayer, i.e., the distance between consecutive planes along the [002] axis in bulk wurtzite ZnS along the major axis of the prolate-shaped dots.⁹

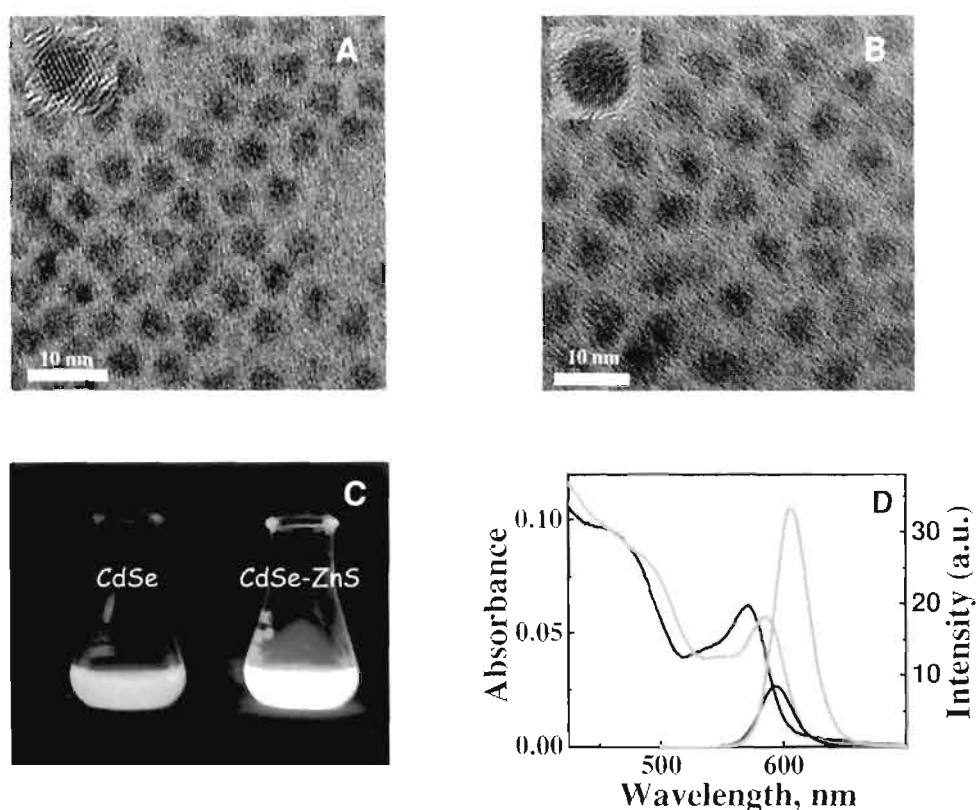


Figure 2.9. Representative HRTEM images of (A) CdSe QDs and (B) CdSe QDs overcoated with 3.9 monolayers of ZnS. (C) Photographs under UV irradiation. (D) Absorption and luminescence spectra of bare CdSe QDs (blue trace) and overcoated with 3.9 monolayers of ZnS (orange trace).

The ZnS overcoated CdSe QDs were characterized by UV-Vis absorption spectroscopy, XRD and HRTEM and these results are discussed. HRTEM images and the absorption and emission spectra of bare QDs having an average core size of 4.2 nm is presented in Figure 2.9A,D. The samples were further overcoated with ZnS shell of varying thickness. Based on HRTEM studies, core-shell QDs were found to be nearly monodisperse. Number of MLs was estimated based on the concentration of diethylzinc and hexamethyldisilathiane used. HRTEM images of core-shell QDs having 3.9 MLs of ZnS shell is presented in Figure 2.9B and other core-shell systems, having varying shell thickness of ZnS, are shown in the experimental section. The absorption as well as the emission spectra underwent a slight bathochromic shift upon overcoating with ZnS shell, accompanied by a dramatic increase in the luminescence quantum yield (Figures 2.9D), which is illustrated in the photograph shown in Figure 2.9C. The absorption and luminescence properties of bare and overcoated QDs have been discussed in detail in various reports.^{9,10,12} Bare QDs possess surface defects due to dangling or unsaturated Cd^{2+} and Se^{2-} sites, which act as traps for excitons, enhancing phonon assisted recombination thereby lowering luminescence quantum yield. An epitaxial growth of ZnS shell over CdSe core passivates the trap states leading to higher luminescence quantum yield.

The bathochromic shift in the absorption and emission spectra (Figure 2.10) observed after overcoating is attributed to the partial leakage of the exciton into the shell material.¹² The luminescence yield of CdSe QDs increased initially with ZnS overcoating, which decreased with further increase in shell thickness (Figure 2.10B).

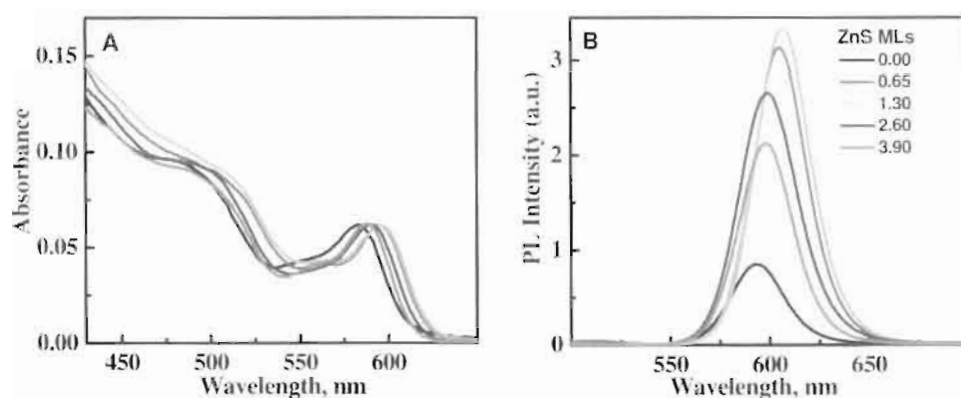


Figure 2.10. Effect of ZnS overcoating (0-3.9 MLs or 0-1.2 nm) (A) on absorption and (B) on emission spectra of CdSe QDs.

Increase in the luminescence quantum efficiency (Figure 2.11) in the initial stages of ZnS overcoating indicates an epitaxial growth of shell, which leads to an effective passivation of surface traps in bare QDs. The subsequent increase in the ZnS MLs resulted in the reduction of PL, which is attributed to the generation of misfit dislocations, resulting from the strain at the interface due to lattice mismatch (12%) between the CdSe and ZnS.⁹



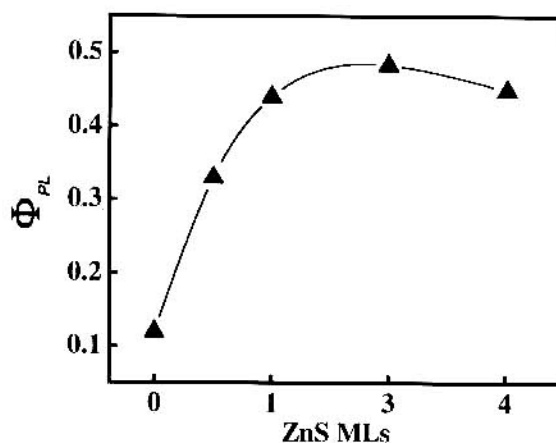


Figure 2.11. Effect of ZnS overcoating (up to 3.9 MLs) on PL quantum yield (Φ_{PL}) of CdSe QDs.

2.2.2. Effect of Electron Donors

We selected electron donors such as phenothiazine (PT) and N-methylphenothiazine (NMPT) to probe the viability of charge transfer process with photoexcited QDs, as a function of thickness of the shell. Comparison of redox potentials of CdSe QDs having a diameter of 4.2 nm (valence band edge redox potential 1.61 V against NHE)²⁴ with phenothiazine and N-methylphenothiazine (E_{ox} of PT and NMPT are 0.85 and 1.03 V, respectively; against NHE)²⁵ indicate that a photoinduced charge transfer process between these systems is thermodynamically feasible. Upon addition of varying concentrations of PT (0-7 mM) to bare CdSe QDs, (in toluene) the absorption spectral profile remained more or less unaffected, while the luminescence underwent dramatic quenching as shown in Figure 2.12A. Based on the absorption spectral studies, the possibility of any chemical degradation of QDs is completely ruled out. In all the cases, QDs were selectively excited

(490 nm) and the possibility of energy transfer process was ruled out due to absence of any spectral overlap of the donor-acceptor pair. Stern-Volmer plot for luminescence quenching, upon addition of PT, followed a nonlinear behavior (Figure 2.12B) and is attributed to the existence of more than one electronic state or a combination of static and dynamic quenching mechanisms.^{26,27} These aspects are discussed in detail in Sections 2.2.3.

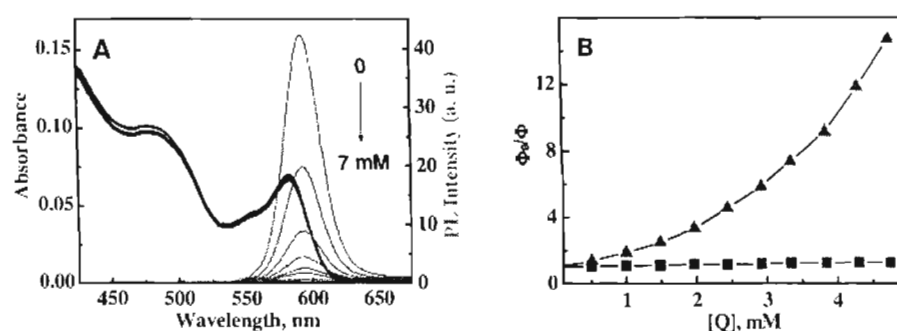


Figure 2.12. (A) Absorption and luminescence spectra of bare CdSe QDs in toluene, upon successive additions of 1 mM PT; excited at 490 nm (OD~0.09). (B) Corresponding Stern-Volmer plot showing the effect of PT (▲) and NMPT (■) on the luminescence intensity of bare CdSe QDs.

Further, the effect of N-methylphenothiazine (NMPT; methyl derivative of PT) and other electron donors such as phenoxazine (PO) and phenoxathiin (PI) on PL of bare CdSe QDs were investigated (Chart 2.1.).

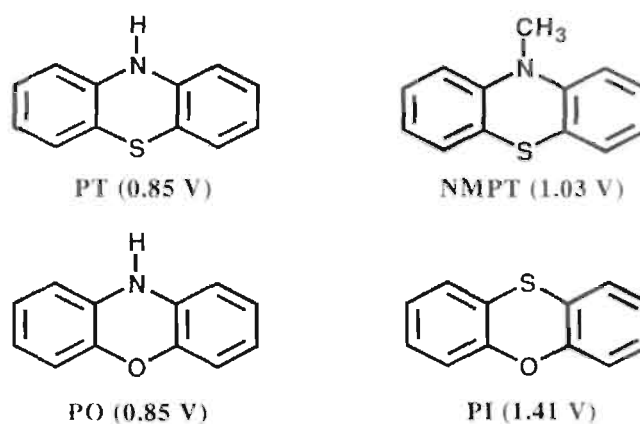


Chart 2.1. Electron donors used in luminescence quenching experiments with bare QDs along with their oxidation potential against NHE.^{27,28}

Interestingly, the luminescence of bare CdSe QDs was practically unaffected upon addition of **NMPT** (Figure 2.12B), even though the process was thermodynamically favorable. It is anticipated that the hole scavenger fails to interact with the surface of QD, plausibly due to the steric restrictions imposed by the *N*-methyl group in **NMPT**. The spectral changes observed on addition of varying concentration of phenoxazine (**PO**) were similar to that of **PT**: the absorption profile (Figure 2.13B) remained unaffected on addition of **PO** (0-10 mM) whereas a dramatic quenching in the luminescence was observed. In contrast, the addition of phenoxathiin (**PI**) had no affect on the PL of bare QDs (Figure 2.13C), since the process is thermodynamically unfavorable (E_{ox} of **PI** is 1.41 V against NHE).²⁸

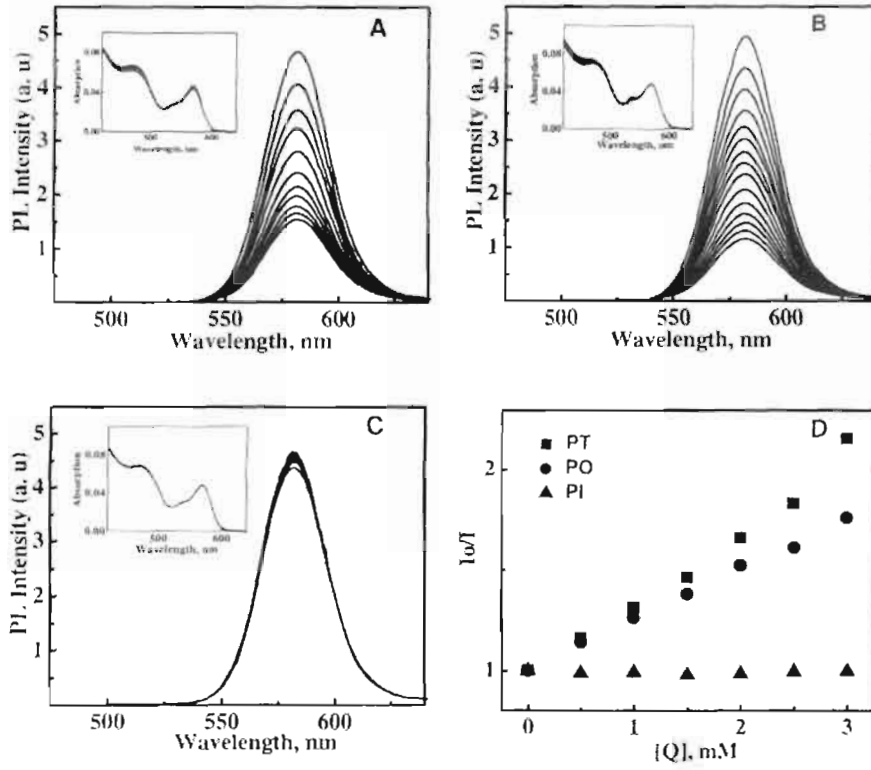


Figure 2.13. Effect of (A) PT, (B) PO, and (C) PI (0–10 mM) on the luminescence intensity of bare CdSe QDs. Excited at 490 nm, OD ~ 0.07, in toluene. (Insets) Respective absorption spectra in toluene. (D) Relative luminescence intensity as a function of quencher concentration.

A better insight on photoinduced charge transfer process can be obtained by considering the thermodynamics of the process using Rehm-Weller equation, by estimating the driving force from electrochemically and spectroscopically measured quantities.^{29,30} In a recent investigation, van Beek *et al.* have demonstrated the light induced electron transfer process between the quantum dots and polythiophene and estimated the driving force for photoinduced charge separation using the equation 2.6;³¹

$$\Delta G^\circ = E_{\text{ox}}(\text{D}) - E_{\text{red}}(\text{A}) - \epsilon_{00} + C \quad (2.6)$$

where ΔG° is the driving force for photoinduced charge separation, $E_{\text{ox}}(\text{D})$ represents the oxidation potential of the donor, $E_{\text{red}}(\text{A})$ is the reduction potential of the acceptor (CdSe QD), and ϵ_{00} stands for the zero-zero excitation energy, i.e., the smallest bandgap calculated from the absorption onset of QD, and C is a solvent-dependent term (the constant C is expected not to exceed a few tenths of an electron volt). From Figure 2.12A, ϵ_{00} was estimated as 2.07 eV, corresponding to an absorption onset of 600 nm. Free energy changes were calculated for various electron donors used in our studies and the results are summarized in Table 2.2.

Table 2.2. Free energy changes associated with photoinduced charge transfer process between CdSe QDs and various electron donors.

<i>Electron Donors</i>	<i>$E_{\text{ox}}(\text{D})$, V vs NHE</i>	<i>ΔG°, eV</i>
PT	0.85	+0.02 + C
PO	0.85	+0.02 + C
NMPT	1.03	+0.20 + C
PI	1.41	+0.58 + C
PPD	0.26	-0.57 + C

* $E_{\text{red}}(\text{A}) = -1.24$ V against NHE, and $\epsilon_{00} = 2.07$ eV.

The estimated ΔG° value for the photoinduced charge separation with CdSe is close to zero for **PT**, **PO** and **NMPT** indicating feasibility of the electron transfer process. The luminescence studies show a dramatic

quenching in all these systems except for **NMPT**. In the case of **NMPT**, the hole scavenger fails to interact with the surface of QD due to the steric restrictions imposed by the methyl group. However, the estimated ΔG° value is found to be more positive in the case of **PI** and no luminescence quenching was observed.

2.2.3. Optimization of Shell Thickness

Ideally, the large bandgap material used as shell should form a uniform layer over QDs. any voids on the surface can affect the photostability and induce leakage of the core material leading to cytotoxic effects.¹³ We have analyzed the overcoated sample carefully by using HRTEM, and these 2D images could not provide any information other than an increase in the overall size of the material. One of the objectives of the present investigation is to develop a simple methodology for estimating the optimum thickness of overcoating material, which can inhibit the undesired electron transfer without losing the luminescence property.

The PL quenching experiments were further carried out with a series of core-shell QDs of varying shell thickness, using PT as electron donor. For this purpose CdSe QDs overcoated with 0-3.9 MLs of ZnS were used. Experiments were carried out in toluene and the QD samples were excited at 490 nm, so that CdSe core is selectively excited (bulk bandgap of ZnS is 3.6 eV corresponding to an absorption onset ~350 nm).³² As in the case of bare QDs, the luminescence was quenched for core-shell QDs with low shell

thickness in presence of **PT** (Figure 2.14A,B). In contrast, the luminescence quenching efficiency was found to decrease with an increase in ZnS shell thickness (>2 MLs) as shown in Figure 2.14C,D.

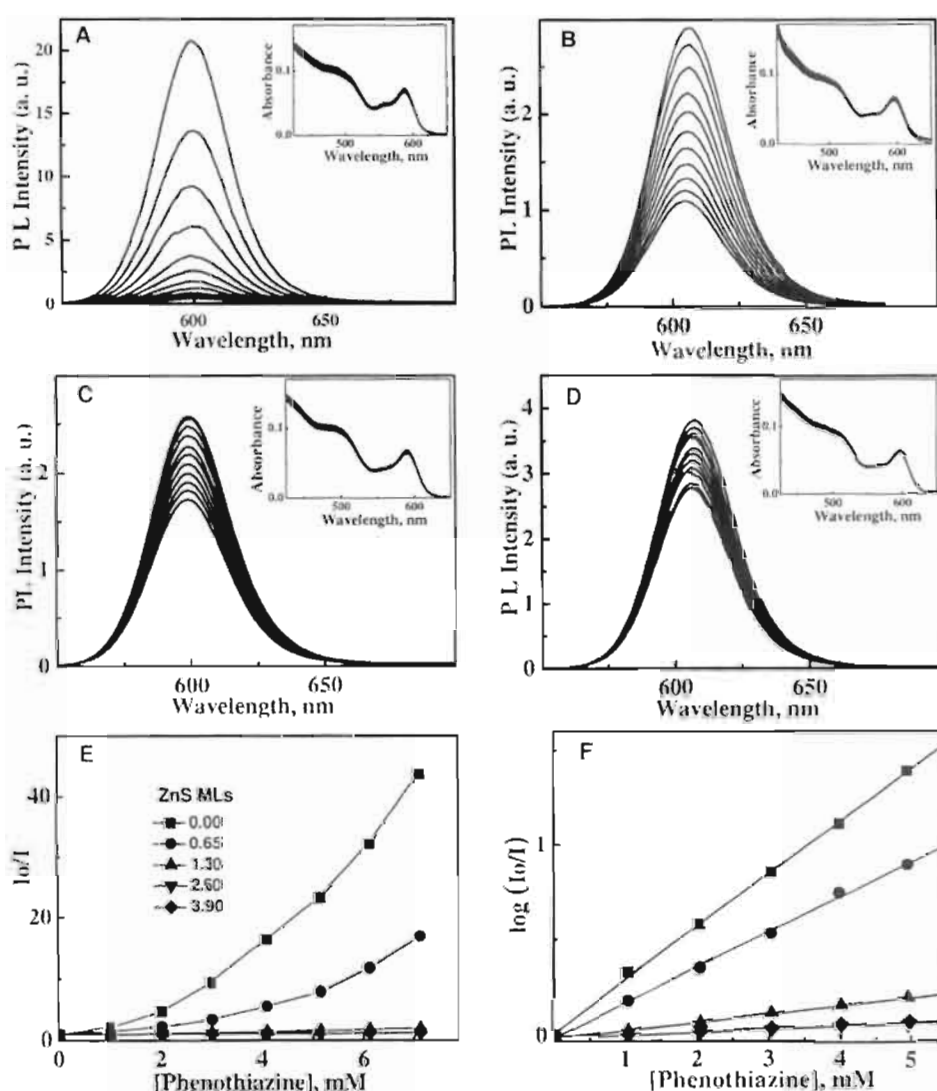


Figure 2.14. Effect of PT (0-10 mM) on photoluminescence and (inset) absorption spectra of CdSe QDs with (A) 0.65, (B) 1.3, (C) 2.6 and (D) 3.9 MLs of ZnS; Excited at 490 nm, OD ~ 0.10 , in toluene. (E) Relative changes in the luminescence intensity including for bare QDs and (F) Plot for $\log(I_0/I)$ against varying concentration of PT.

Relative changes in the luminescence intensity (I_0/I ; I_0 and I represents the PL intensity in absence and presence of **PT** respectively) CdSe QDs possessing 0, 0.65, 1.3, 2.6 and 3.9 monolayers of ZnS in presence of **PT** are presented in Figure 2.14E.

The nonlinear effects observed in the PL quenching of CdSe QDs has been reported by various groups^{26,33} and in our study the relative PL intensity (I_0/I) showed an exponential relationship with the concentration of **PT**, as per equation 2.7.^{4,6}

$$I_0/I = e^{\alpha[\text{PT}]}$$
(2.7)

where ' α ' represents the static quenching constant. A plot of $\log(I_0/I)$ versus the concentration of PT shows a linear relationship (Figure 2.14F), and the ' α ' values for CdSe QDs possessing 0.0, 0.65, 1.3, and 2.6 monolayers of ZnS are deduced as 277, 184, 42, and 12 M^{-1} , respectively, from the linear fit plots. The ' α ' values remained more or less the same for CdSe-ZnS QDs possessing shell thickness more than 2.6 monolayers ($\sim 12 \text{ M}^{-1}$).

To explore the luminescence quenching mechanism further, experiments were repeated as a function of temperature (at 298 K and 323 K) and results are shown in Figure 2.15. It was observed that the quenching rate decreases considerably at elevated temperature for both bare (' α ' at 298 and 323 K is 290 and 151 M^{-1} , respectively; inset of Figure 2.15A) and overcoated samples (' α ' at 298 and 323 K is 174 and 96 M^{-1} , respectively; inset of Figure 2.15B). PT forms a weak complex with QD surface [QD---PT] which

dissociates at higher temperature preventing photoinduced charge transfer process.

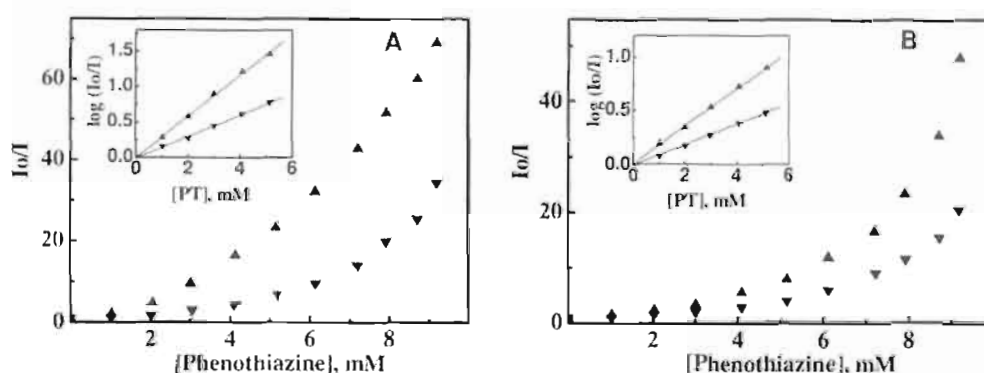


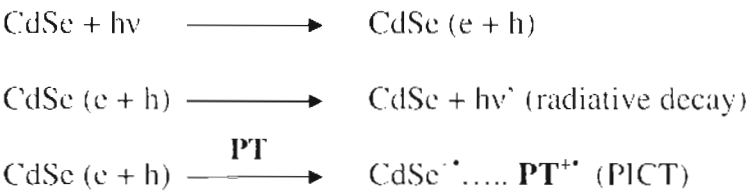
Figure 2.15. Relative changes in the luminescence intensity of (A) bare CdSe QDs and (B) ZnS overcoated (0.65 MLs) CdSe QDs upon the addition of PT at 323 and 298 K respectively. Inset shows the corresponding plots of $\log(I_0/I)$ against the concentration of PT.

Time correlated single photon counting studies (TCSPC) for bare and overcoated CdSe QD samples were carried out, and the results for bare QDs are shown in Table 2.3. Luminescence decay kinetics of CdSe QDs showed multiexponential decay characteristics. The origin of multiexponential emission decay for metal chalcogenides has already been investigated in detail, and is attributed to trapping sites within the nanoparticle,³³ and to the blinking effects.^{34,35} The lifetime and amplitude components of bare (and ZnS over coated) CdSe QDs did not show any significant changes in presence of PT (Table 2.3). This result further confirms that the interaction of PT with QDs is static in nature.

Table 2.3. TCSPC data for bare CdSe QDs in presence of **PT**.

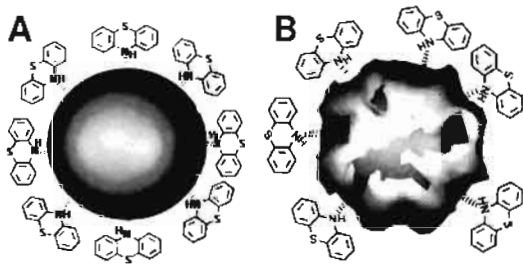
[PT], mM	τ_1 , ns	τ_2 , ns	τ_3 , ns	τ_{avg} , ns	χ^2
0	4.0(16%)	14(61%)	46(23%)	31	1.12
2	3.9(17%)	13(62%)	43(21%)	30	1.18
4	3.7(18%)	13(62%)	43(20%)	27	1.12
6	3.9(18%)	13(63%)	44(19%)	28	1.15
8	3.8(16%)	13(64%)	50(20%)	32	1.14

Bare CdSe QDs form weak complex with **PT** and efficiently scavenges the photoexcited hole formed in the valance band. Various photochemical process are presented below.



Bawendi and coworkers have reported that overcoating QD with a thin layer of ZnS (1.3 < MLs) can lead to a non-uniform ZnS shell.⁹ In the case of QDs with 0.65 and 1.3 MLs of ZnS, **PT** complexes through the voids in the shell as illustrated in Scheme 2.1.

Scheme 2.1. Complexation of **PT** with (A) bare and (B) ZnS overcoated CdSe QDs having voids.



Luminescence quenching in fluorophores is discussed based on several models.³⁶⁻³⁹ including the Perrin model.³⁹ In a recent study, Scaiano and coworkers have reported that the quenching radius, i.e., the donor-acceptor distance is influenced by the size of quantum dots.⁴ The quenching radius can be better viewed as an ‘action radius’ for the quencher and can be obtained by using Perrin analysis as given by the equation 2.8. It assumes that an effective quenching sphere exists about the donor (or acceptor, in current study) and if the quencher molecule is outside the quenching sphere it does not quench at all.

$$\alpha = N_A V \quad (2.8)$$

where ‘ α ’ is the static quenching constant, ‘ N_A ’ is Avogadro’s number and ‘ V ’ is the quenching volume. For example, in the case of a quencher molecule such as TEMPO, the quenching radius (0.9 nm) can reach across the nanoparticle when its size is smaller, where as for larger QDs, the interaction is restricted with the excitons near the surface.³⁹ The quenching volume of the bare and overcoated QDs was estimated, and these results are presented as Table 2.4. The quenching volume was found to decrease with an increase in number of ZnS MLs. It also indicates that the overcoating prevents charge-transfer interaction of PT with QD, at higher shell thickness.

Table 2.4: Quenching volume of bare and ZnS overcoated CdSe QDs

ZnS MLs	α , M ⁻¹	V, cm ³
0	277	46 x 10 ⁻²⁰
0.65	184	31 x 10 ⁻²⁰
1.30	42	7 x 10 ⁻²⁰
2.60	12	2 x 10 ⁻²⁰

In order to obtain quantitative information on the optimum shell thickness, which can suppress the undesired electron transfer process and provide maximum radiative decay, PL quantum yield (Φ_L) and the static quenching constant (α) for CdSe-ZnS core-shell QDs were plotted as a function of ZnS monolayers (Figure 2.16).

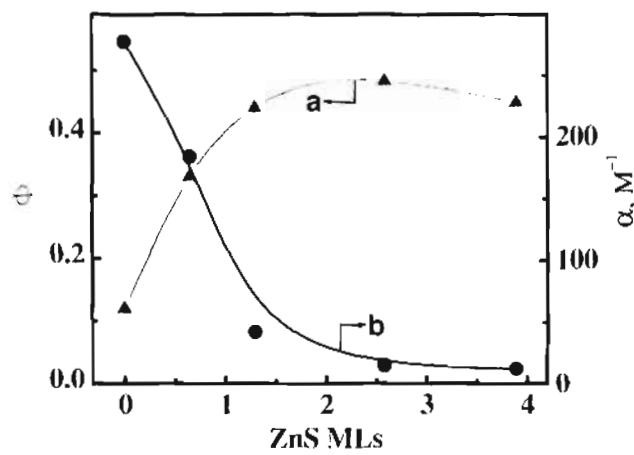


Figure 2.16. Changes in the PL quantum yield (Φ) and static quenching constant (α) as a function of number of ZnS MLs.

The luminescence quantum yield increases with the number of ZnS monolayers (Φ_L (bare) 0.08, Φ_L (1.3) 0.44, and Φ_L (2.6) 0.48) and further

decreases slightly ($\Phi_f(3.9) = 0.44$), whereas the static quenching constant dramatically decreases. On the basis of the ' Φ_f ' and ' α ' values presented in Figure 2.17, it is concluded that two monolayers (corresponding to 0.65 nm) of ZnS shell is the optimum shell thickness for a 4.2 nm diameter CdSe quantum dot, which inhibit charge transfer processes and provide maximum PL quantum yield.

2.3. Conclusions

It has been demonstrated that the ZnS shell in CdSe-ZnS QDs plays an important role not only in modulating the luminescence quantum yield but also in regulating the charge carrier transfer dynamics from excited core to electron donors. Steady state and time-resolved luminescence studies suggest that the electron donors bind to the surface of CdSe QDs leading to luminescence quenching. Time resolved luminescence experiments as well as the temperature dependent studies further confirm that the interaction is static in nature. Further photoinduced charge-transfer dynamics between CdSe quantum dots (QDs) possessing varying monolayers of ZnS and hole scavengers such as phenothiazine (PT) was investigated. Based on the studies it is concluded that two monolayers of ZnS shell is the optimum shell thickness for a 4.2 nm diameter CdSe quantum dot, which inhibit charge transfer processes and provide maximum luminescence quantum yield. Luminescent core-shell QDs, with optimum shell thickness, which do not involve any electron-transfer interactions, are ideal for bioimaging, and

methodologies presented here are useful for probing the overcoating process in semiconductor QDs.

2.4. Experimental Section

2.4.1. Materials and Methods

General details of solvents, reagents and equipments/instruments used for synthesis, characterisation and studies are provided in the Appendix. Reagents such as trioctylphosphine oxide (TOPO), trioctylphosphine (TOP), cadmium oxide (CdO), Se powder, dodecylamine (DDA), hexadecylamine (HDA), tetradecylphosphonic acid (TDPA), phenothiazine (PT), phenoxazine (PO), phenoxathiin (PI), diethyl zinc (DEZ) and hexamethyldisilathiane (HMDST) were purchased from Aldrich and used as such, except PT, PO and PI, which were further purified by recrystallisation from dry benzene.

2.4.2. Synthesis of TOPO capped CdSe QDs

A pot mixture containing CdO (0.067 g, 0.52 mmol), dodecylamine (3.8 g, 20.72 mmol), TOPO (2.7 g, 6.9 mmol) and tetradecylphosphonic acid (0.40 g, 1.44 mmol) was heated to 300 °C under vacuum, until CdO dissolves completely to produce an optically clear solution. At this temperature, an injection mixture containing TOPSe (selenium powder in TOP, 83 μ L, 0.083 mmol) in TOP (5.2 mL, 2.5 mmol) was introduced. After desired crystal growth, the reaction was arrested by reducing the reaction temperature down

to ambient conditions. The QDs thus obtained was purified by reprecipitation with methanol.

2.4.3. Synthesis of CdSe-ZnS Core-Shell QDs

In a typical procedure, to grow a ZnS shell of 0.4 nm thickness on CdSe core (4.2 nm), a pot mixture containing CdSe QDs (11.6 μM), TOPO (4 g, 10.3 mM) and HDA (2 g, 8.3 mM) was heated to 160 $^{\circ}\text{C}$ under inert atmosphere. A solution of DEZ (47.9 μL , 1 M solution in hexane) and HMDST (8.9 μL , 0.049 mM) in TOP (3 mL) was added drop wise, under gentle stirring, over a period of 30 minutes. Then the reaction mixture was cooled to room temperature followed by addition of 10 mL 50% butanol/hexane mixture. Finally, the CdSe-ZnS core-shell QDs were purified by reprecipitation with methanol and redissolved in toluene. QDs were characterized by HRTEM (Figure 2.17) and XRD analysis (Figure 2.18).

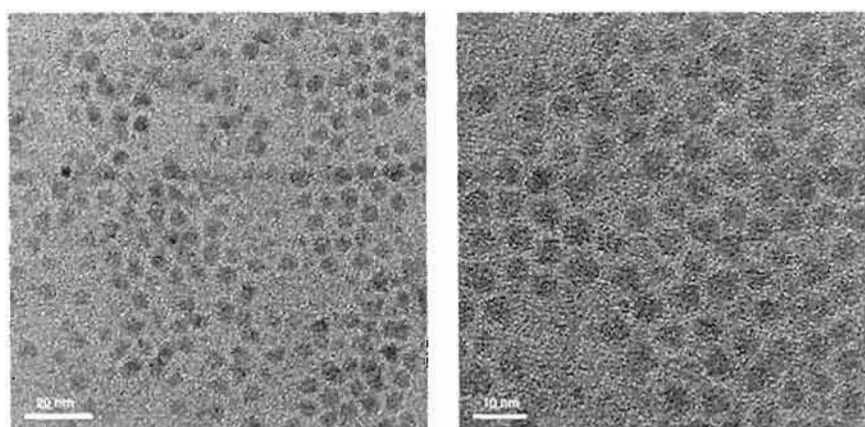


Figure 2.17. HRTEM images of ZnS (2.6 MLs) overcoated CdSe

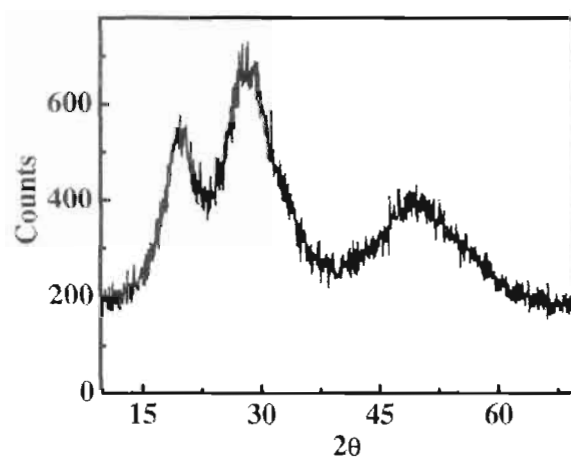
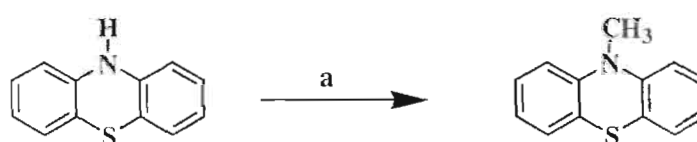


Figure 2.18. Powder XRD pattern of ZnS overcoated (2.6 MLs) CdSe QDs.

2.4.4. Synthesis of N-methylphenothiazine (NMPT)⁴⁰⁾



(a) CH_3I , NaH, dry THF, dark, 24 h, rt.

Phenothiazine (2 g, 10 mM) dissolved in dry tetrahydrofuran (15 mL) was stirred with NaH (0.36 g, 15 mM) under argon atmosphere in dark for 1 h to produce the N sodium salt. Methyl iodide (1.9 g, 20 mM) was added, and the solution was further stirred for 24 h at room temperature to give N-methylphenothiazine, which was extracted with diethyl ether. After treating the ether layer with anhydrous sodium sulfate, solvent was evaporated to give solid product which was chromatographed over neutral aluminum using hexane to yield 90 mg (42 %) as pure product: mp 100-101 °C; IR (KBr) ν_{max} 3739, 3608, 3055, 2887, 2818, 2353, 1782, 1573, 1556, 1454, 1330, 1265,

1138, 1039, 864, 758, 532.35, 503, 455, 435 cm^{-1} ; ^1H NMR (CDCl_3 , 300 MHz) δ 3.37 (3H, s), 6.79-7.16 (aromatic 8H, m), ^{13}C NMR (CDCl_3 , 75 MHz) δ 35.31 (alkyl), 114.04, 122.46, 123.51, 127.18, 127.37, 145.83, FAB(m/z):Found ($\text{C}_{13}\text{H}_{11}\text{NS}$) 213.10, Exact Mass: 213.06. The absorption and emission spectra of **PT** and **NMPT** are shown in Figure 2.19.

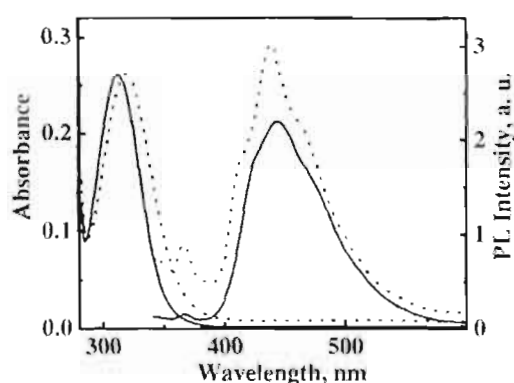


Figure 2.19. Absorption and emission spectra of **PT** (solid line) and **NMPT** (dotted line) in toluene, excited at 330 nm.

2.5. References

1. Kamat, P. V. *J. Phys. Chem. C* **2007**, *111*, 2834.
2. Medintz, I. L.; Uyeda, H. T.; Goldman, E. R.; Mattoussi, H. *Nat. Mater.* **2005**, *4*, 435.
3. Anderson, N. A.; Lian, T. *Annu. Rev. Phys. Chem.* **2005**, *56*, 491.
4. Laferrière, M.; Galian, R. E.; Maurel, V.; Scaiano, J. C. *Chem. Commun.* **2006**, 257.
5. Maurel, V.; Laferrière, M.; Billone, P.; Godin, R.; Scaiano, J. C. *J. Phys. Chem. B* **2006**, *110*, 16353.

6. Clarke, S. J.; Hollmann, C. A.; Zhang, Z.; Suffern, D.; Bradforth, S. E.; Dimitrijevic, N. M.; Minarik, W. G.; Nadeau, J. L. *Nat. Mater.* **2006**, *5*, 409.
7. Katari, J. E. B.; Colvin, V. L.; Alivisatos, A. P. *J. Phys. Chem.*, **1994**, *98*, 4109.
8. Kloepper, J. A.; Bradforth, S. E.; Nadeau, J. L. *J. Phys. Chem. B* **2005**, *109*, 9996.
9. Dabbousi, B. O.; Rodriguez-Viejo, J.; Mikulec, F. V.; Heine, J. R.; Mattoussi, H.; Ober, R.; Jensen, K. F.; Bawendi, M. G. *J. Phys. Chem. B* **1997**, *101*, 9463.
10. Peng, X.; Schlamp, M. C.; Kadavanich, A. V.; Alivisatos, A. P. *J. Am. Chem. Soc.* **1997**, *119*, 7019.
11. Reiss, P.; Bleuse, J.; Pron, A. *Nano Lett.* **2002**, *2*, 781.
12. Peng, X. A.; Peng, X. G. *J. Am. Chem. Soc.* **2001**, *123*, 183.
13. Derfus, A. M.; Chan, W. C. W.; Bhatia, S. N. *Nano Lett.* **2004**, *4*, 11.
14. Kuno, M.; Lee, J. K.; Dabbousi, B. O.; Mikulec, F. V.; Bawendi, M. G. *J. Chem. Phys.* **1997**, *106*, 9869.
15. Baranov, A. V.; Rakovich, Yu. P.; Donegan, J. F.; Perova, T. S.; Moore, R. A.; Talapin, D. V.; Rogach, A. L.; Masumoto, Y.; Nabiev, I. *Phys. Rev. B* **2003**, *68*, 165306/1.
16. Lu, L.; Xu, X.; Liang, W.; Lu, H. *J. Phys.: Condens. Matter.* **2007**, *19*, 406221.

17. Lange, H.; Machón, M.; Artemyev, M.; Woggon, U.; Thomsen, C. *Phys. Stat. Sol. Rapid Research Letters*, **2007**, *1*, 274.
18. Grabolle, M.; Ziegler, J.; Merkulov, A.; Nann, T.; Resch-genger, U. *Ann. N. Y. Acad. Sci.* **2008**, *1130*, 235.
19. Klimov, V. I. *Los Alamos Science*, **2003**, *28*, 214.
20. Yu, W.; Qu, L.; Guo, W.; Peng, X. *Chem. Mater.* **2003**, *15*, 2854.
21. Patterson, A. L. *Phy. Rev.* **1939**, *56*, 978.
22. Kissinger, N. J. S.; Jayachandran, M.; Perumal, K.; Raja, S. *Bull. Mater. Sci.*, **2007**, *30*, 547.
23. Ge, J.; Xu, S.; Zhuang, J.; Wang, X.; Peng, Q.; Li, Y. *Inorg. Chem.* **2006**, *45*, 4922.
24. Burda, C.; Green, T. C.; Link, S.; El-Sayed, M. A. *J. Phys. Chem. B* **1999**, *103*, 1783.
25. Kochi, J. K.; Sun, D.; Rosokha, S. V. *J. Am. Chem. Soc.* **2004**, *126*, 1388.
26. Landes, C.; Burda, C.; Braun, M.; El-Sayed, M. A. *J. Phys. Chem. B* **2001**, *105*, 2981.
27. Sharma, S. N.; Pillai, Z. S.; Kamat, P. V. *J. Phys. Chem. B* **2003**, *107*, 10088.
28. Matsui, M.; Miyamoto, Y.; Shibata, K.; Takase, Y. *Bull. Chem. Soc. Jpn.* **1984**, *57*, 2526-2530.
29. Kavarnos, G. J. *Fundamentals of Photoinduced Electron Transfer*. VCH; New York, **1993**.

30. Wan, J.; Ferreira, A.; Xia, W.; Chow, C. H.; Takechi, K.; Kamat, P. V.; Jones, G.; Vullev, V. I. *J. Photochem. Photobiol., A* **2008**, *197*, 364.
31. Beek, R. V.; Zoombelt, A. P.; Jenneskens, L. W.; vanWalree, C. A.; Mello Doneg, C. D.; Veldman, D.; Janssen, R. A. J. *Chem. Eur. J.* **2006**, *12*, 8075.
32. Li, L. S.; Pradhan, N.; Wang, Y.; Peng, X. *Nano Lett.* **2004**, *4*, 2261.
33. Jin, W. J.; Fernández-Argüelles, M. T.; Costa-Fernández, J. M.; Pereiro, R.; Sanz-Medel, A. *Chem. Commun.* **2005**, 883.
34. Chestnoy, N.; Harris, T. D.; Hull, R.; Brus L. E. *J. Phys. Chem.* **1986**, *90*, 3393.
35. Nirmal, M.; Brus, L. *Acc. Chem. Res.* **1999**, *32*, 407.
36. Turro, N. J. *Modern Molecular Photochemistry*. Benjamin Cummings Publishing Co.: Menlo Park, CA, **1978**.
37. Zelent, B.; Kusba, J.; Gryczynski, I.; Johnson, M. L.; Lakowicz, J. R. *J. Phys. Chem.* **1996**, *100*, 18592.
38. Eftink, M. R.; Ghiron, C. A. *J. Phys. Chem.* **1976**, *80*, 486.
39. Noyes, R. M. *Prog. React. Kinet.* **1961**, *1*, 131.
40. Sakaguchi, M.; Hu, M.; Kevan, L. *J. Phys. Chem.* **1990**, *94*, 870- 874.

Silica Overcoated CdSe Quantum Dots for Biological Applications

Abstract

Silica overcoated, water soluble CdSe QDs were synthesized and characterized and carried out its *in vitro* cytotoxicity analysis. The two-photon absorption (TPA) properties of silica overcoated QDs were investigated in detail and their potential use in cell imaging was explored. Trioctylphosphine oxide (TOPO) capped CdSe QDs synthesized in organic medium was made water soluble by overcoating with silica shell using two different silica precursors: aminopropyl trimethoxysilane (APS) and tetraethyl orthosilicate (TEOS). CdSe QDs overcoated with TEOS yielded stable water soluble core-shell systems with high silica shell thickness, however their luminescence properties were found to be poor. In contrast, APS overcoated QDs were found to be luminescent with good quantum yield. Cytotoxicity analysis based on MTT assay in human bone marrow derived mesenchymal stem cells (hMSC), showed that silica coated CdSe QDs are cytocompatible in nanomolar levels. Multiphoton absorption studies showed that silanised QDs possess improved two-photon absorption (TPA) characteristics in water compared to the TOPO capped QDs in organic medium. This allowed the excitation of QDs in biological water window using near-infrared (NIR) radiation. These results indicate that silica overcoated CdSe QDs are useful for biological labeling, imaging and sensing applications.

3.1. Introduction

Quantum dots of II-VI and III-V semiconductors offer numerous applications in biomedical science, particularly for the detection of ions and molecules, drug and gene delivery, cellular imaging, diagnosis and treatment of diseases.¹⁻⁵ These systems possess unique properties compared to the conventional organic fluorophores; the most significant one is the size, shape and composition dependent optical properties.⁶ Broad absorption spectrum allows simultaneous excitation of various QDs using single excitation wavelength and the narrow luminescence of QDs allows multiple signal collection, avoiding spectral overlap. QDs possess higher molar extinction coefficient, large two-photon absorption cross section, high luminescence quantum yield and longer luminescence lifetime compared to conventional dyes. The longer lifetime is particularly useful for investigating living cells by eliminating autofluorescence. Large two-photon absorption cross section of QDs permits the use of NIR wavelength for excitation (imaging by exciting in the biological water window). Recent studies have been focused on the design of QD based bioprobes, which possess specific activity and their interactions with biomolecules.³ Among various II-VI and III-V semiconductor QDs, cadmium chalcogenides are widely investigated since the synthetic protocols for these systems are optimized. However, the cytotoxicity associated with these systems and the poor solubility in aqueous medium limits their use in biological applications.^{6a}

3.1.1. Toxicological Effect of Quantum Dots

As mentioned in the previous section, the cytotoxic effects of cadmium based QDs, is a major concern, particularly the use of these systems for *in vivo* studies.^{7a-c} The cytotoxic effect of bulk CdSe is well documented while the cytocompatibility of their ‘nano’ analogues is still under investigation. Cadmium and zinc have similar atomic structure and chemical behavior. However, the latter is considered as an essential element, while the former one is highly toxic having no (known) role in animal metabolism.^{7d} Recent reports indicate that the cadmium ions (Cd^{2+}) is responsible for the toxicological effects in cadmium chalcogenide based QDs.⁸ The surface of QD is susceptible to oxidation, unless properly protected, resulting in the release of free Cd^{2+} ions. This leads to cell death and these aspects were investigated in detail by Parak and coworkers (Figure 3.1).^{8a} The sulfhydryl group of critical mitochondrial proteins can take up the free cadmium ions in cell, leading to oxidative stress and mitochondrial malfunctioning, called as cadmium hepatotoxicity.⁹

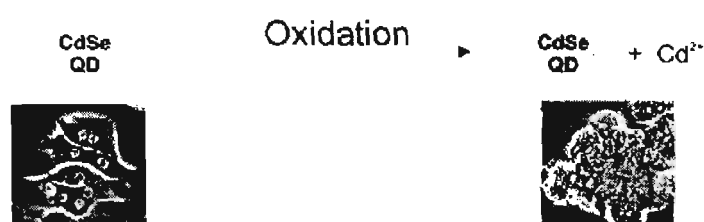
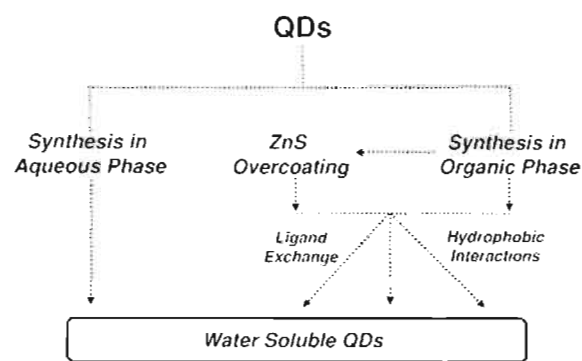


Figure 3.1. Photographs showing the Cd^{2+} induced (released from CdSe QDs) cell death, in liver culture model (adapted from reference 8b).

Any measure that can prevent the oxidation and escape of Cd^{2+} from QD surface can reduce the toxicity of CdSe QDs. For example, overcoating with ZnS is found to be an effective strategy for suppressing the cytotoxic effects of CdSe QDs (and enhancing the luminescence quantum yield).⁸ Apart from this, water solubility of QDs is an essential criterion for their use in biological systems. Various reports on the synthesis of water soluble QDs with reduced toxicological effects are discussed below.

3.1.2. Synthesis of Water Soluble QDs

Highly monodisperse QDs can be prepared by following high temperature organometallic synthesis; however, their solubility is limited to nonpolar medium. These QDs can be made soluble in water by exchanging with ligands having hydrophilic moiety. Alternatively, QDs can be directly synthesized in water, but the monodispersity is low compared to the former method. Various approaches for the synthesis of water soluble QDs are summarized in Figure 3.2.¹⁰ Among these, the most recommended method is silanisation, where QDs are overcoated with a silica shell.^{10a} The cytotoxicity effects are reduced, since the core constituents are well protected inside the silica shell.¹¹ Silica coating based on ‘reverse microemulsion’ method is the most versatile approach which was developed simultaneously by Ying and coworkers¹² and Nann and coworkers.¹³



3.2. A schematic representation of various strategies towards water soluble QDs.

3.1.3. Quantum Dots for Multiphoton Fluorescence Imaging

In vivo bioimaging tools are mainly been hampered by poor tissue penetration of visible light. In contrast, NIR radiation has less scattering and absorption by biological tissue, eliminating interference from autofluorescence. Optical imaging using NIR radiation in the biological water window (Figure 3.3) is more appropriate for larger organisms (and for deep tissue imaging).¹⁴

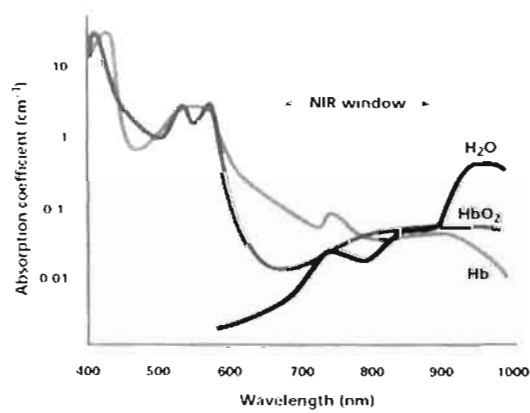


Figure 3.3. Biological water (NIR) window: the absorbance by biological molecules is minimum compared to the visible region. (adapted from reference 14)

Multiphoton imaging is a novel technique wherein biological samples are excited using NIR wavelengths, offering local excitation at the focal point of the objective with least specimen damage. Multiphoton absorption is a nonlinear process resulting from the simultaneous absorption (no intermediate state exists) of more than one photon of longer wavelength ($h\nu_2$) by the chromophore as illustrated in Figure 3.4. Whether it is a single photon or multiphoton process, the luminescence ($h\nu_{pl}$) is independent of the mode of the excitation. Various aspects on multiphoton processes and its applications are summarized in recent reviews.¹⁵ Other than photostability and brightness, QDs also possess excellent multiphoton absorption (MPA) characteristics, two or three orders higher than conventional fluorophores. These aspects make QDs a promising candidate for multiphoton induced fluorescence imaging.¹⁶

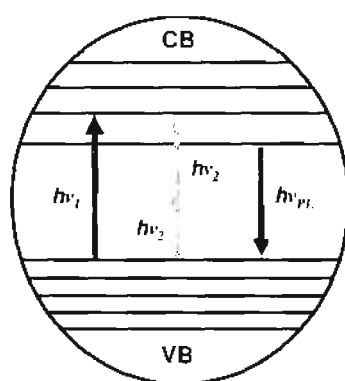


Figure 3.4. Two photon absorption process in QDs; total energy is conserved as $h\nu_1 = 2h\nu_2$. Also, the luminescence is independent of mode of excitation process.

In the present study, we have developed a modified 'reverse microemulsion' procedure which was adopted for overcoating CdSe QDs with silica. Details of the synthesis and characterization are presented in the subsequent sections. Further, the cytotoxicity analysis and nonlinear optical properties of silica overcoated CdSe QDs were investigated and the results are also presented.

3.2. Results and Discussion

3.2.1. Overcoating of CdSe QDs with Silica

CdSe QDs capped with TOPO was synthesized by following the high temperature organometallic synthesis method as described in Chapter 2. Absorption and luminescence spectra of QDs are presented in Figure 3.6. The absorption profile showed the characteristic excitonic peaks and the luminescence spectrum was found to be narrow (FWHM ~35 nm). HRTEM results confirmed that the QDs are monodisperse, having an average size of 4.3 nm (Figure 3.7A). QDs obtained were found to be soluble in nonpolar solvents.

QDs were further overcoated with silica shell by following a 'reverse microemulsion method' to render water solubility and to impart cytocompatibility. (Details of the procedure adopted for overcoating with silica are provided in the experimental section). TOPO layer on CdSe was first exchanged with silica precursors and then introduced into a

microemulsion system, formed by cyclohexane as oil phase and igeal as the surfactant. After the place exchange reaction, the pH of the medium was increased. The alkoxy groups of silica precursors initially undergo hydrolysis followed by condensation to yield silica shell (Stöber process) and the core-shell QDs thus obtained were found to be soluble in aqueous media. A schematic representation of the overall process is given in Figure 3.5.

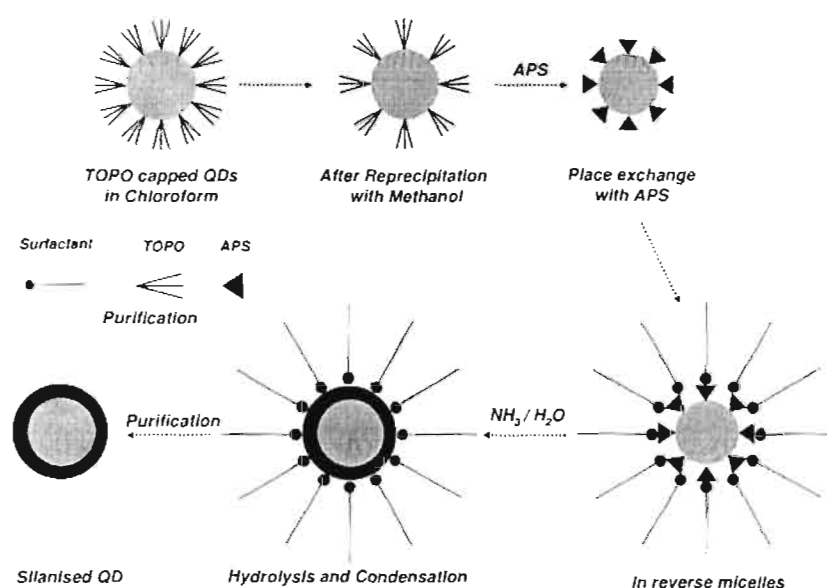


Figure 3.5. A schematic representation of the silanisation procedure adopted.

In the present study, silica overcoated QDs were prepared using tetraethyl orthosilicate (TEOS) or aminopropyl silane (APS) as silica precursor and both yielded water soluble nanohybrid systems. However, their photophysical properties showed considerable difference. Overcoated QDs were characterized using various spectroscopic techniques and transmission electron microscope (TEM) as presented below.

Absorption spectral features of silica overcoated CdSe QDs, prepared using TEOS as precursor were found to be similar to that of TOPO capped QDs. These results indicate that the overall size and electronic structure of the QDs were not affected upon overcoating (Figure 3.6A). However, the overcoating results in a dramatic quenching in the luminescence of QDs (Figure 3.6B). This is attributed to the poor passivation of QD surface by the TEOS, on removal of TOPO.¹⁷

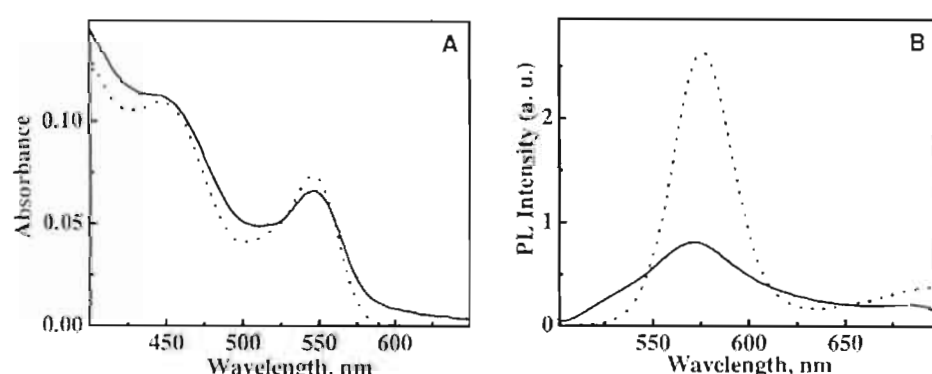


Figure 3.6. (A) Absorption and (B) luminescence spectra of CdSe QDs: TOPO capped (dotted trace) and silica (TEOS) overcoated (solid trace).

HRTEM images of TOPO capped and silica overcoated CdSe QDs are presented in Figure 3.7. From the TEM images, it was observed that more than one CdSe QDs are entrapped in the silica shell and the overall diameter of the nanohybrid system was found to be ~40 nm. Even though silica overcoating provided solubility in water, the poor luminescence properties and large shell thickness limit their use in biological imaging and sensing.

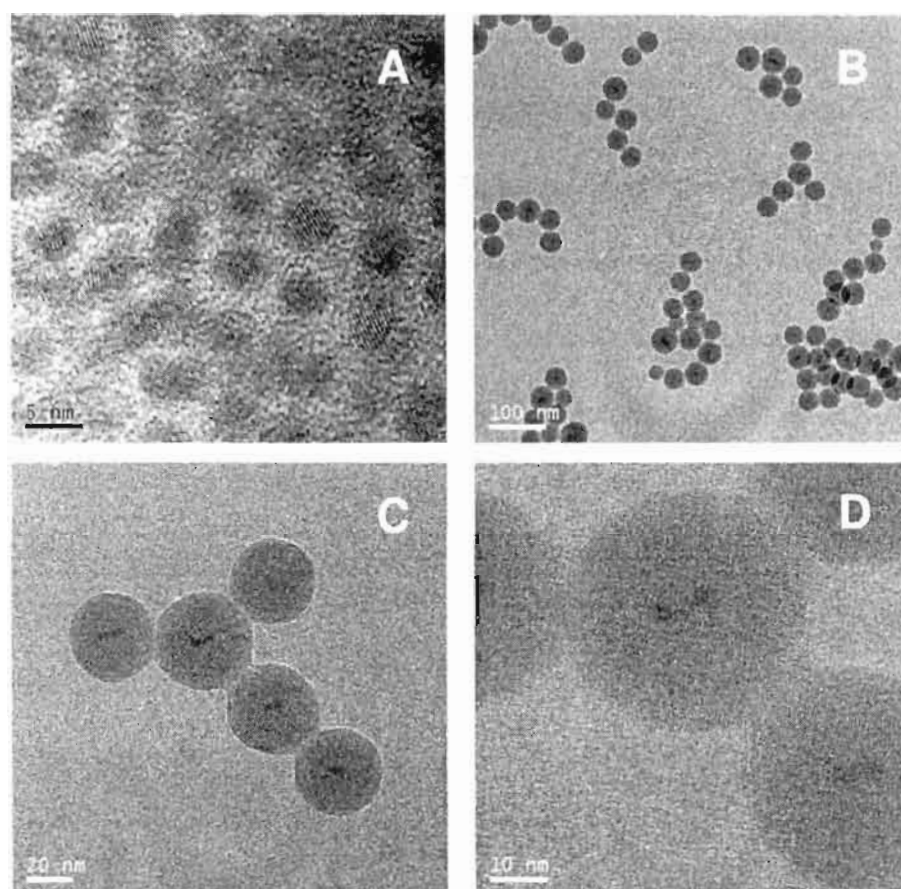


Figure 3.7. HRTEM images of CdSe QDs (4.3 nm) (A) TOPO capped and (B-D) silica (TEOS) overcoated.

Further, we have used aminopropyl silane as precursor for overcoating, which yielded highly luminescent and water soluble CdSe QDs with excellent shelf life. Details of the synthesis and purification are presented in the experimental section. The absorption and luminescence spectral profiles of the silica overcoated CdSe QDs, using APS as precursor, are similar to TOPO capped QDs (Figure 3.8). Overcoated QDs were luminescent and stable under physiological buffer conditions (pH 7.3), which make them a promising candidate for biological applications. Photophysical properties of CdSe QDs

capped with TOPO and overcoated with silica are summarized in Table 3.1. A hypsochromic shift (4-7 nm) was observed in the absorption (first excitonic band) and in the luminescence maximum with an enhancement in luminescence yield upon overcoating (14% for silica overcoated and 9% for TOPO capped) with silica. Primary amines (due to their Lewis base character) are reported as good surface capping agents for CdSe QDs.¹⁸ The amino group in APS efficiently passivates the QD surface upon overcoating, eliminating shallow trap states and thereby facilitating the band edge luminescence exclusively. Thus the enhancement in the luminescence property may be attributed to the surface reconstruction and the formation of a thin silica shell. The full width at half maximum (FWHM) of the luminescence band before and after overcoating is estimated as 35 and 39 nm, respectively.

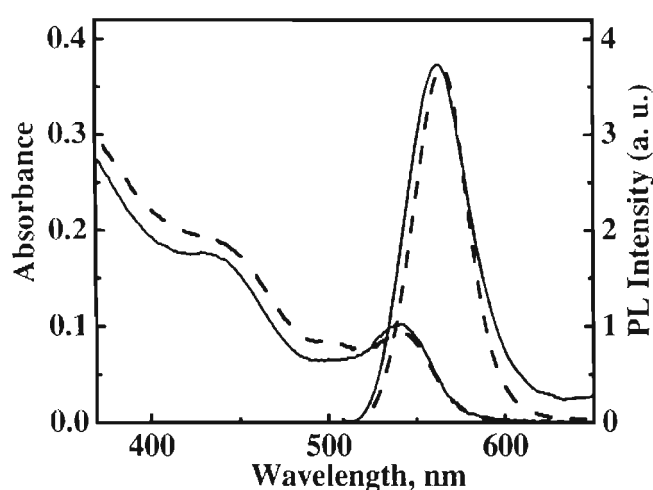


Figure 3.8. Absorption and luminescence spectra of CdSe QDs: (dotted trace) TOPO capped in chloroform and (solid trace) silica (APS) overcoated in PBS (pH 7.3).

Table 3.1. Comparison of photophysical properties of CdSe QDs capped with TOPO and overcoated with silica.

QD	First Excitonic Absorption Wavelength, nm	Luminescence Wavelength, nm	FWHM, nm	QY (%) (standard used: Rhodamine 6G)
CdSe/TOPO	551	565	35	09
CdSe/APS	547	557	39	14

A better idea about the size and distribution of the silica overcoated QDs can be obtained from the high resolution transmission electron microscope images presented in Figure 3.9. When APS was used as precursor for silica overcoating, the overall increase in size was found to be nominal (~1.5 nm). Based on the spectroscopic studies and TEM analysis, it is further concluded that silica overcoated QDs, using APS as precursor are superior in photophysical properties and possess uniform size distribution. In contrast, silica overcoated QDs, using TEOS as precursor, resulted in the formation of a thick shell and their photophysical properties were poor.

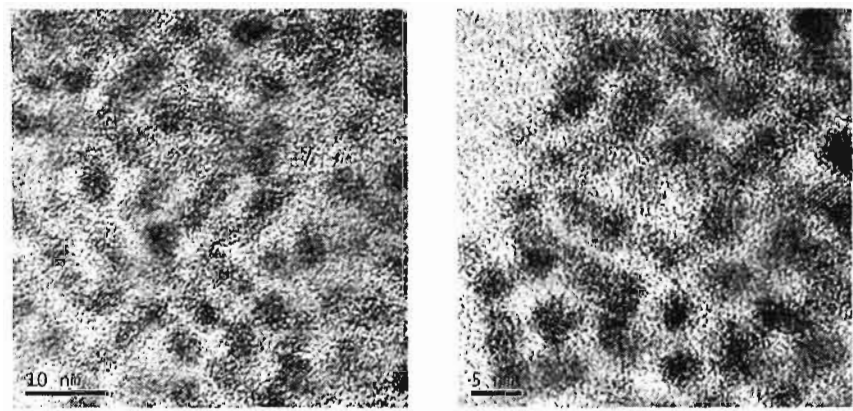


Figure 3.9. HRTEM images of silica (APS) overcoated CdSe QDs.

Place exchange of TOPO with APS on QD surface was further probed using FTIR (ATR) spectroscopy. FTIR spectrum of CdSe QDs before and after overcoating with silica is presented in Figure 3.10. Sharp peak at 1130 cm^{-1} is attributed to the P=O stretching band which is $\sim 20\text{ cm}^{-1}$ lower compared to free TOPO. This shift may be due to the noncovalent interaction of P=O to Cd^{2+} sites on the CdSe QD surface. The bands at 1466 cm^{-1} and at $2800\text{--}3000\text{ cm}^{-1}$ arise from the CH_2 bending and C-H stretching respectively, from the alkyl groups of TOPO. The peak at 1600 cm^{-1} is attributed to N-H bending mode from the octadecylamine used as a co-capping agent in the synthesis. Upon overcoating with APS, the peaks corresponding to TOPO disappeared with a concomitant increase in the intensity of the peak at 1600 cm^{-1} , corresponding to the amine bending mode. These results confirm the substitution of TOPO with APS.^{19a}

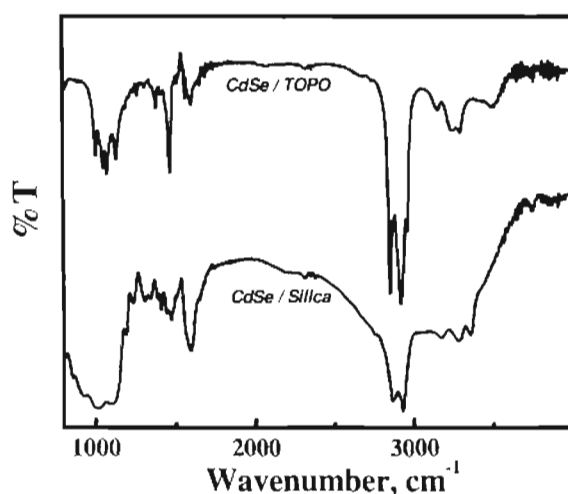


Figure 3.10. FTIR spectra of CdSe QDs before and after over coating with silica; disappearance of band at 1466 cm^{-1} and a change in the relative peak intensity at $\sim 2900\text{ cm}^{-1}$ (alkyl stretching) and at 1600 cm^{-1} (N-H bending) proves the substitution of TOPO with APS.

Energy dispersive X-ray spectroscopic technique (EDS) is an analytical tool used for the elemental analysis and chemical characterization of nanomaterials. In the present study, we have used EDS for probing the substitution of TOPO layer by silica shell and these results are presented in Figure 3.11. EDS spectra of both TOPO capped and silica overcoated CdSe QDs showed characteristic ' $K\alpha$ ' and ' $L\alpha$ ' energy lines corresponding to cadmium and selenium. For silica overcoated QDs, the signal corresponding to phosphorous (2.01 keV) was replaced with that of silicon at 1.74 keV, ensuring the exchange of TOPO with APS on the QD surface.^{19b}

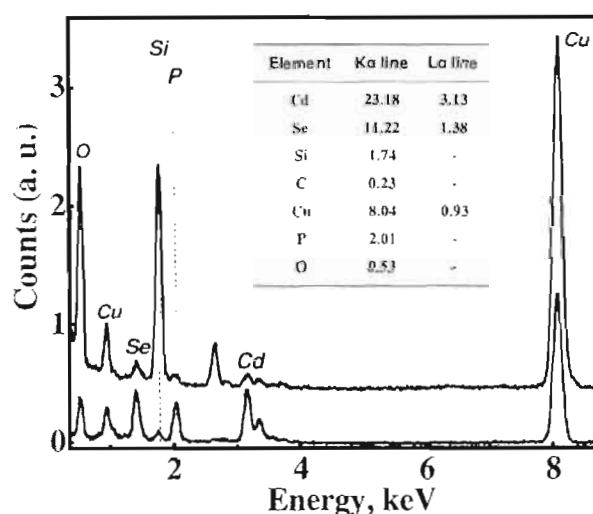


Figure 3.11. EDS spectra of CdSe QDs. (Bottom trace) TOPO capped (Top trace) silica overcoated.

Above results suggest that we have succeeded in synthesizing water soluble and luminescent core-shell QDs by overcoating with silica, using APS as precursor. Silanised QDs were found to be stable for weeks in PBS buffer (pH 7.3) and the luminescence properties were found to be insensitive to pH

as well as the ionic strength of the medium (Figure 3.19, Experimental Section). Toxicological effects and nonlinear optical properties of QDs overcoated with silica, using APS as precursor is presented below.

3.2.2. *In Vitro* Cell Cytotoxicity Studies

The cytotoxicity of silica overcoated CdSe QDs (prepared using APS as precursor) was evaluated in human mesenchymal stem cells (hMSC) with MTT viability assay.²⁰ It is a colourimetry based assay, wherein the live cells reduce MTT to a colored product, formazan. The formazan formed can be quantified using UV-Vis absorption spectroscopy, which in turn gives the amount of live cells. Briefly, the protocol involves doping the cells with QDs and the cell viability was monitored as a function of QD concentration and time (Detailed description of the method is provided in the experimental section). In a typical procedure, 1×10^4 cells were seeded onto 96 well plate (NUNC). After 7 days in culture, 100 μ L of MTT solution (5 mg/mL stock in PBS) was added to each of these wells and incubated for 4 h at 37 °C. The crystals formed were then dissolved in isopropanol and the absorbance at 540 nm was measured using an ELISA plate reader. Figure 3.12 shows the cell viability in terms of metabolic activity, obtained from MTT assay. On treating with live cells under identical conditions, it was observed that the silica overcoated QDs were least cytotoxic, whereas TOPO capped QDs induced cell death (Figure 3.13). This is attributed to the less leakage of CdSe core constituents in to the cell medium, compared to the TOPO capped QDs. These

results, based on *in vitro* studies suggest that the silica overcoating substantially reduces the cytotoxic effects, making these QDs suitable for biological applications. Further, we have used these QDs for labeling and imaging of cells, under a fluorescence microscope (DM 6000, Leica). A representative image of mesenchymal stem cells mixed with red emitting silica overcoated CdSe QDs is presented in Figure 3.13.

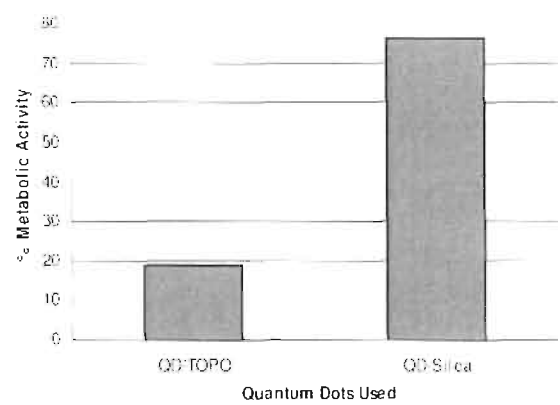


Figure 3.12. Comparison of cytotoxic effects of bare QDs and silica over coated CdSe QDs based on MTT assay (after 7 days).



Figure 3.13. Mesenchymal stem cells added with red emitting silica overcoated CdSe QDs.

3.2.3. Two-Photon Absorption Studies

The multiphoton absorption characteristics of CdSe QDs capped with TOPO in toluene and silica overcoated (using APS as precursor) in water was investigated as follows. QD samples were excited using femtosecond (fs) laser pulse (pulse width <100 fs) at three different wavelengths (720, 800 and 820 nm). The two-photon absorption cross-section (σ_{2PA}) was calculated using fluorescein in water (pH 13) as the reference (σ_{2PA} 36 GM at 800 nm).²¹

A comparison of luminescence spectra of TOPO capped QDs in toluene, recorded by exciting the sample at 400 nm (using xenon arc lamp) and at 800 nm (using fs laser pulse) is presented in Figure 3.14. Irrespective of the excitation wavelength, the luminescence spectra was found to be identical for QDs, with a luminescence maximum at ~575 nm. From the absorption spectrum (inset, Figure 3.14), it is clear that the QDs are not having any absorption at 800 nm. This indicates that the luminescence obtained by exciting at 800 nm is involving a multiphoton process.

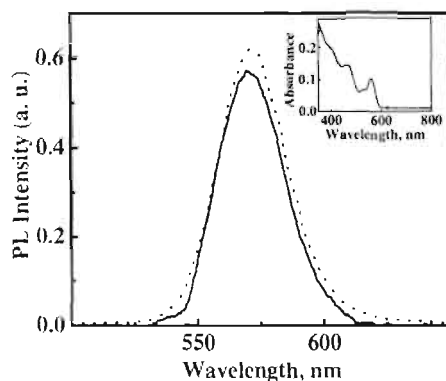


Figure 3.14. Luminescence spectra of TOPO capped CdSe QDs in toluene: (dotted trace) excited at 400 and (solid trace) excited at 800 nm. (inset) Absorption spectrum.

Luminescence intensity of the QDs was monitored as a function of excitation energy to obtain a better understanding on the number of photons absorbed by the sample, while exciting at longer wavelengths. QDs were excited at 800 nm, using laser pump power (average power = pulse energy \times repetition rate) varying from 120 to 700 mW, and the results are shown in Figure 3.15A. For a comparison, experiments were done at identical conditions with a standard dye-fluorescein (Figure 3.15B). It was found that the luminescence intensity of the CdSe QDs (and the fluorescein) decreased on lowering the excitation energy. The extent of multiphoton excitation is proportional to the intensity raised to the n^{th} power, where n represents the number of photons absorbed.²² A logarithmic plot of luminescence intensity as a function of excitation energy gave a straight line and the number of photons absorbed was extracted from the slope (Figures 3.16A,B). For QDs and fluorescein, slope values obtained are 1.85 and 2.06 respectively, indicating that in both cases the luminescence is by a two-photon excitation process.

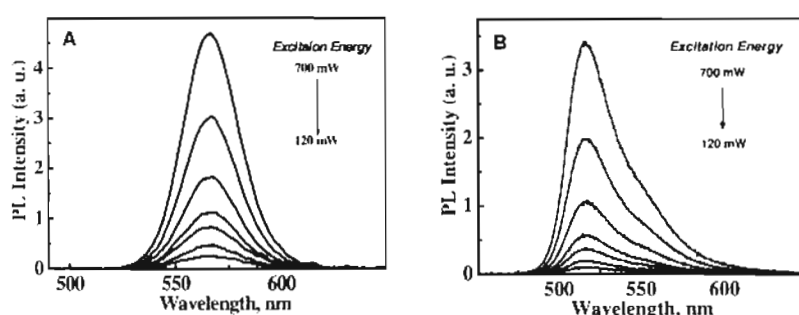


Figure 3.15. Two-photon induced luminescence spectra of (A) CdSe QDs, capped with TOPO in toluene (B) Fluorescein dye in 0.1 N NaOH, excited using 800 nm laser pulse at various laser powers.

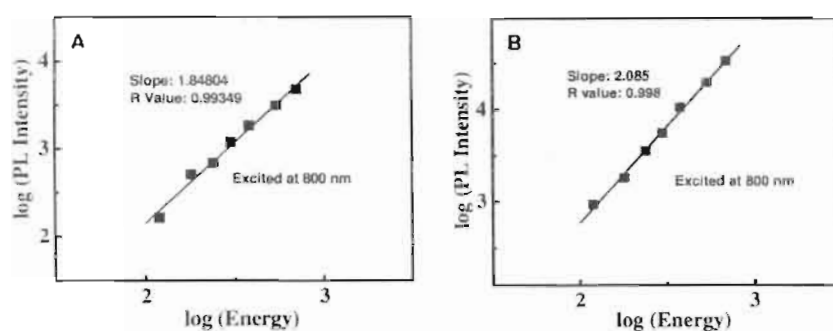


Figure 3.16. Logarithmic plots of PL intensity against excitation energy for (A) CdSe QDs, capped with TOPO and (B) Fluorescein dye.

Further, we have extended the experiments with silica overcoated CdSe QDs in water and the results are given in Figure 3.17. Similar to TOPO capped QDs, silica overcoated QDs also showed identical luminescence spectra, when excited at 400 and 800 nm. This confirms that the QDs possess same electronic structure before and after overcoating with silica, undergoing multiphoton induced excitation process.

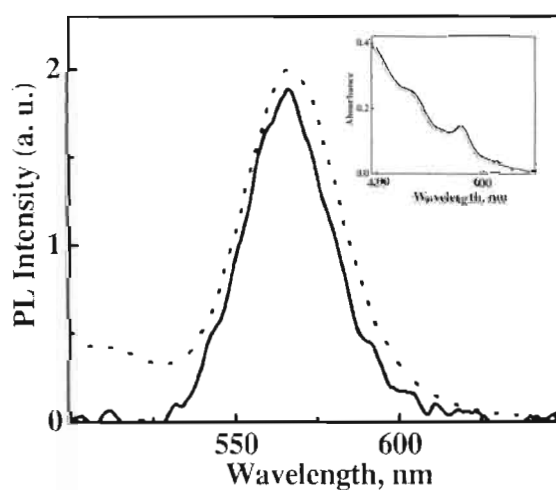


Figure 3.17. Luminescence spectra of silica overcoated CdSe QDs in PBS, excited at 400 (dotted line) and at 800 nm (solid line). (inset) Absorption spectrum.

Luminescence intensity of silanised QDs was found to decrease on lowering the excitation energy (at 800 nm) as obtained in case of TOPO capped QDs. The respective logarithmic plot (\log (incident energy) vs. \log (luminescence intensity)) showed that the luminescence obtained is by a two-photon induced excitation process. A comparison of two-photon induced luminescence spectra of CdSe QDs, capped with TOPO and overcoated with silica is shown in the Figure 3.18A-C. The samples were excited at 780, 800 and 820 nm with fs laser pulse of identical power (700 mW).

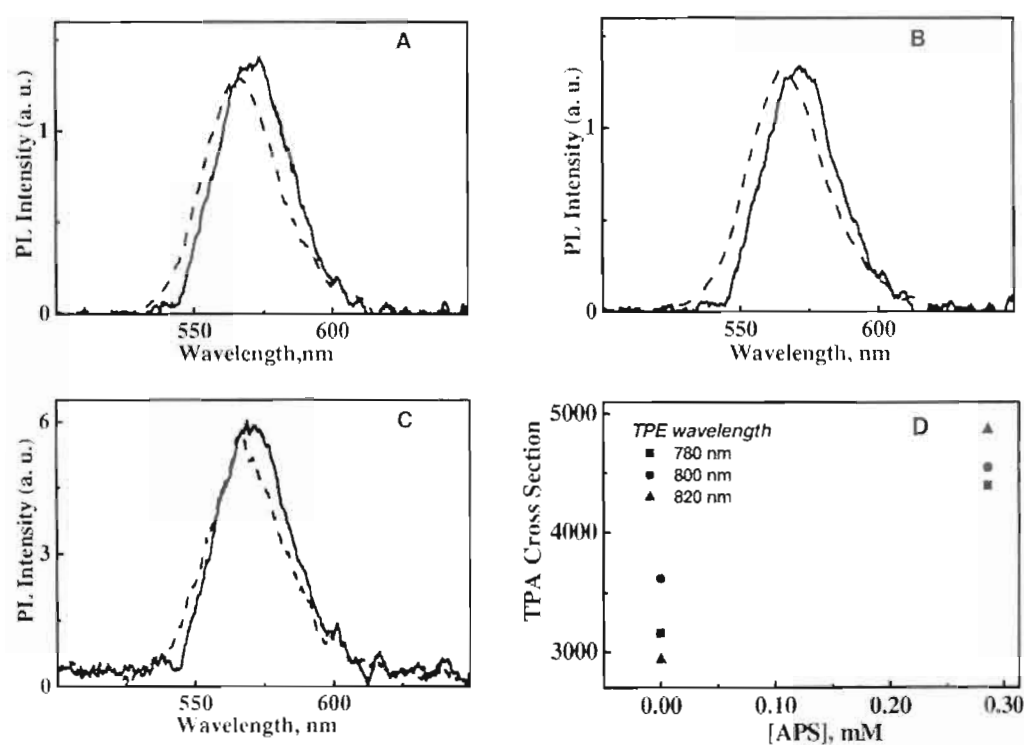


Figure 3.18. Two-photon induced luminescence spectra of CdSe QDs, capped with TOPO in toluene (dashed line) and silica overcoated in aqueous media (solid line), excited at (A) 780, (B) 800 and (C) 820 nm with (fs) laser pulse. (D) A comparison of two-photon absorption cross-sections for TOPO capped and silica overcoated CdSe QDs.

The two-photon absorption cross section (σ_{2PA}) was estimated using fluorescein as reference, using the relation given below (equation 3.1).²³

$$\sigma_{2PA} = \sigma_r (F \cdot C_r \cdot \eta_r \cdot \phi_r) / (F_r \cdot C \cdot \eta \cdot \phi) \tag{3.1}$$

where ' σ_{2PA} ' stands for TPA cross section, 'F' for the luminescence peak area, 'C' for the concentration, ' η ' for the refractive index of the solvents, ' ϕ ' for single photon excited quantum yield and the subscript 'r' corresponds to reference used. The results obtained for CdSe QDs capped with TOPO and silica is given in the Figure 3.18D and the values are given in Table 3.2.

Table 3.2. Comparison of two-photon absorption cross sections for TOPO capped and silica overcoated CdSe QDs.

Sample	σ_{2PA} (GM)*		
	780 nm	800 nm	820 nm
CdSe/TOPO	3160	3620	2937
CdSe/APS	4391	4544	4864

*1 GM = 10^{-50} (cm⁴ s/photon)

It is observed that the two-photon absorption cross section of silica coated CdSe QDs is higher compared to the corresponding TOPO coated QDs. It is attributed to the effective QD surface passivation by the amino groups of the silica precursor used, compared to TOPO.

3.3. Conclusions

A modified protocol for overcoating silica on CdSe QDs, based on reverse microemulsion method was developed. Among two silica precursors used (TEOS and APS), APS yielded stable QDs in water, with good luminescence quantum yield. Further, cytotoxicity analysis with human mesenchymal stem cells (hMSC), by following MTT assay showed that silica overcoated CdSe QDs are cytocompatible. Based on nonlinear optical studies it is concluded that the silanised QDs possess better two-photon absorption properties compared to the TOPO analogues. In conclusion, silica overcoated CdSe QDs are ideally suited for optical imaging using NIR radiation in the biological water window and an extremely versatile candidate for various biological investigations.

3.4. Experimental Section

3.4.1. Materials and Methods

General details of solvents, reagents and equipments used for synthesis, characterisation and studies are provided in the Experimental section. Aminopropyl trimethoxysilane (APS) and tetraethyl orthosilicate (TEOS) and igepal CO-520 were purchased from Aldrich and used as such. PBS buffer (pH 7.3) was prepared by diluting 2 mL of the stock solution (sodium dihydrogen phosphate (0.100 g) and disodium hydrogen phosphate (0.620 g) in 10 mL distilled water) after adding sodium chloride (0.870 g) to 100 mL with distilled water. UV-Vis absorbance spectrum for MTT assay

was recorded on a Hidex-Chameleon spectrophotometer. Cell images were captured using DM6000 (Lieca) fluorescence microscope. Multiphoton excitation experiments were performed using Ti:Sapphire pulsed laser source 'Millennia V' (pulse width <100 fs, repetition rate 82 MHz), equipped with CCD detector (CDP 2022S) and the signals were deconvoluted using optics spectra suit software. Two-photon absorption cross section was obtained by comparison with fluorescein dye in 0.1N NaOH (pH 13), as reference.

3.4.2. Silica Overcoating of CdSe QDs Using TEOS

Igepal CO-520 (1.3 mL) was dissolved in cyclohexane (10 mL) by stirring under inert atmosphere for 30 minutes. TOPO capped CdSe QDs in chloroform was added drop wise (400 μ L, \sim 14 μ M) along with TEOS (0.075 g, 0.36 mM) over a period of 30 minutes under stirring. To this mixture, ammonia solution (150 μ L, 33 wt %) was added drop wise and stirring was continued for 24 hours. The silanised QDs obtained were precipitated with methanol, washed once with butanol and ethanol and redissolved in distilled water.

3.4.3. Silica Overcoating of CdSe QDs using APS

A mixture of TOPO capped CdSe QDs in chloroform (400 μ L, \sim 14 μ M) and APS (0.075 g, 0.36 mM) was vortexed for thirty minutes, in an inert atmosphere. This mixture was added to Igepal CO-520 (1.3 mL) in cyclohexane (10 mL) and stirred for 30 minutes under dry conditions. Again

ammonia solution (150 μ L, 33 wt%) was added drop wise and the stirring was continued for 24 hours. The silanised QDs were appeared as globules, sticking onto the walls of the glass vial, which was purified by washing with dry chloroform. QDs were redissolved in PBS buffer (150 mM, pH 7.3) for studies.

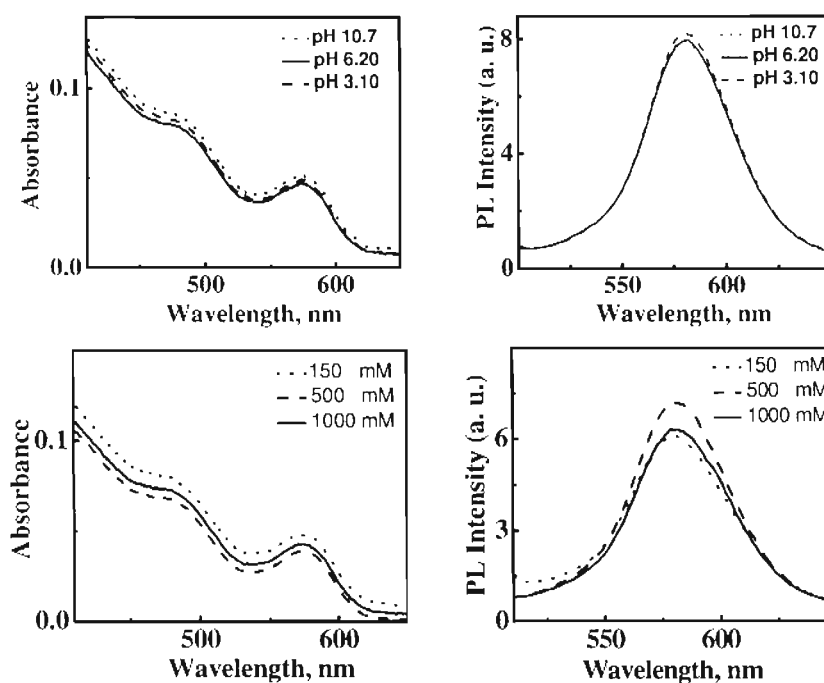


Figure 3.19. Effect of pH (top row) and ionic strength (bottom row) of the medium on absorption and luminescence spectra of silanised (APS) CdSe QDs.

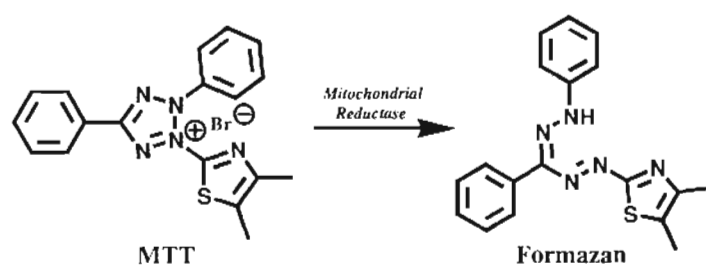
3.4.4. Cell Culturing

Bone marrow was collected from volunteers after getting consent. Mesenchymal stem cells were isolated and expanded in culture flasks (T25-NUNC) with alpha MEM supplemented with 10% FBS, 100 units/mL of penicillin and 100 μ g/mL of streptomycin (Gibco, India), incubated at 37 $^{\circ}$ C

in humid atmosphere and 5% CO₂. The medium was changed after 3 days to remove non-adherent cells and subsequently renewed twice a week. After attaining 80% confluence cells were trypsinised and fifth passage cells were used for experiments.

3.4.5. MTT Assay

A universally accepted method for quantifying the cell poisoning effect is MTT assay, a colourimetric measure of mitochondrial activity, which is directly correlated to the cell viability.²⁰ Metabolically active cells (live cells) are able to reduce the MTT, a tetrazolium salt [(3-[4,5-dimethylthiazol-2-yl]-2,5-diphenyltetrazolium bromide)], to colored formazan crystals, while dead cells do not. Formazan was dissolved in appropriate solvent and the absorbance (at 540 nm), was measured, which gives the concentration of formazan produced and in turn the amount of live cells.



Scheme 3.1. Scheme showing the reduction of MTT to formazan.

3.5. References

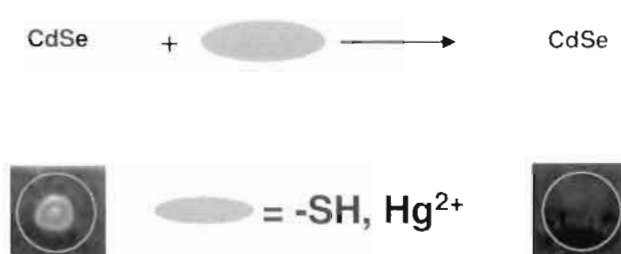
1. De, M.; Ghosh, P. S.; Rotello, V. M. *Adv. Mater.* **2008**, 20, 4225.
2. Sokolova, V.; Epple, M. *Angew. Chem. Int. Ed.* **2008**, 47, 1382.

3. (a) Biju, V.; Itoh, T.; Anas, A.; Sujith, A.; Ishikawa, M. *Anal. Bioanal. Chem.* **2008**, *391*, 2469. (b) Yu, W. W.; Chang, E.; Drezek, R.; Colvin, V. L. *Biochem. Biophys. Res. Commun.* **2006**, *348*, 781.
4. (a) Katz, E.; Willner, I. *Angew. Chem. Int. Ed.* **2004**, *43*, 6042. (b) Michalet, X.; Pinaud, F.; Lacoste, T. D.; Dahan, M.; Bruchez, M. P.; Alivisatos, A. P.; Weiss, S. *Single Mol.* **2001**, *2*, 261.
5. Niemeyer, C. M. *Angew. Chem. Int. Ed.* **2001**, *40*, 4128.
6. (a) Smith, A. M.; Nie, S. *Analyst* **2004**, *129*, 672. (b) Bailey, R. E.; Smith, A. M.; Nie, S. *Physica E* **2004**, *25*, 1.
7. (a) Tsay, J. M.; Michalet, X. *Chemistry and Biology* **2005**, *12*, 1159. (b) Klostranec, J. M.; Chan, W. C. W. *Adv. Mater.* **2006**, *18*, 1953. (c) Hardman, R. *Environ. Health Perspect.* **2006**, *114*, 165. (d) Berman, E. *Toxic Metals and Analysis* Heydon and Sons Ltd., London, **1980**.
8. (a) Kirchner, C.; Liedl, T.; Kudera, S.; Pellegrino, T.; Javier, A. M.; Gaub, H. E.; Stölzle, S.; Fertig, N.; Parak, W. J. *Nano Lett.* **2005**, *5*, 331. (b) Derfus, A. M.; Chan, W.C.W.; Bhatia, S. N. *Nano Lett.* **2004**, *4*, 11.
9. Rikans, L. E.; Yamano, T. *J. Biochem. Mol. Toxicol.* **2000**, *14*, 110.
10. (a) Pellegrino, T.; Kudera, S.; Liedl, T.; Javier, A. M.; Manna, L.; Parak, W. J. *Small* **2005**, *1*, 48. (b) Caruso, F. *Adv. Mater.* **2001**, *13*, 11.
11. Tan, T. T.; Selvan, S. T.; Zhao, L.; Gao, S.; Ying, J. Y. *Chem. Mater.* **2007**, *19*, 3112.

12. Selvan, S. T.; Patra, P. K.; Ang, C. Y.; Ying, J. Y. *Angew. Chem. Int. Ed.* **2007**, *46*, 2448.
13. Darbandi, M.; Thomann, R.; Nann, T. *Chem. Mater.* **2005**, *17*, 5720.
14. Weissleder, R. *Nat. Biotechnol.* **2001**, *19*, 316.
15. (a) He, G. S.; Tan, L.-S.; Zheng, Q.; Prasad, P. N. *Chem. Rev.* **2008**, *108*, 1245. (b) Ma, Y. F. J.; Lee, S. H. *Mater. Sci. Rep.* **1993**, *9*, 53.
16. Larson, D. R.; Zipfel, W. R.; Williams, R. M.; Clark, S. W.; Bruchez, M. P.; Wise, F. W.; Webb, W. W. *Science* **2003**, *300*, 1434.
17. Koole, R.; van Schooneveld, M. M.; Hilhorst, J.; de Mello Donegá, C.; 't Hart, D. C.; van Blaaderen, A.; Vanmaekelbergh, D.; Meijerink, A. *Chem. Mater.* **2008**, *20*, 2503.
18. (a) Nosea, K.; Fujitaa, H.; Omataa, T.; Otsuka-Yao-Matsuoaa, S.; Nakamuraa, H.; Maeda, H. *J. Lumin.* **2007**, *126*, 21. (b) Foos, E. E.; Wilkinson, J.; Mäkinen, A. J.; Watkins, N. J.; Kafafi, Z. H.; Long, J. P. *Chem. Mater.* **2006**, *18*, 2886.
19. (a) Trindade, T.; O'Brien, P.; Zhang, X. *Chem. Mater.* **1997**, *9*, 523. (b) Ge, J.-P.; Xu, S.; Zhuang, J.; Wang, X.; Peng, Q.; Li, Y.-D. *Inorg. Chem.* **2006**, *45*, 4922.
20. David M. L.; Morgan, D. M. L.; *Polyamine Protocols* (Methods in Biology), **2008**, *79*, 179.
21. Albota, M. A.; Xu, C.; Webb, W. W. *Appl. Opt.* **1998**, *37*, 7352.

22. (a) Lakowicz, J. R. *Principles of Fluorescence Spectroscopy*; 3rd Edn. Springer: New York, **2006**. (b) Lakowicz, J. R. (Ed.) *Topics in Fluorescence Spectroscopy*; Volume 5, Plenum Press: New York, **1997**.
23. (a) Wang, L.; Tao, X.; Shi, J.; Yu, X.; Jiang, M. *J. Phys. Chem. B* **2006**, *110*, 19711. (b) Oulianov, D. A.; Tomov, I. V.; Dvornikov, A. S.; Rentzepis, P. M. *Opt. Commun.* **2001**, *19*, 235.

Silica Overcoated CdSe Quantum Dots as Sensors



Abstract

The use of silica overcoated CdSe QDs for the selective detection and quantification of (i) biologically important molecules under physiologically relevant conditions and (ii) trace quantities of Hg^{2+} ions in the presence of interfering metal ions have been demonstrated. Amino acids and peptides containing free sulfhydryl group (cysteine, homocysteine and glutathione) selectively quenched the luminescence of silica overcoated CdSe QDs by an electron transfer process. The ability of this core-shell nanohybrid system to detect free thiols, in the presence disulphides have been utilized for the estimation of free thiol content in human blood serum samples. Among the various metal ions, Hg^{2+} selectively quenched the emission of silanised QDs in aqueous medium with a concomitant bathochromic shift in the absorption and emission band. Mercuric ions react with CdSe QDs to yield quantum sized HgSe on its surface, which further modifies the band edge recombination process.

4.1. Introduction

Selective detection of biologically important molecules and environmentally toxic metal cations has been an active area of interest.^{1a} Most of the earlier sensing systems were based on organic molecules and inorganic complexes.^{1b} More recently, attention has been focused on the design of QD based hybrid systems for sensing applications, due to their fascinating optical properties, which are tunable with size and shape.^{1c-f} QDs can undergo electron or energy transfer process when bound to an analyte. The redox potential of QDs can be conveniently tuned by varying the size; i.e., QDs can act as an electron donor or acceptor without varying the chemical composition.^{1g,h} Photoexcitation of QDs results in the formation of electron-hole pair (exciton). Any process which can influence the radiative recombination of the electron and hole can alter the luminescence from the QDs. Analytes with appropriate redox potential can interact with QDs and scavenge the photogenerated electrons in the conduction band or holes in the valence band leading to reduced rate of electron-hole radiative recombination. A schematic illustration of various processes is provided in Figure 4.1., where ED and EA represent the electron donor and acceptor, respectively. To facilitate the electron or hole transfer, the redox level of (i) EA should be lower than the conduction band edge or (ii) ED should be higher than valence band edge of the QD.

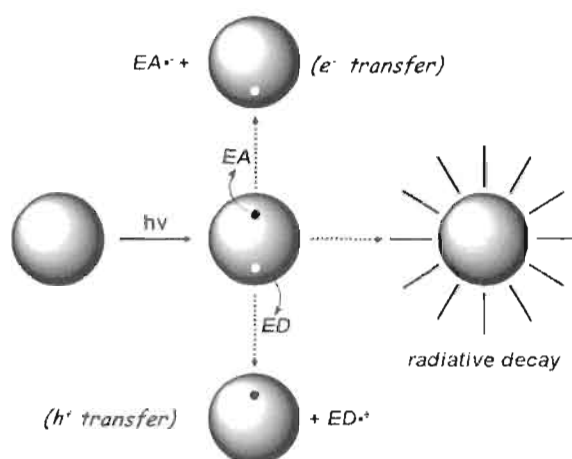


Figure 4.1. Illustration of various light induced electron transfer process in QDs. EA and ED represents analytes resulting in the suppression of QD luminescence.

A typical example was reported by Benson and coworkers for maltose sensing, where the QD luminescence was restored (switch on) upon analyte recognition (Figure 4.2).² Cadmium selenide QDs overcoated with ZnS (CdSe-ZnS) was conjugated to a Ru(II) complex functionalized with maltose binding protein (MBP). This hybrid QD possessed low luminescence due to electron injection from Ru(II) complex. Protein conformation varies upon binding with maltose and the electron transfer is attenuated as the Ru donor moves away from QD, restoring its luminescence. It is possible to tune the electron transfer process between QD and donor/acceptor, by varying the distance and several systems based on this concept have been reported.³

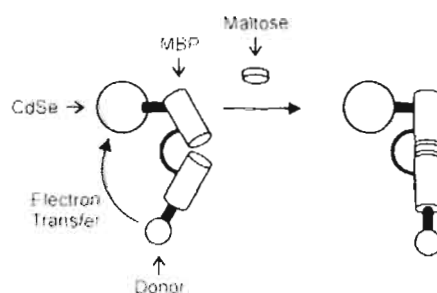


Figure 4.2. QD based maltose sensor: binding of maltose results in a change in protein conformation. This inhibits the electron transfer from Ru(II) to QD, leading to the restoring of QD luminescence (*adapted from reference 2*).

It is not necessary that the target sensing should always be mediated by binding with receptor moiety; direct interaction of analyte on to the surface of QDs by electrostatic interaction can also result in signaling by photoinduced electron transfer process.⁴ The analyte interaction with QD can lead to luminescence enhancement (turn on sensor) or quenching (turn off sensor). It is reported by Rivas *et al.* that Cu(II) ions quenched the luminescence of CdSe QDs in aqueous media which was restored in the presence of cyanide ion as it scavenges the quencher as CuCN (Figure 4.3).^{4c}



Figure 4.3. QD based luminescence 'turn ON' sensor. The Cu(II) on QD surface quenches QD luminescence, which is restored in the presence of CN⁻ (*adapted from reference 4*).

QD sensors based on Förster energy transfer have been reported for the detection of various analytes and these aspects are summarized in References 5-11. QD based pH sensors, by synchronizing both electron and energy transfer process have been reported by Raymo and coworkers.¹²

Herein, we report the use of silica overcoated CdSe QDs described in Chapter 3 for the detection of biologically important molecules and environmentally hazardous metal ions from aqueous medium. The first part of this chapter focuses on the selective detection of (i) amino acids such as cysteine and homocysteine and (ii) peptides such as glutathione in presence of interfering molecules. The second part of the chapter describes the use of silica overcoated CdSe QDs for the selective detection of Hg^{2+} ions.

4.2. Detection of Sulfhydryl Containing Biomolecules

Development of simple probes with high selectivity and sensitivity for quantitative detection of sulfhydryl containing bioanalytes is of great interest for biomedical community.^{13a,b} For example, sulfhydryl containing biologically relevant molecules such as cysteine (Cys), homocysteine (Hcy) and glutathione (GSH) are of particular attention, as they play vital role in metabolic process in living cells by maintaining biological redox homeostasis.^{13c} Selective detection and quantification of these biologically important analytes is of great relevance; however their structural similarity incorporating both carboxylic and amino groups is the major difficulty associated with the development of sensors for their selective detection.

Various approaches for analysis of these bioanalytes were developed based on electroanalytical techniques,¹³ spectrophotometric method based on Ellman's reagent,¹⁴ high performance liquid chromatography (HPLC) techniques, capillary electrophoresis separation or by immunoassays based on derivatisation with fluorescent/phosphorescent reagents.¹⁵ All these methods require either expensive reagents or equipments. Recently Xia and coworkers have investigated the interaction of 3-mercaptopropionic acid capped CdTe QDs and Cys/Hcy by varying the pH of the medium.^{16a} Authors observed an enhancement in the luminescence of QDs in the presence of Cys and Hcy in acidic medium, where as the luminescence was quenched in basic medium. In another report, calixarene appended CdSe QDs were utilized as sensor for methionine and phenylalanine based on the luminescence enhancement.^{16b} A novel QD based sensing technique for the selective detection of sulfhydryl containing amino acids and peptides, at physiologically relevant conditions is presented below. To the best of our knowledge, this is the first report on the development of a sensor, based on silica overcoated CdSe QD for the selective detection of biologically important analytes.

4.2.1. Results and Discussion

Details on the synthesis and photophysical properties of silica overcoated CdSe QDs are presented in Chapter 3. Effect of various amino acids and peptides on luminescence properties of silica overcoated CdSe QDs was investigated. Silica overcoated CdSe QDs in PBS (pH 7.3) were excited

at 460 nm (OD ~ 0.1). The absorption spectrum of QDs showed characteristic excitonic transition at ~ 550 nm and the luminescence maximum at ~ 560 nm (Figure 4.4). The photoluminescence intensity of the silica overcoated CdSe QDs was found to be sensitive to sulfhydryl containing biomolecules. For example, the luminescence was quenched upon addition of Cys (0-40 μM), whereas the absorption spectrum remained unaffected as shown in the Figure 4.4A (inset). Since the absorption spectral profile remained unaltered, in presence of varying amounts of Cys, one can rule out the possibility of any chemical degradation of QDs, which can lead to a reduced luminescence intensity.

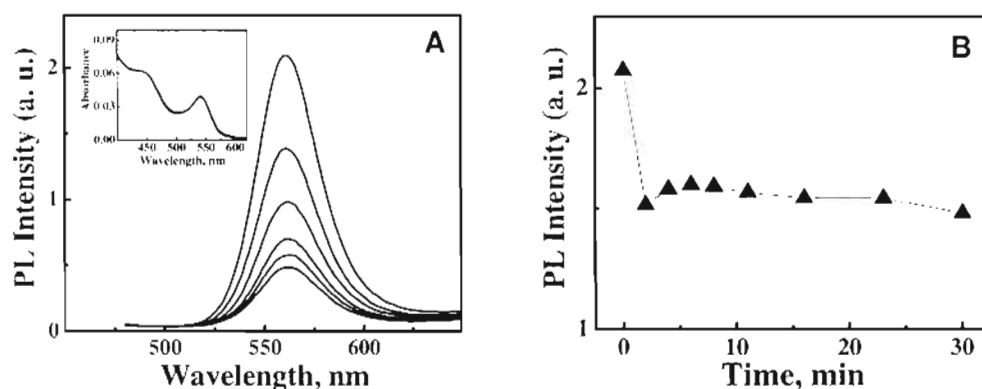


Figure 4.4. (A) Effect of Cys (0-40 μM) on the absorption (inset) and luminescence spectra of silica overcoated CdSe QDs (0.20 μM) in PBS (pH 7.3), excited at 460 nm. (B) Luminescence intensity of QDs in presence of Cys (5 μM) as a function of time.

Further a fixed concentration of Cys (5 μM) was added to QDs and monitored the variation in luminescence intensity as a function of time (Figure 4.4B). Luminescence intensity was decreased instantaneously on addition of Cys and remained unaltered on keeping for long time. Interaction

between QDs and Cys was analysed by monitoring the luminescence intensity of QDs as a function of Cys concentration. The luminescence quenching was analyzed using Stern-Volmer equation (4.1);

$$I_0/I = 1 + K_{sv}[Q] \quad (4.1)$$

where ' I_0 ' and ' I ' are luminescence intensity in the absence and presence of quencher respectively, ' K_{sv} ' is the Stern-Volmer constant. A plot of relative luminescence intensity against concentration of quencher, followed a linear behavior (Figure 4.5A), indicating the presence of either dynamic or static interaction. The Stern-Volmer constant (K_{sv}) was estimated from the slope of the linear fit as $8.9 \times 10^4 \text{ M}^{-1}$. The average lifetime (τ_{avg}) of silica overcoated CdSe QDs was determined as 22 ns based on SPC analysis. The bimolecular quenching constant (k_q) was estimated as $4.1 \times 10^{12} \text{ M}^{-1}\text{s}^{-1}$; the extremely high value of K_q indicates that the luminescence quenching process arises through a static interaction of cysteine with QD and not by a diffusion controlled process.¹⁷

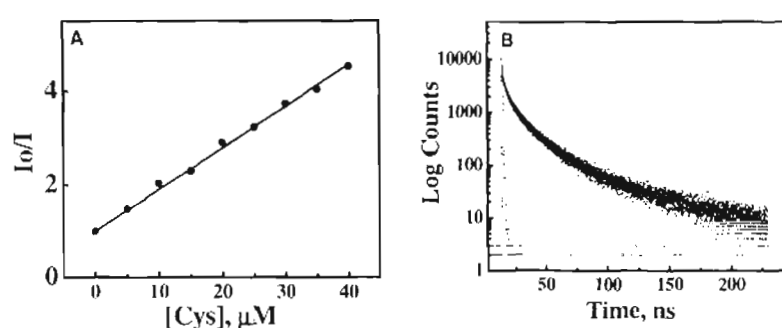


Figure 4.5. (A) Stern-Volmer plot for quenching of QD luminescence in the presence of Cys. (B) Effect of Cys (0-40 μM) on exciton lifetime of silica overcoated CdSe QDs.

The static quenching process was further confirmed based on time correlated single photon counting studies. Silanised QDs showed triexponential decay and the average lifetime of 22 ns remained unchanged in the presence of Cys (0-40 μM ; Figure 4.5B) indicating that the Cys undergoes a static interaction with silanised QDs.¹⁸ Based on the steady state and time resolved luminescence studies, the observed quenching in luminescence of QDs was attributed to the complexation with Cys. Among the twenty α -amino acids, none of the amino acids other than Cys showed any variation in the luminescence intensity of silica overcoated CdSe QDs, confirming the selectivity (Figure 4.6; luminescence spectra are provided in the Experimental section). These results indicate that the Cys binds to the QD surface through the thiol (-SH) functional group. Interestingly, we observed similar effect in the presence of other sulfhydryl containing biologically important molecules such as homocysteine (Hcy) and glutathione (GSH), on luminescence of silica overcoated CdSe QDs. These results are presented in Figure 4.7. The luminescence of QDs underwent dramatic quenching while the absorption spectrum remained unaltered.

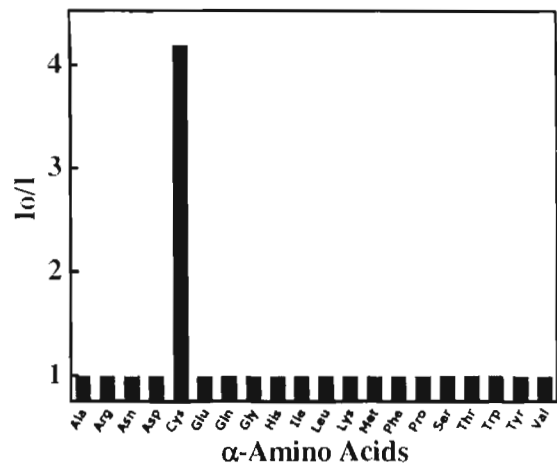


Figure 4.6. Graph showing the selectivity of Cys among the twenty α -amino acids. [Cys] = 40 μ M, others 320 μ M, in PBS.

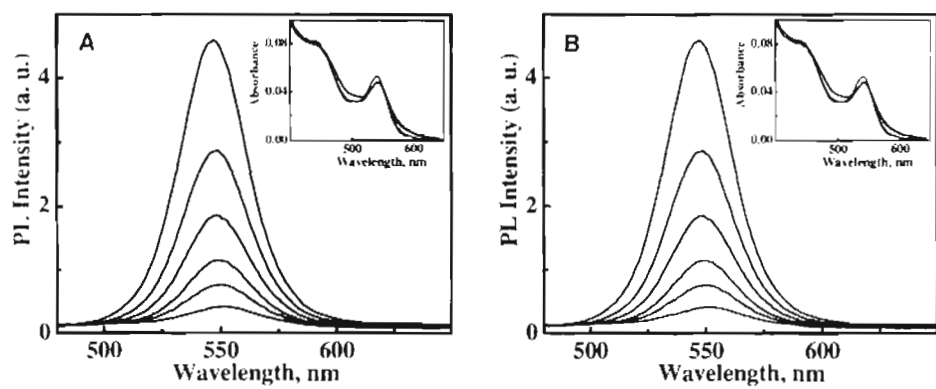


Figure 4.7. Absorption (insets) and luminescence spectra of silica overcoated CdSe QDs (0.20 μ M) in PBS, in the presence of (A) Hcy (0-73 μ M) and (B) GSH (0-76 μ M).

Analysis of the relative photoluminescence intensity as a function of quencher concentration showed a linear relationship (Stern-Volmer plot) for Hcy and GSH. In both the cases, ' K_q ' was found to be in the order of $10^{12} \text{ M}^{-1} \text{ s}^{-1}$ (Table 4.1), as in the case of Cys, ruling out the possibility for a diffusion controlled process.

Table 4.1. Comparison of quenching constants (K_{sv} and K_q) for QD interaction with Cys, Hcy and GSH.

Analytes	K_{sv}, M^{-1}	$K_q, M^{-1} s^{-1}$
Cys	89254	4.1×10^{12}
Hcy	94190	4.3×10^{12}
GSH	90433	4.1×10^{12}

The exciton decay analysis of QDs in presence of varying concentration of Hcy and GSH provided similar results; the average exciton lifetime remained constant in absence and presence of both the analytes (Figure 4.8). These results indicate that the quencher-QD interaction in the case of Hcy and GSH is associative in nature as in the case of Cys. These observations confirmed that the sulfhydryl containing molecules interact with CdSe QD resulting in the quenching of luminescence. This is supported by the fact that the sulfhydryl group (-SH) has a strong affinity towards CdSe surface.¹⁹ Interestingly, the molecules such as Cystine (Cyt) having a disulphide linkage (-S-S-) and methionine (-S-CH₃) did not influence the luminescence of QDs (Figure 4.9).

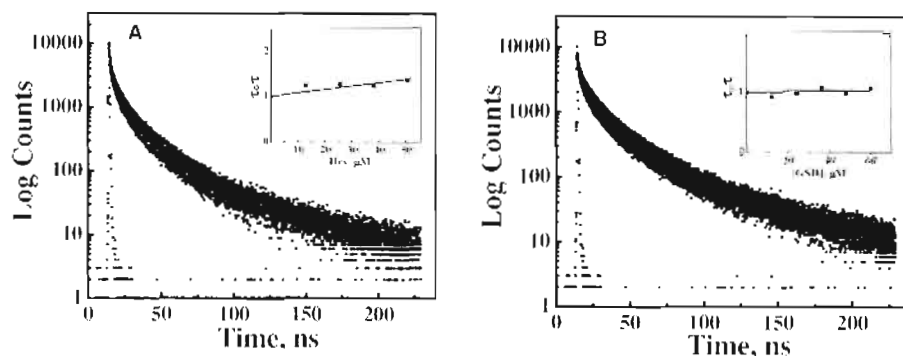


Figure 4.8. Effect of (A) Hcy and (B) GSH on exciton lifetime of silica overcoated CdSe QDs. (Insets) Respective relative changes in average life times (τ_0/τ) with respect to the quencher concentration.

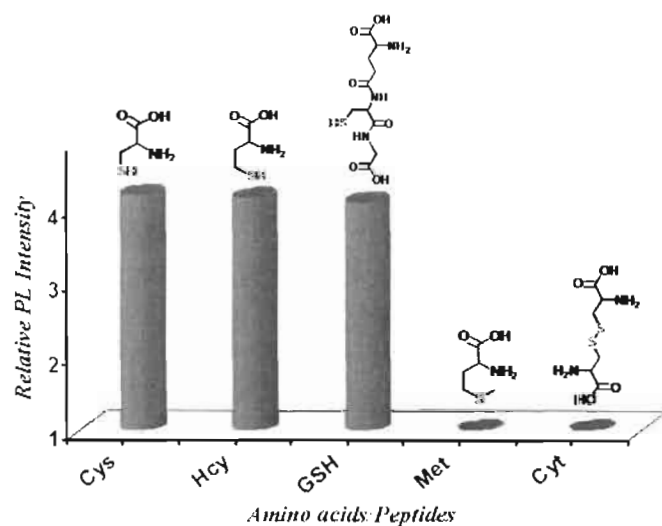


Figure 4.9. Relative luminescence intensity (I_0/I) of silica overcoated CdSe QDs in the presence of Cys, Hcy, GSH, Met and Cyt.

Above observations unambiguously confirm the role of thiol functionality (-SH) in quenching the luminescence of silanised CdSe QDs. It is reported that the thiol group quenches the luminescence of TOPO capped CdSe QDs in organic solvents through a hole transfer mechanism. Meijerink and coworkers explained this process based on the difference in the redox

levels between the valence band edge of CdSe QDs and thiols as illustrated in Figure 4.10.^{20a} Trapping of photoexcited hole formed in QD valence band by the thiol moiety, results in luminescence quenching. In contrast, the valence band of CdTe is positioned at higher redox levels with respect to that of thiols, thus eliminating hole-trapping process.

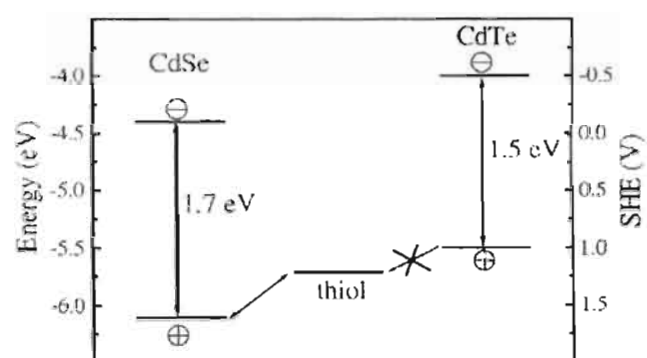


Figure 4.10. Redox positions of CdSe, CdTe band edges and thiol, shown both on a vacuum scale and with respect to SHE.^{20a}

Recently, Hollingsworth and coworkers showed that in aqueous media “thiolate anion (RS^-)” is the active species affecting the optical properties of CdSe QDs, rather than “thiol” (RSH) moiety.^{20b} The photogenerated hole in the valence band of CdSe QD are trapped by the thiolate ion, resulting in the formation of a ‘thyl radical’ (RS^\bullet) which undergoes coupling to yield non-coordinating disulfide (RSSR) as shown below.



The silica overcoated CdSe QDs can be visualized as a core-shell system consisting of CdSe core and silica shell. Iwasaki *et al.* showed that in case of CdS/SiO₂ core-shell system, the silica shell is sufficiently porous for small molecules and ionic species such as amines, Cd²⁺ and OH⁻ to penetrate from the bulk solution to the interior of the silica shell, while larger molecules such as methyl viologen cannot penetrate.²¹ Based on this, in present system, the penetration of quencher through the silica shell may be ruled out. Another possibility is that the silica shell around CdSe core is non-uniform and the quencher undergoes a direct interaction with CdSe core through the voids in the shell. This assumption was supported by the HRTEM images, which showed the presence of a thin silica shell over the QD core as shown in the Figure 4.11. The formation of silica shell on CdSe core can proceed through the dimerisation of APS molecules, through a siloxane bridge (-Si-O-Si-) as illustrated in Figure 4.12. One of the amino groups of APS is bound to QD surface while other projecting out with an overall length of ~1.5 nm for APS dimer. This also suggests that the silica shell formed is of very low thickness (~1.5 nm) while APS is used as silica precursor. Based on these results, we assume that the thin silica shell may contain void spaces which allows the direct interaction of analytes having thiol functionality with the CdSe core.

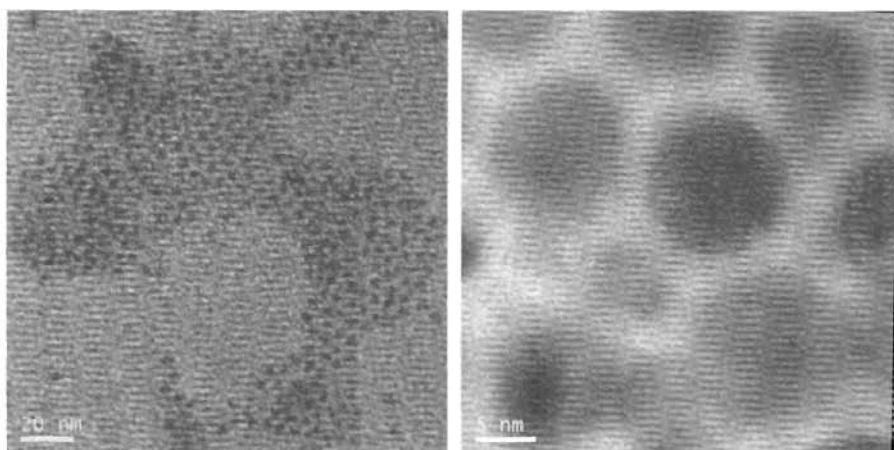


Figure 4.11. HRTEM images of silica overcoated CdSe QDs, illustrating the presence of very thin silica shell over QD core.

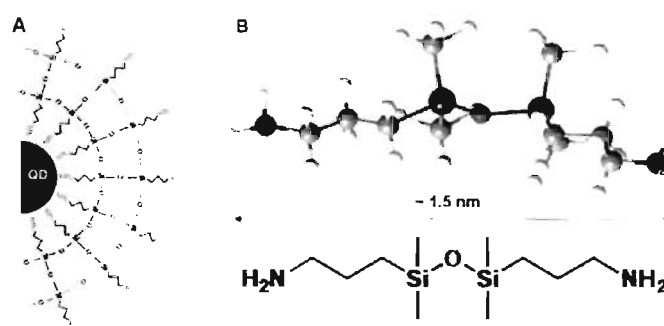


Figure 4.12. (A) Schematic illustration of silica shell formed on QD core by APS (not to scale) and (B) overall length of an APS dimer on QD surface obtained from minimum energy optimized structure using Chem3D.

Analysis of Total Free Thiols in Human Blood Serum: Amount of ‘free thiols’ in human blood serum is a biological marker for many diseases.^{13c} Most of the commercialized techniques for analysis of amino acids and peptides in blood serum are sophisticated, time consuming, and expensive.^{17a-b}

Using silica overcoated CdSe QDs, herein we present a simple fluorimetric method for the analysis of low molecular weight amino thiols in blood serum.

Serum samples (**S1**, **S2** and **S3**) were collected from three volunteers and the total thiol content was analyzed as explained below. In a typical procedure, silica overcoated CdSe QDs was diluted with PBS (pH 7.3) to a final concentration of 0.17 μM , and 10 μL of this solution was mixed with an equal volume of blood serum. Luminescence of QDs was monitored under UV light using a gel documentation system (UVP, Cambridge, UK) and imaging was done using a CCD camera. Serial dilutions of serum (1:2, 1:10, 1:100 and 1:1000) in PBS were used for the experiments. Photographs recorded under UV illumination after mixing serum (of various concentrations) with QDs is shown in Figure 4.13 (left panel). In case of **S1**, luminescence of QD was not affected on addition of serum of any concentration levels (Figure 4.13, first row). In contrast, **S2** and **S3** turned off the luminescence of QDs at higher serum concentrations (Figure 4.13, second and third row). Luminescence of QDs was totally quenched at dilution of 1:2 in the case of **S2**, where the luminescence was turned off even at a dilution of 1:10 in the case of **S3**. These results indicate that **S3** has a higher 'free thiol' content compared to **S2**.

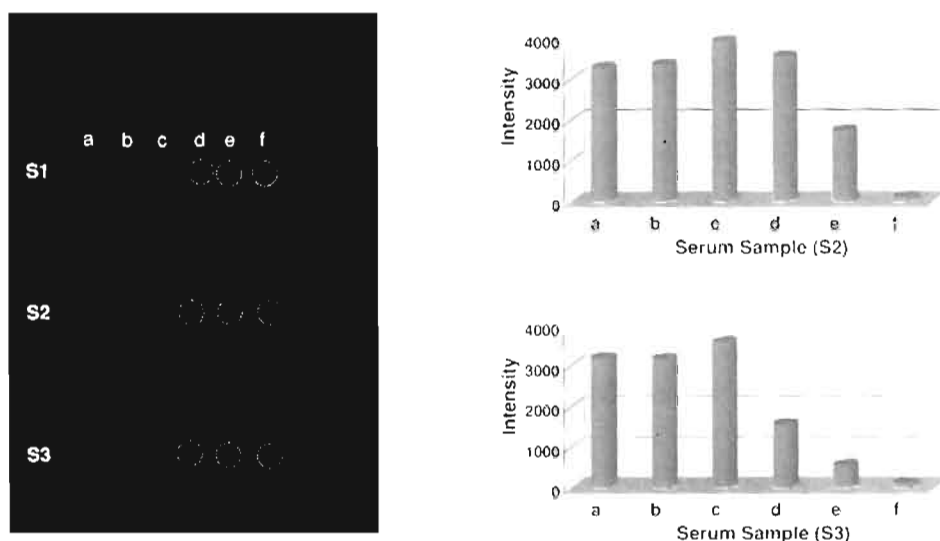


Figure 4.13. (left panel) Analysis of human blood serum sample using silica overcoated CdSe QDs. a-f: QD drops (0.17 μM , in PBS,) on glass slides. **S1**, **S2** and **S3** correspond to three serum samples used. Serum concentration increases from c-f (dilution in the order 1:1000, 1:100, 1:10 and 1:2); a and b for control experiments. In case of **S2** and **S3**, the QD luminescence was quenched at higher concentrations (indicated by circles). (right panel) Graphs obtained from densitometry analysis of photograph, for **S2** and **S3**.

Further the densitometric analysis (Visionworks[®]LS analysis software) of the photographs were carried out to estimate relative distribution of the 'free thiol' content in **S2** and **S3** and the results are presented in the Figure 4.13 (right panel). A comparison of the luminescence intensity at dilutions 1:100, 1:10 and 1:2 ('d', 'e' and 'f' in the right panel of Figure 4.14) for **S2** and **S3** gives the difference in thiol content in serum samples. The luminescence was more suppressed in the case of **S3**, even at higher dilutions, indicating that this serum sample contains higher amount of 'free thiols'.

A detailed investigation with higher number of serum samples is recommended to explore the potential of these materials for application in clinical laboratories for routine analysis.

4.3. Selective Detection of Hg^{2+} Using Silanised QDs

Mercury is having prime role among the heavy metals, in offering major threat to environmental contamination.²² Determination of mercury content in samples is challenging due to its high volatility, even at ambient temperatures. Various instrumental methods of analysis for the determination of mercury include gas chromatography, neutron activation analysis, atomic absorption spectroscopy, cold vapor atomic fluorescence spectrometry, cyclic voltammetry, microcantilevers etc.^{23a-c} However, these methods involve multistep sample preparation and/or sophisticated instrumentation. The use of QDs for the selective detection of mercury ions have been reported based on CdS and CdTe QDs.²⁴ We have investigated the potential use of silanised CdSe QDs as a luminescent probe for the selective detection of Hg^{2+} from aqueous media.

4.3.1. Results and Discussion

CdSe QDs were synthesized and overcoated with silica using aminopropyl silane as described in Chapter 3. Silanised CdSe QDs used in the present study showed an absorption profile with characteristic peak at 575 nm, corresponding to first excitonic transition and the luminescence

maximum centered at 582 nm (blue trace in Figure 4.14) with FWHM of ~50 nm. Effect of various metal ions on photophysical properties of silica overcoated CdSe QDs (0.16 μM) in PBS (pH 7.3) were investigated by exciting at 480 nm (absorbance~0.08) and luminescence intensity was collected at the peak maximum. Interestingly, the absorption as well as the luminescence spectra showed a considerable red shift ($\Delta\lambda\sim 25$ nm) in presence of Hg^{2+} ions (0-14 μM ; Figure 4.14). These spectral changes were followed by a decrease in the luminescence intensity and broadening of the band. Further, the exciton lifetime of silanised CdSe QDs was measured as a function of mercuric ion concentration. Silanised CdSe QDs showed a triexponential exciton decay characteristics with an average lifetime of 18 ns. A substantial reduction in the average lifetime, was observed on addition of Hg^{2+} (6 μM ; Figure 4.15) suggesting an interaction between QDs and metal ions and various possibilities are discussed below.

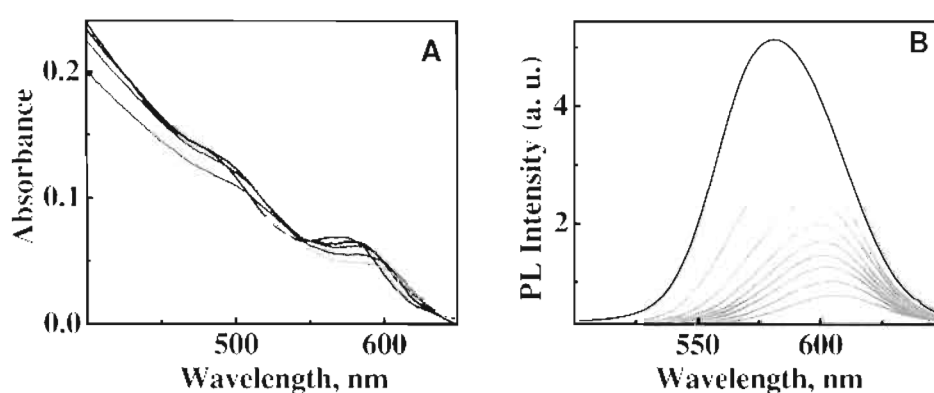


Figure 4.14. (A) Absorption and (B) luminescence spectra of silica overcoated CdSe QDs (0.16 μM), in presence of Hg^{2+} (0-14 μM) in PBS (pH 7.3), excited at 480 nm.

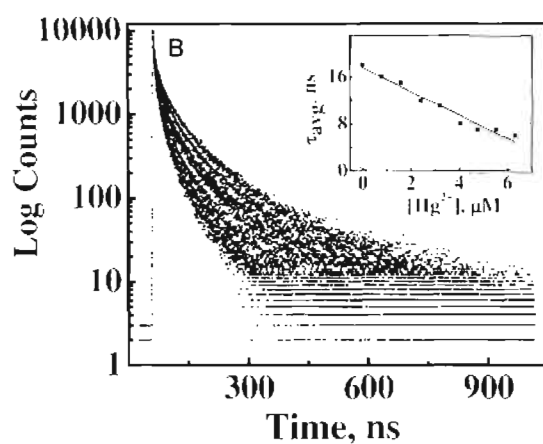


Figure 4.15. Effect of Hg^{2+} on exciton decay lifetimes of silica overcoated CdSe QDs. Excited at 441 nm.

It is possible to account for the red shift in the first excitonic transition in absorption spectrum of QDs in terms of (i) an increase in the overall size of the QDs due to Ostwald's ripening^{25a} or (ii) a metal ion induced aggregation of QDs.^{25b,c} These possibilities can also result in luminescence quenching and broadening of the band as the electronic levels of QD are influenced in either case (Figure 4.16). HRTEM images recorded in the absence and presence of Hg^{2+} are presented in Figure 4.17. The average size of QD and its distribution remained unchanged in presence of Hg^{2+} and the possibility of aggregation and Ostwald's ripening was ruled out. The possibility of a hole transfer cannot be accounted in the present case since Hg^{2+} cannot be easily oxidized.

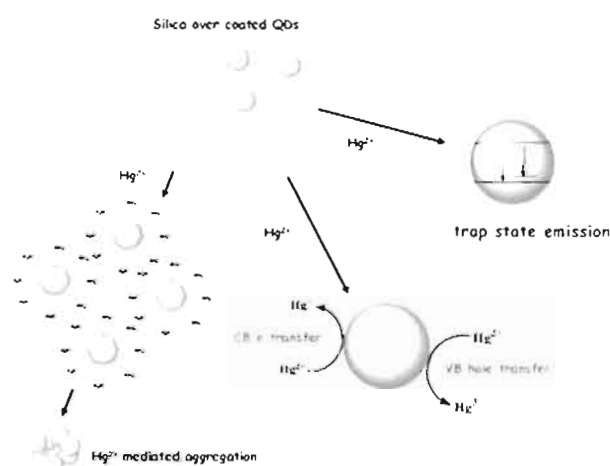


Figure 4.16. Plausible mechanisms for the observed red shift in absorption and luminescence profiles as well as for the PL quenching of silica over coated CdSe QDs upon addition of Hg^{2+} .

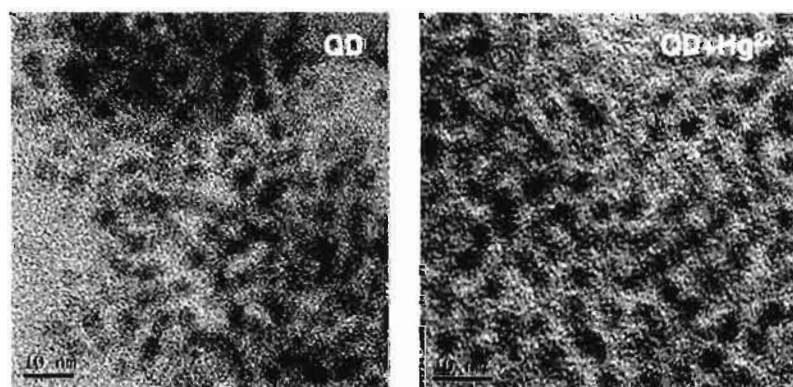


Figure 4.17. HRTEM images of silica overcoated CdSe QDs in before and after adding Hg^{2+} , showing absence of size increase or aggregation in presence of mercuric ion.

The red shift in absorption and luminescence maxima as well as the broadening of luminescence profile in the presence of Hg^{2+} can be explained based on the interaction of metal ions with QDs, leading to the generation of new trap states with low-lying energy levels. The shift in the excitonic band in

the absorption spectrum on addition of Hg^{2+} corresponds to a reduction in the energy gap of QDs from 2.14 eV (CdSe band edge luminescence) to 2.04 eV. This can be attributed to the generation of new energy levels close to valence and conduction band edges. Weller and coworkers have earlier reported a red shift in the excitonic absorption peak and reduction in band edge emission in the case of CdS QDs on addition of mercuric ions (Figure 4.18).²⁶ Based on spectroscopic investigations, authors have concluded the formation of quantum sized HgS on CdS surface, which influences the electronic structure of QDs by generating new nonradiative decay channels having lower energy states. Cadmium telluride QDs also react with mercuric ions resulting in the formation of quantum sized HgTe on the surface. It is also reported that Cu^{2+} can react with (i) CdS leading to the formation of quantum sized CuS on QD surface and (ii) CdSe to yield quantum sized CuSe.²⁷

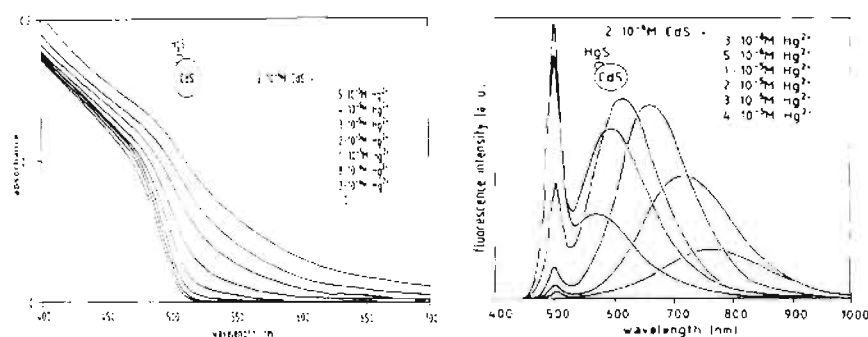
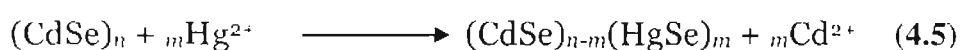


Figure 4.18. Effect of Hg^{2+} on absorption and luminescence spectra of CdS QDs in water which is attributed to the formation of quantum size HgS on CdS surface.²⁶

In the present case, Hg^{2+} can react with CdSe QDs (equation 4.1) leading to the formation of quantum sized HgSe on QD surface opening a

new channel for exciton decay. The red shift in absorption and luminescence maxima as well as the broadening of luminescence profile can be thus attributed to the formation of HgSe on QD surface. It is also supported by the fact that the solubility product of HgSe ($-\log K_{sp} = 65$) is lower compared to that of CdSe ($-\log K_{sp} = 35$).³⁸



In the absence of HgSe formation, the excitons formed in CdSe QDs undergo radiative recombination (bandgap energy 2.14 eV). Quantum sized HgSe on CdSe surface further modifies the band edge recombination process: the electrons relax to the low lying conduction band of HgSe and the radiative exciton recombination from this energy level results. A schematic representation of various energy levels is presented in Figure 4.19. A substantial reduction in the average lifetime, from 22 ns to 7 ns, was observed on addition 6 μM of Hg^{2+} (Figure 4.15). The observed decrease in the exciton decay lifetimes in presence of Hg^{2+} is due to the new decay channels, which depopulates of excitons. It is earlier reported by Iwasaki *et al.* that small ionic species can penetrate through silica overcoated CdS QDs.²¹ As discussed in the earlier part of this Chapter, the silica shell formed around CdSe QD is found to be thin (~ 1.5 nm). Hg^{2+} ions can interact with CdSe core either through the void spaces in the shell or by penetrating through the thin porous silica layer.

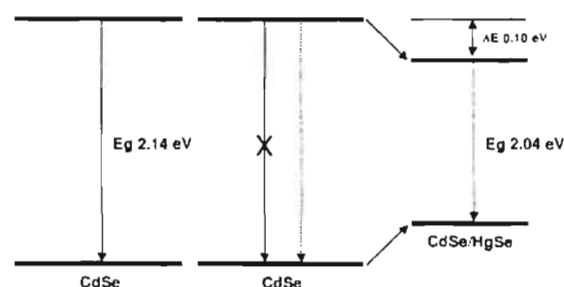


Figure 4.19. Exciton recombination pathways in CdSe QDs (solid arrow) and in presence of HgSe on CdSe QD surface (dashed arrow).

We have further investigated the interaction of various metal ions including alkali, alkaline earth and transition metals and the results are presented in Figure 4.20. Interestingly, addition of these metal ions does not influence the spectral properties of CdSe QDs even at higher concentration of $\sim 100 \mu\text{M}$. To confirm the selectivity of Hg^{2+} ions, quenching studies were carried out in the presence of various metal cations (Figure 4.20). A mixture of various metal cations (Li^+ , Na^+ , K^+ , Mg^{2+} , Ca^{2+} , Ba^{2+} , Mn^{2+} , Fe^{2+} , Co^{2+} , Ni^{2+} , Cu^{2+} , Zn^{2+} , Cd^{2+} , Al^{3+} , Pb^{2+} ; $100 \mu\text{M}$ each) was added to a solution of QDs ($0.20 \mu\text{M}$) in PBS. The decrease in the luminescence intensity was found negligible ($\sim 10\%$; trace 'b' in Figure 4.20B). Further, addition of Hg^{2+} ions ($8 \mu\text{M}$) to this solution resulted in a substantial reduction in the luminescence intensity (trace 'c' in Figure 4.20B), indicating the possibility of using silica overcoated CdSe QDs for the selective detection of mercury containments in the presence of other interfering metal ions.

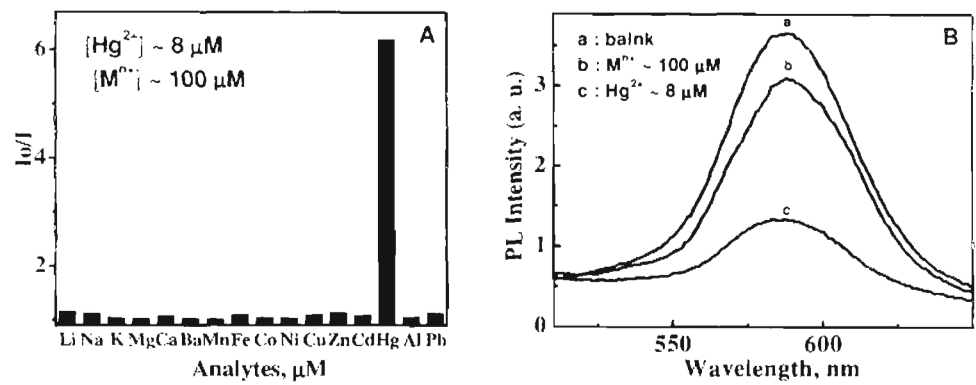


Figure 4.20. (A) Effect of various metal ions on PL intensity of silica overcoated CdSe QDs in PBS. (B) Selectivity of Hg^{2+} in presence of other interfering and non-interfering metal ions.

4.4. Conclusions

Luminescence properties of silica overcoated CdSe QDs in aqueous media were found to be sensitive to sulfhydryl containing bioanalytes and mercuric ions. Luminescence of QDs was turned off in presence of micromolar quantities of thiol containing biomolecules such as cysteine, homocysteine and glutathione and found to be insensitive to their oxidized forms (disulphides). Further, we have demonstrated the use of this water soluble luminescent material for the analysis of total free thiols present in human blood samples. Based on various experiments, it was confirmed that the quenching of luminescence occurs through a hole transfer process. HRTEM analysis showed that the silica shell is very thin or non-uniform and the analytes can interact with CdSe core through the voids.

We have also demonstrated the use of silica overcoated CdSe QDs in the selective detection of Hg^{2+} in presence of interfering metal ions, with a limit of detection (LOD) of 1.5 ppm (according to 3σ IUPAC definition). The photophysical properties of QDs were dramatically influenced by mercuric ions: a bathochromic shift in the absorption and emission spectra along with a decrease in the luminescence intensity was observed. It is anticipated that the mesoporous, thin silica shell is permeable to Hg^{2+} ion, allowing interaction with CdSe core surface. The spectral changes are attributed to the formation of quantum sized HgSe on CdSe surface. The absorption and emission properties of silica overcoated CdSe QDs are insensitive to various metal ions such as Li^+ , Na^+ , K^+ , Mg^{2+} , Ca^{2+} , Ba^{2+} , Mn^{2+} , Fe^{2+} , Co^{2+} , Ni^{2+} , Cu^{2+} , Zn^{2+} , Cd^{2+} , Al^{3+} , Pb^{2+} , even at 0.1 mM concentration, making this system highly selective for mercuric ions. In conclusion, fluorimetric method presented here allows the detection of sulfhydryl containing bioanalytes (at physiologically relevant conditions) and mercuric ions in the presence other interfering metal ions, without the aid of any specialized instruments.

4.5. Experimental Section

4.5.1. Materials and Methods

General details of solvents, reagents and equipments used for synthesis, characterisation and studies are provided in the Appendix. Amino acids, peptides and metal salts used for studies were purchased from Aldrich and used as such. Blood serum analysis experiments were carried out using a

gel documentation system (UVP, Cambridge, UK) equipped with (black and white) CCD camera. Densitometry analysis of the photographs were done using visionworks®LS analysis software.

4.5.2. TCSPC Analysis of QD Luminescence

Table 4.2. PL decay fit data in presence of Cys.

[Cys], μM	τ_1 , ns	τ_2 , ns	τ_3 , ns	τ_{avg} , ns	χ^2
0.0	0.59(07%)	5.9(29%)	24.4(64%)	22.5	1.19
13.9	0.51(09%)	4.6(27%)	21.0(64%)	19.6	1.19
27.8	0.47(10%)	4.8(30%)	22.0(60%)	20.2	1.13
41.3	0.75(08%)	5.2(30%)	21.2(62%)	19.4	1.17
54.9	0.47(11%)	4.3(29%)	20.1(60%)	18.5	1.19

Table 4.3. PL decay fit data in presence of Hcy.

[Hcy], μM	τ_1 , ns	τ_2 , ns	τ_3 , ns	τ_{avg} , ns	χ^2
0	0.61(04%)	5.6(25%)	22.8(71%)	21.40	1.19
12.8	0.62(05%)	4.4(29%)	18.6(66%)	17.31	1.19
25.5	0.44(08%)	3.7(30%)	18.2(62%)	16.85	1.13
38.1	0.50(09%)	4.2(34%)	19.1(57%)	17.31	1.17
50.7	0.77(10%)	4.5(35%)	17.6(55%)	15.66	1.19

Table 4.4. PL decay fit data in presence of GSH.

[GSH], μM	τ_1 , ns	τ_2 , ns	τ_3 , ns	τ_{avg} , ns	χ^2
0.0	0.90(5%)	6.9(28%)	24.9(67%)	22.98	1.18
12.3	1.10(7%)	7.6(32%)	27.4(61%)	24.79	1.16
24.5	0.91(7%)	6.4(31%)	25.8(62%)	23.58	1.19
36.7	0.82(8%)	5.6(31%)	23.3(61%)	21.29	1.11
48.7	0.82(9%)	6.1(36%)	25.9(55%)	23.16	1.06
60.7	0.79(9%)	5.6(36%)	24.1(55%)	21.56	1.04

4.5.3. Effect of Amino acids (~ 300 μ M) on QD Luminescence

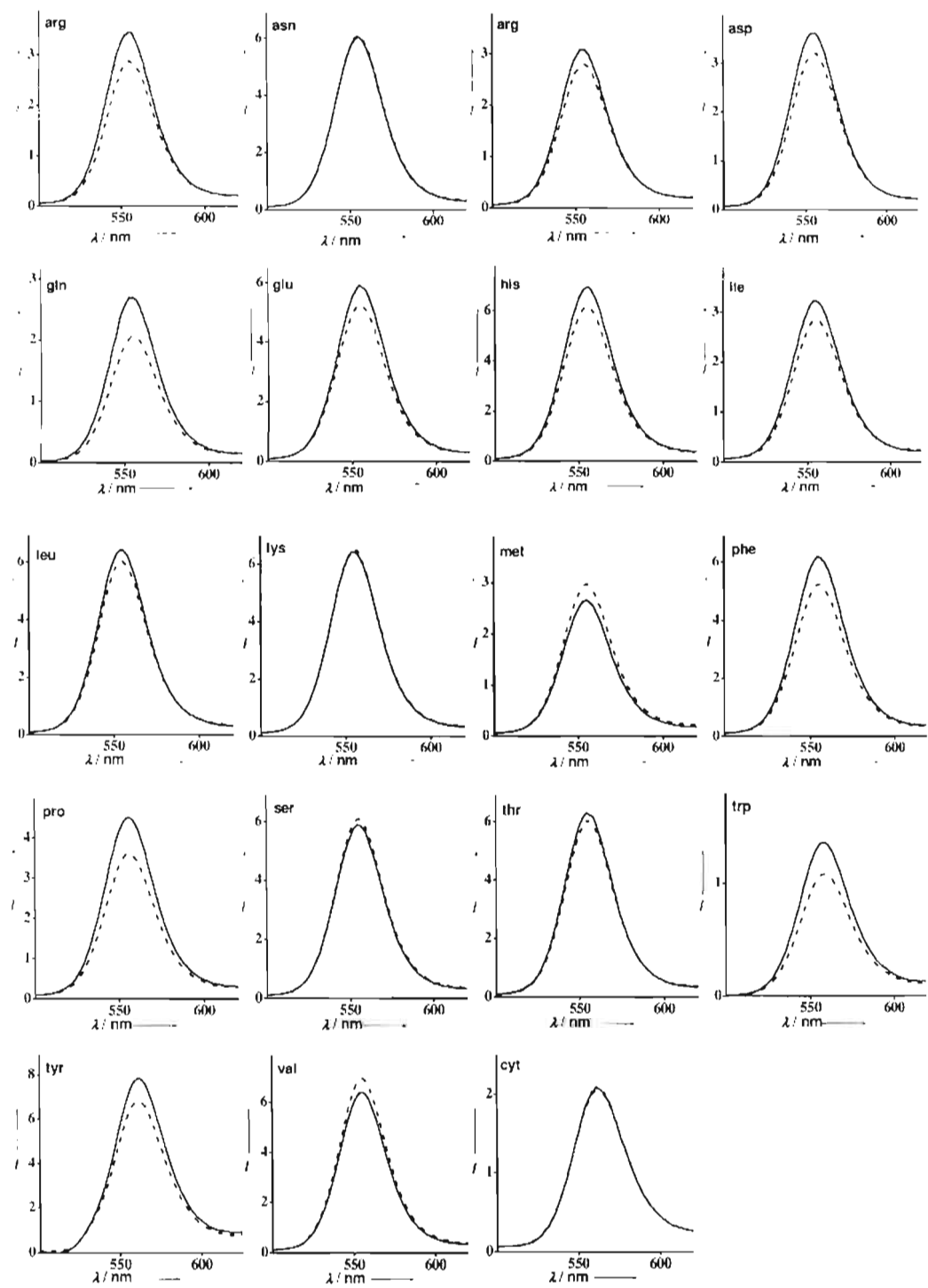


Figure 4.21. Effect of α -amino acids including cystine (~320 μ M) on PL of silica over coated CdSe QD (0.20 μ M, excited at 460 nm, in PBS).

4.5.4. TCSPC Analysis of QD luminescence in presence of Hg²⁺

Table 4.5. PL decay fit data in presence of Hg²⁺.

[Hg ²⁺], μM	τ ₁ , ns	τ ₂ , ns	τ ₃ , ns	τ _{avg} , ns	χ ²
0	0.79 (13%)	4.8 (32%)	20.0(55%)	18	1.07
0.81	0.81 (15%)	4.3 (35%)	18.6 (50%)	16	1.17
1.62	0.75 (12%)	3.9 (35%)	16.9 (53%)	15	1.11
2.42	0.68 (12%)	3.3 (38%)	7.90 (50%)	12	1.16
3.21	0.57 (14%)	2.8(43%)	13.0 (43%)	11	1.12
4.05	0.54 (14%)	2.3 (40%)	9.60 (46%)	8	1.14
4.78	0.56 (20%)	2.3 (40%)	8.90 (40%)	7	1.00
5.55	0.55 (19%)	2.2 (38%)	7.70 (43%)	6	1.02
6.33	0.48 (14%)	2.2 (32%)	14.3 (54%)	7	1.10

4.6. References

1. (a) Mascini, M.; Tombelli, S. *Biomarkers* **2008**, *13*, 637. (b) Chow, C.-F.; Chiu, B. K. W.; Lam, M. H. W.; Wong, W.-Y. *J. Am. Chem. Soc.* **2003**, *125*, 7802. (c) Alivisatos, P. *Nat. Biotechnol.* **2004**, *22*, 47. (d) Raymo, F. M.; Yildiz, I. *Phys. Chem. Chem. Phys.* **2007**, *9*, 2036. (e) Somers, R. C.; Bawendi, M. G.; Nocera, D. G. *Chem. Soc. Rev.* **2007**, *36*, 579. (f) Costa-Fernández, J. M.; Pereiro, R.; Sanz-Medel, A. *TrAC, Trends Anal. Chem.* **2006**, *25*, 207. (g) Duonghong, D.; Ramsden, J.; Gratzel, M. *J. Am. Chem. Soc.* **1982**, *104*, 2917. (h) Anderson, N. A.; Lian, T. *Annu. Rev. Phys. Chem.* **2005**, *56*, 491.

2. Sandros, M. G.; Shete, V.; Benson, D. E. *Analyst* **2006**, *131*, 229.

3. Ji, X.; Zheng, J.; Xu, J.; Rastogi, V. K.; Cheng, T.-C.; DeFrank, J. J.;

- Leblanc, R. M. *J. Phys. Chem. B*, **2005**, *109*, 3793.
4. (a) Yildiz, I.; Tomasulo, M.; Raymo, F. M. *Proc. Nat. Acad. Sci. U.S.A.* **2006**, *103*, 11457. (b) Shang, L.; Zhang, L.; Dong, S. *Analyst* **2009**, *134*, 107. (c) Touceda-Varela, A.; Stevenson, E. I.; Galve-Gasiòn, J. A.; Dryden, D. T. F.; Mareque-Rivas, J. C. *Chem. Commun.* **2008**, 1998.
5. Medintz, I. L.; Clapp, A. R.; Brunel, F. M.; Tiefenbrunn, T.; Uyeda, H. T.; Chang, E. L.; Deschamps, J. R.; Dawson, P. E.; Mattoussi, H. *Nat. Mater.* **2006**, *5*, 581.
6. Oh, E.; Lee, D.; Kim, Y. P.; Cha, S. Y.; Oh, D. B.; Kang, H. A.; Kim, J.; Kim, H. S.; *Angew. Chem. Int. Ed.* **2006**, *45*, 7959.
7. Zhang, C.-Y.; Yeh, H. C.; Kuroki, M. T.; Wang, T.-H. *Nat. Mater.* **2005**, *4*, 826.
8. Tang, B.; Cao, L.; Xu, K.; Zhuo, L.; Ge, J.; Li, Q.; Yu, L. *Chem. Eur. J.* **2008**, *14*, 3637.
9. Goldman, E. R.; Medintz, I. L.; Whitley, J. L.; Hayhurst, A.; Clapp, A. R.; Uyeda, H. T.; Deschamps, J. R.; Lassman, M. E.; Mattoussi, H. *J. Am. Chem. Soc.* **2005**, *127*, 6744.
10. Gill, R.; Willner, I.; Shweky, I.; Banin, U. *J. Phys. Chem. B* **2005**, *109*, 23715.
11. (a) Medintz, I. L.; Mattoussi, H. *Phys. Chem. Chem. Phys.* **2009**, *11*, 17. (b) Algar, W. R.; Krull, U. J. *Anal. Bioanal. Chem.* **2008**, *391*, 1609. (c)

- Sapsford, K. E.; Berti, L.; Medintz, I. L. *Angew. Chem. Int. Ed.* **2006**, *45*, 4562.
12. Tomasulo, M.; Yildiz, I.; Kaanumalle, S. L.; M. Raymo, F. M. *Langmuir* **2006**, *22*, 10284.
13. (a) Herzog, G.; Arrigan, D. W. M. *Analyst* **2007**, *132*, 615. (b) White, P. C.; Lawrence, N. S.; Davis, J.; Compton, R. G. *Electroanal.* **2002**, *14*, 89. (c) Wang, W.; Rusin, O.; Xu, X.; Kim, K. K.; Escobedo, J. O.; Fakayode, S. O.; Fletcher, K. A.; Lowry, M.; Schowalter, C. M.; Lawrence, C. M.; Fronczek, F. R.; Warner, I. M.; Strongin, R. M. *J. Am. Chem. Soc.* **2005**, *127*, 15949.
14. Ellman, G. L. *Arch. Biochem. Biophys.* **1959**, *82*, 70.
15. Nekrassova, O.; Lawrence, N. S.; Compton, R. G. *Talanta* **2003**, *60*, 1085.
16. (a) Xia, Y.-S.; Zhu, C. *Microchim. Acta* **2009**, *164*, 34. (b) Wang, X.; Wu, J.; Li, F.; Li, H. *Nanotechnology* **2008**, *19*, 205501.
17. (a) Mourice, R. E.; Camillo, A. G. *Anal. Biochem.* **1981**, *114*, 199. (b) Billone, P. S.; Maretti, L.; Maurel, V.; Scaiano, J. C. *J. Am. Chem. Soc.* **2007**, *129*, 14150.
18. Lakowicz, J. R. *Principles of Fluorescence Spectroscopy* (3rd Ed). Springer, New York, **2006**.
19. Rikans, L. E.; Yamano, T. *J. Biochem. Mol. Toxicol.* **2000**, *14*, 110.

20. (a) Wuister, S. F.; Donegá, C. M.; Meijerink, A. *J. Phys. Chem. B* **2004**, *108*, 17393. (b) Jeong, S.; Achermann, M.; Nanda, J.; Ivanov, S.; Klimov, V. I.; Hollingsworth, J. A. *J. Am. Chem. Soc.* **2005**, *127*, 10126.
21. (a) Iwasaki, K.; Torimoto, T.; Shibayama, S.; Takahashi, H.; Ohtani, B. *J. Phys. Chem. B* **2004**, *108*, 11946. (b) Iwasaki, K.; Torimoto, T.; Shibayama, T.; Nishikawa, T.; Ohtani, B. *Small* **2006**, *2*, 854.
22. Berman, E. *Toxic Metals and Analysis*. Heydon and Sons Ltd., London, **1980**.
23. (a) Nolan, M. A.; Kounaves, S. P. *Anal. Chem.* **1999**, *71*, 3567. (b) Xu, X.; Thundat, T. G.; Brown, G. M.; Ji, H.-F. *Anal. Chem.* **2002**, *74*, 3611. (c) Bloom, N.; Fitzgerald, W. F. *Anal. Chim. Acta* **1988**, *208*, 151.
24. (a) Chen, J.; Gao, Y. C.; Guo, C.; Wu, G. H.; Chen, Y. C.; Lin, B. *Spectrochim. Acta, Part A* **2008**, *69*, 572. (b) Xia, Y.-S.; Zhu, C.-Q. *Talanta* **2008**, *75*, 215. (c) Li, H.; Zhang, Y.; Wang, X.; Gao, Z. *Microchim. Acta* **2008**, *160*, 119. (d) Li, H.; Zhang, Y.; Wang, X.; Xiong, D.; Bai, Y. *Mater. Lett.* **2007**, *61*, 1474.
25. (a) Tonti, D.; Mohammed, M. B.; Al-Salman, A.; Pattison, P.; Chergui, M. *Chem. Mater.* **2008**, *20*, 1331. (b) Koole, R.; Liljeroth, P.; de Mello Doneg, C.; Vanmaekelbergh, D.; Meijerink, A. *J. Am. Chem. Soc.* **2006**, *128*, 10436. (c) Yoon, J.; Ohler, N. E.; Vance, D. H.; Aumiller, W. D.; Czarnik, A. W. *Tetrahedron Lett.* **1997**, *38*, 3845.

-
26. (a) Eychmüller, A.; Hässelbarth, A.; Weller, H. *J. Lumin.* **1992**, 53, 113.
(b) Hässelbarth, A.; Eychmüller, A.; Giersig, M.; Mews, A.; Weller, H. *J. Phy. Chem.* **1993**, 97, 5333.
27. (a) Isarov, A. V.; Chrysochoos, J. *Langmuir* **1997**, 13, 3142. (b) Callan, J. F.; Mulrooney, R. C. *Phys. Status Solidi C*. **2009**, 1.
28. Szabo, J. P.; Cocivera, M. *Can. J. Chem.* **1988**, 66, 1065.

APPENDIX

1. General Outline for Materials and Methods

Chemicals and solvents used for the reactions and spectroscopic studies were of analytical and spectroscopic grade, and were further purified by following standard protocols wherever necessary.¹ The electronic absorption spectra were recorded on a Shimadzu model UV-3101, or 2401 PC UV-Vis-NIR scanning spectrophotometer. Emission spectra were collected using SPEX-Fluorolog F112X spectrofluorimeter equipped with a 450W Xenon arc lamp and spectra obtained were corrected using the program supplied by the manufacturer. FTIR and ATR studies were performed on a Shimadzu IR Presige-21 FTIR spectrometer. The photoluminescence lifetimes were measured using an IBH picosecond time correlated single photon counting (TCSPC) system with an excitation source of 440 nm (pulse width <200 ps) and luminescence decay profiles were deconvoluted using IBH data station software V2.1. The average life time was deduced from relation below:²

$$I(t) = \sum_{i=1}^n a_i \exp(-t/\tau_i)$$
$$\tau_{avg} = \frac{a_1\tau_1^2 + a_2\tau_2^2 + a_3\tau_3^2}{a_1\tau_1 + a_2\tau_2 + a_3\tau_3}$$

where 't' represents time, 'τ' lifetime, and 'a' is pre-exponential factor.

X-ray diffraction patterns were recorded using Philips X'Pert Pro. X-ray diffractometer with Cu K α radiation (1.5406 Å) and spectra were analysed using X'Pert Highscore software. For high resolution transmission electron microscopic (HRTEM) and energy dispersive X-ray spectroscopic (EDS) studies, a drop of nanoparticle solution was placed on a carbon coated Cu grid and the solvent was allowed to evaporate. Specimens were examined on a JEOL 3010 300 kV or on a FEI Tecnai G² S-TWIN 300 kV transmission electron microscope.

All melting points were determined with a Mel-Temp-II melting point apparatus and are uncorrected. Preliminary characterization of organic compounds was carried out using Shimadzu GCMS-QP2010 gas chromatograph-mass spectrometer (GCMS). ¹H and ¹³C NMR spectra were recorded on a 300 MHz Bruker Avance DPX spectrometer and high resolution mass spectra (HRMS) were recorded on JEOL JMS 600H mass spectrometer.

To measure relative quantum yields of QDs, rhodamine 6G in ethanol ($\Phi_1 = 0.91$) was used as the reference, which offers a good spectral overlap with that of QD emission. Both reference and QD was excited at the same wavelength, where the absorbance was kept at ~0.10 and the quantum yield (Φ) was obtained by using following equation;³

$$\Phi_{\text{QD}} = \Phi_{\text{R}} \frac{F_{\text{QD}} A_{\text{R}} \eta_{\text{QD}}^2}{F_{\text{R}} A_{\text{Q}} \eta_{\text{R}}^2}$$

where the subscript R and QD stands for reference and quantum dots respectively, 'A' for absorbance, 'F' for area under the emission peak and 'η' represents refractive index of the solvent used.

Further details of specific reagents or instrumentation setup used are provided in the concerned chapters.

2. References

1. (a) Armarego, W. L. F.; Chai, C. L. L. *Purification of Laboratory Chemicals*. (5th Ed), Elsevier Science, USA, **2003**. (b) Vogel, A. I. *A Text Book of Practical Organic Chemistry*. Longman, London, **1989**.
2. Selmarten, D.; Jones, M.; Rumbles, G.; Yu, P.; Nedeljkovic, J.; Shaheen, S. *J. Phys. Chem. B* **2005**, *109*, 15927.
3. Lakowicz, J. R. *Principles of Fluorescence Spectroscopy* (3rd Ed). Springer, New York, **2006**.

LIST OF PUBLICATIONS

1. An approach for optimizing the shell thickness of core-shell quantum dots using photoinduced charge transfer.
Vinayakan, R.; Shanmugapriya, T.; Nair, P. V.; Ramamurthy, P.; Thomas, K. G. *J. Phys. Chem. C* **2007**, *111*, 10146.
2. Synthesis of CdS nanorods and nanospheres: shape tuning by controlled addition rate of sulphide at room temperature.
T. Shanmugapriya, **R. Vinayakan**, K. George Thomas, P. Ramamurthy. (*Under revision, J. Phys. Chem. C*)
3. Silanised CdSe QDs for the selective detection of biothiols.
R. Vinayakan and K. George Thomas
(*Under submission to Angew. Chem. Int. Ed.*)
4. Silanised CdSe QDs for the selective detection of Hg^{2+} in aqueous media.
R. Vinayakan and K. George Thomas
(*Under submission to Chem. Commun.*)
5. *In vitro* cytotoxicity analysis and imaging using silanised CdSe QDs.
M. Vibin, **R. Vinayakan**, and Annie Abraham. (*To be submitted*).